



ELSEVIER

New Astronomy Reviews 45 (2001) 663–742

New Astronomy
Reviews

www.elsevier.com/locate/newar

Advective accretion disks and related problems including magnetic fields

G.S. Bisnovatyi-Kogan^{a,*}, R.V.E. Lovelace^b

^a*Space Research Institute, Profsoyuznaya 84/32, Moscow 117810, Russia*

^b*Department of Astronomy, Cornell University, Ithaca, NY 14853, USA*

Received 30 June 2001

Abstract

Accretion disk theory was first developed assuming local heat balance where the energy produced by viscous heating was emitted from the sides of the disk. One of the important inventions of this theory was the phenomenological treatment of the turbulent viscosity, known as the “alpha” prescription, where the $(r\phi)$ component of the stress tensor was approximated by αp , where α is a dimensionless constant and p is the pressure. This prescription played a role in the accretion disk theory as important as the mixing-length theory of convection for stellar evolution. Sources of turbulence in accretion disks are discussed, including hydrodynamical turbulence and convection and the role and of ordered and disordered magnetic fields. In parallel with the optically thick geometrically thin accretion disk models, a new branch of the optically thin accretion disk models was discovered, with a larger thickness for the same total luminosity. The choice between these solutions should be made on the basis of a stability analysis. The ideas underlying the necessity for including advection in accretion disk theory are presented and models with advection are reviewed. The low-luminosity, optically thin accretion disk models with advection are discussed, and the limits on advection dominated accretion flows (ADAF) imposed by the presence of a magnetic field are analyzed. The behavior of accretion disks in the presence of ordered and disordered magnetic fields are discussed. The interaction of an accretion disk with a rotating magnetized star is reviewed including the formation of magnetohydrodynamic (MHD) outflows, magnetic braking of the star’s rotation, and the propeller effect. The problems of the MHD origin of jets from magnetized disks are discussed including the ejection of mass, energy, angular momentum, and magnetic flux from the disk in both in the hydromagnetic and Poynting flux regimes. Recent MHD simulation results are discussed. © 2001 Published by Elsevier Science B.V.

1. Introduction

Accretion is the main source of energy in many astrophysical objects, including different types of binary stars, binary X-ray sources, and quasars and

active galactic nuclei (AGN). While the first development of accretion theory started a long time ago (Bondi and Hoyle, 1944; Bondi, 1952), intensive development of this theory began after the discovery of the first X-ray sources (Giacconi et al., 1962) and quasars (Schmidt, 1963). Accretion on to stars, including neutron stars, terminates at an inner boundary. This may be the stellar surface or the outer boundary of a magnetosphere for a strongly magnetized star. In this case all gravitational energy of the

*Corresponding author.

E-mail addresses: gkogan@mx.iki.rssi.ru (G.S. Bisnovatyi-Kogan), rv11@cornell.edu (R.V.E. Lovelace).

infalling matter is transformed into heat and radiated outward.

The situation is quite different for accretion to black holes, which are deduced to be present in some binary X-ray sources in the galaxy, as well as in AGN. Here, matter falls in to the event horizon of the black hole and no radiation escapes from within it. The efficiency of accretion is not known a priori in contrast with the case of accretion on to a star, and depends strongly on factors such as the angular momentum of the incoming matter and the magnetic field embedded in it. Schwartzman (1971) first showed that for spherical accretion of nonmagnetized gas the efficiency of radiation may be as small as 10^{-8} for low mass accretion rates. He showed that the presence of a magnetic field in the accreting matter can increase the efficiency up to about 10%. Heating of the matter due to magnetic field annihilation in the flow raises further the efficiency up to about 30% (Bisnovatyi-Kogan and Ruzmaikin, 1974; Meszáros, 1975). In the case of a geometrically thin accretion disk, which occurs when the matter is supplied with large angular momentum, the radiation efficiency is about one-half the efficiency of accretion on to a star with a radius equal to the radius of the last stable orbit. Matter cannot emit all the gravitational energy because part of the energy is absorbed by the black hole. In the case of geometrically thick but optically thin accretion disks, the situation approaches the case of spherical accretion, and therefore the presence of a magnetic field also plays a critical role.

Here we first discuss the development of the theory of a disk accretion, starting from the creation of the so-called “standard model,” and then reviewing recent developments connected with the role of advection. The flow of papers (see e.g. references in Narayan et al., 1996; Menon et al., 1999) considering advection dominated accretion flows (ADAF) as a solutions for many astrophysical problems should be treated with some caution because of the restrictive assumptions. The assumptions include neglect of the magnetic field and the associated magnetic field annihilation in heating of accretion plasma flow, and considering heating of electrons due *only* to binary collisions with protons (ions). These assumptions were critically analyzed in several papers (Bis-

novatyi-Kogan and Lovelace, 1997, 2000; Quataert, 1998; Blackman, 1999).

Competition between rapid accumulation of observational data, mainly from the Hubble Space Telescope and X-ray satellites, and the rapid construction of theoretical models for their explanation sometimes creates a situation where a model is disproved during the time of its publication. Some ADAF models give examples of this situation. One is connected with an explanation of the unusual non-monotonic spectrum of the galaxy NGC 4258. It was claimed (Lasota et al., 1996), that such spectrum may be explained only by an ADAF model. Observations (Herrnstein et al., 1998; Cannizzo et al., 1998) gave data in the radio and optical/UV regions showing a spectral maximum where a suspected minimum had been explained by an ADAF model, and posing constraints on the ADAF model. Restrictions on the ADAF model have also been obtained from radio observations of elliptical galaxies (Wrobel and Herrnstein, 2000). Another example is connected with an attempt to prove the existence of the event horizon in black holes systems using an ADAF model. Fig. 7 from the work of Menon et al. (1999) (Fig. 2 from Narayan et al., 1997) was considered to be proof of the existence of the event horizon of black holes and at the same time as a triumph of the ADAF model. However, the data used for these figures appears to be incomplete and a full set of observational data altered this picture (Chen et al., 1998).

Here, we analyze physical processes in optically thin accretion flows at low accretion rates *including* the influence of a magnetic field. We show, that account of the magnetic field amplification and annihilation in the accretion flow significantly modifies the ADAF solutions. Namely, the radiative efficiency of the accretion flows cannot become less than about 1/3 of the standard accretion disk value. This result brings into question attempts to connect ADAF models with the existence of the event horizon of a black hole, and on the explanation of the low luminosities of nearby super-massive black holes in nearby galactic nuclei.

It appears that the observational features “explained” by ADAF models, in particular, the “under-luminous galactic nuclei” may instead be due to

more complicated physical processes possibly involving magnetic fields. The behavior of accretion disks in the presence of ordered and disordered magnetic fields are discussed. The interaction of an accretion disk with a rotating magnetized star is reviewed including the formation of magneto-hydrodynamic (MHD) outflows, magnetic braking of the star's rotation, and the propeller effect. The problems of the MHD origin of jets from magnetized disks are discussed including the ejection of mass, energy, angular momentum, and magnetic flux from the disk in both in the hydromagnetic and Poynting flux regimes. Recent MHD simulations of the origin of hydromagnetic and Poynting jets from accretion disks are discussed. Energy losses connected with magnetohydrodynamic (MHD) outflows and jets from the accretion disk may be very important and represent an alternative explanation of under-luminous AGN black holes.

2. Foundation of accretion disk theory

2.1. Development of the standard model of disk accretion

Matter falling into a compact object tends to form a disk when its angular momentum is sufficiently high. This happens when matter falling into a black hole comes from a neighboring ordinary star in a binary system, or when the matter results from the tidal disruption of a star whose trajectory of motion approaches sufficiently close to the black hole, so that tidal forces overcome the self-gravity of the star. The first situation is observed in many galactic X-ray sources containing stellar mass black holes (Cherepashchuk, 1996, 2000). Tidal disruption of stars may happen in quasars and active galactic nuclei (AGN), if the model of supermassive black hole surrounded by a dense stellar cluster of Lynden-Bell (1969) is true for these objects.

Models of the structure of accretion disks around a black hole were investigated by Lynden-Bell (1969) and by Pringle and Rees (1972). The modern "standard" theory of the disk accretion was formulated in the papers of Shakura (1972), Novikov and Thorne (1973) and Shakura and Sunyaev (1973). It

is important to note that all authors of the accretion disk theory from the USSR were students (N.I. Shakura) or collaborators (I.D. Novikov and R.A. Sunyaev) of academician Ya.B. Zeldovich, who was not among the authors, but whose influence on them could hardly be overestimated.

The equations of the standard disk accretion theory were first formulated by Shakura (1972). Some corrections and generalization to general relativity (GR) were done by Novikov and Thorne (1973) (see also a correction to their equations in GR made by Riffert and Herold, 1995). The main idea of this theory is to describe a geometrically thin non-self-gravitating disk (of mass M_d which is much smaller than the mass of the black hole M) by hydrodynamic equations averaged over the disk thickness $2h$. Fig. 1 shows the disk geometry.

2.2. Basic equations

Let us start with the Navier–Stokes equations in Cartesian coordinates, describing the motion of a viscous compressible fluid with variable dynamic viscosity η and bulk viscosity η_B coefficients (Chapman and Cowling, 1939; Landau and Lifshitz, 1959)

$$\rho \left(\frac{\partial u_i}{\partial t} + u_k \frac{\partial u_i}{\partial x_k} \right) = - \frac{\partial p}{\partial x_i} + \rho g_i + \frac{\partial}{\partial x_k} \left[\eta \left(\frac{\partial u_i}{\partial x_k} + \frac{\partial u_k}{\partial x_i} - \frac{2}{3} \frac{\partial u_l}{\partial x_l} \delta_{ik} \right) + \eta_B \frac{\partial u_l}{\partial x_l} \delta_{ik} \right], \quad (1)$$

or in vector notation,

$$\rho \left(\frac{\partial \mathbf{u}}{\partial t} + (\mathbf{u} \cdot \nabla) \mathbf{u} \right) = - \nabla p + \rho \mathbf{g} + \nabla_k \left[\eta \left(\nabla_k \mathbf{u} + \nabla \mathbf{u}_k - \frac{2}{3} (\nabla \cdot \mathbf{u}) \underline{\delta} \right) + \eta_B (\nabla \cdot \mathbf{u}) \underline{\delta} \right]. \quad (2)$$

Here, the usual tensor definitions are used with δ_{ik} the Kronecker delta, and $\underline{\delta}$ the unit tensor; g_i is the gravitational acceleration. Summation over repeated indices is assumed. The last term in (1) is the

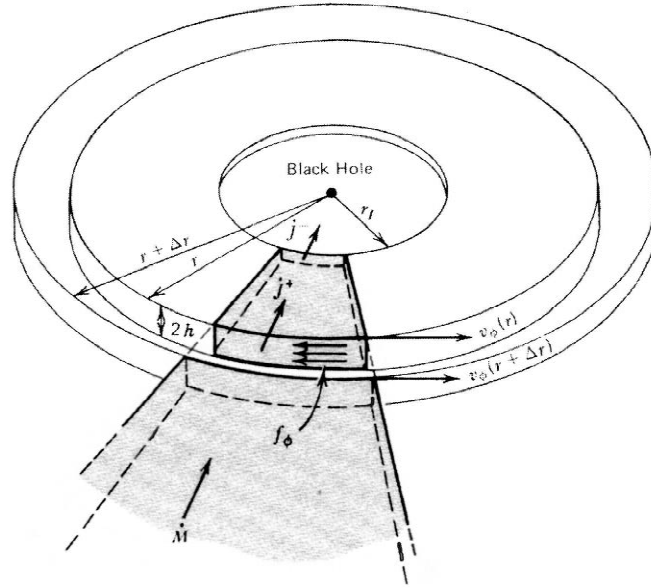


Fig. 1. Geometry of a thin accretion disk from Shapiro and Teukolsky (1983). Here, \dot{M} is the mass accretion rate, j is the total angular momentum flux, and $f_\phi = (1/r^2)\partial(r^2 t_{r\phi})$ is the viscous force with $t_{r\phi} = \eta \partial\Omega/\partial r$ the main component of the viscous stress tensor and η the dynamic viscosity coefficient.

divergence of the viscosity stress tensor σ_{ik} , which is related to the symmetric and divergentless deformation tensor τ_{ik} by the relation

$$\sigma_{ik} = 2\eta\tau_{ik} + \eta_B \frac{\partial u_i}{\partial x_l} \delta_{ik}, \quad \tau_{ik} = \frac{1}{2} \left(\frac{\partial u_i}{\partial x_k} + \frac{\partial u_k}{\partial x_i} - \frac{2}{3} \frac{\partial u_l}{\partial x_l} \delta_{ik} \right). \quad (3)$$

The bulk viscosity η_B is connected with finite rate of relaxation processes (ionization, chemical or nuclear reactions, etc). It is important only for rapid spatial changes (e.g., shocks) which are not considered here. Thus we take $\eta_B = 0$ everywhere below.

For accretion flows, it is natural to express Eq. (1) in cylindrical coordinates (r, ϕ, z) . For transformation to cylindrical coordinates, we need to write in these coordinates the different differential operators on a scalar a , a vector $\mathbf{a} = (a_r, a_\phi, a_z)$ and a tensor.

$$\underline{\mathbf{a}} = \begin{pmatrix} a_{rr} & a_{r\phi} & a_{rz} \\ a_{\phi r} & a_{\phi\phi} & a_{\phi z} \\ a_{zr} & a_{z\phi} & a_{zz} \end{pmatrix}. \quad (4)$$

(a) Gradient of a scalar:

$$\nabla a = \left(\frac{\partial a}{\partial r}, \quad \frac{1}{r} \frac{\partial a}{\partial \phi}, \quad \frac{\partial a}{\partial z} \right). \quad (5)$$

(b) Divergence of a vector:

$$\nabla \cdot \mathbf{a} = \frac{1}{r} \frac{\partial (ra_r)}{\partial r} + \frac{1}{r} \frac{\partial a_\phi}{\partial \phi} + \frac{\partial a_z}{\partial z}. \quad (6)$$

(c) Curl of a vector:

$$\nabla \times \mathbf{a} = \left(\frac{1}{r} \frac{\partial a_z}{\partial \phi} - \frac{\partial a_\phi}{\partial z}, \quad \frac{\partial a_r}{\partial z} - \frac{\partial a_z}{\partial r}, \quad \frac{\partial a_\phi}{\partial r} + \frac{a_\phi}{r} - \frac{1}{r} \frac{\partial a_r}{\partial \phi} \right). \quad (7)$$

(d) Gradient of a vector:

$$\nabla \mathbf{a} = \begin{pmatrix} \frac{\partial a_r}{\partial r} & \frac{\partial a_\phi}{\partial r} & \frac{\partial a_z}{\partial r} \\ \frac{1}{r} \frac{\partial a_r}{\partial \phi} - \frac{a_\phi}{r} & \frac{1}{r} \frac{\partial a_\phi}{\partial \phi} + \frac{a_r}{r} & \frac{1}{r} \frac{\partial a_z}{\partial \phi} \\ \frac{\partial a_r}{\partial z} & \frac{\partial a_\phi}{\partial z} & \frac{\partial a_z}{\partial z} \end{pmatrix}. \quad (8)$$

(e) Divergence of a tensor:

$$\nabla \cdot \mathbf{a} = \begin{pmatrix} \frac{\partial a_{rr}}{\partial r} + \frac{1}{r} \frac{\partial a_{\phi r}}{\partial \phi} + \frac{\partial a_{zr}}{\partial z} + \frac{a_{rr} - a_{\phi\phi}}{r} \\ \frac{\partial a_{r\phi}}{\partial r} + \frac{1}{r} \frac{\partial a_{\phi\phi}}{\partial \phi} + \frac{\partial a_{z\phi}}{\partial z} + \frac{a_{r\phi} + a_{\phi r}}{r} \\ \frac{\partial a_{rz}}{\partial r} + \frac{1}{r} \frac{\partial a_{\phi z}}{\partial \phi} + \frac{\partial a_{zz}}{\partial z} + \frac{a_{rz}}{r} \end{pmatrix}. \quad (9)$$

(f) Laplacian of a scalar:

$$\nabla^2 a \equiv (\nabla \cdot \nabla) a = \frac{\partial^2 a}{\partial r^2} + \frac{1}{r} \frac{\partial a}{\partial r} + \frac{1}{r^2} \frac{\partial^2 a}{\partial \phi^2} + \frac{\partial^2 a}{\partial z^2}. \quad (10)$$

(g) Laplacian of a vector:

$$\nabla^2 \mathbf{a} \equiv (\nabla \cdot \nabla) \mathbf{a} = \begin{pmatrix} \frac{\partial^2 a_r}{\partial r^2} + \frac{1}{r} \frac{\partial a_r}{\partial r} - \frac{a_r}{r^2} + \frac{1}{r^2} \frac{\partial^2 a_r}{\partial \phi^2} - \frac{2}{r^2} \frac{\partial a_\phi}{\partial \phi} + \frac{\partial^2 a_r}{\partial z^2} \\ \frac{\partial^2 a_\phi}{\partial r^2} + \frac{1}{r} \frac{\partial a_\phi}{\partial r} - \frac{a_\phi}{r^2} + \frac{1}{r^2} \frac{\partial^2 a_\phi}{\partial \phi^2} + \frac{2}{r^2} \frac{\partial a_r}{\partial \phi} + \frac{\partial^2 a_\phi}{\partial z^2} \\ \frac{\partial^2 a_z}{\partial r^2} + \frac{1}{r} \frac{\partial a_z}{\partial r} + \frac{1}{r^2} \frac{\partial^2 a_z}{\partial \phi^2} + \frac{\partial^2 a_z}{\partial z^2} \end{pmatrix}. \quad (11)$$

For the transformation of Eq. (3) to cylindrical coordinates we have

$$\tau_{ik} = \frac{1}{2} (\nabla_k \mathbf{u} + \nabla \mathbf{u}_k) - \frac{1}{3} (\nabla \cdot \mathbf{u}) \delta_{ik}, \quad (12)$$

with

$$2\tau_{ik} = \begin{pmatrix} \frac{4}{3} \frac{\partial u_r}{\partial r} - \frac{2}{3} \left(\frac{u_r}{r} + \frac{1}{r} \frac{\partial u_\phi}{\partial \phi} + \frac{\partial u_z}{\partial z} \right) & \frac{\partial u_\phi}{\partial r} + \frac{1}{r} \frac{\partial u_r}{\partial \phi} - \frac{u_\phi}{r} \\ \frac{\partial u_\phi}{\partial r} + \frac{1}{r} \frac{\partial u_r}{\partial \phi} - \frac{u_\phi}{r} & \frac{4}{3} \left(\frac{1}{r} \frac{\partial u_\phi}{\partial \phi} + \frac{u_r}{r} \right) - \frac{2}{3} \left(\frac{\partial u_r}{\partial r} + \frac{\partial u_z}{\partial z} \right) \\ \frac{\partial u_z}{\partial r} + \frac{\partial u_r}{\partial z} & \frac{1}{r} \frac{\partial u_z}{\partial \phi} + \frac{\partial u_\phi}{\partial z} \\ \frac{\partial u_z}{\partial r} + \frac{\partial u_r}{\partial z} & \\ \frac{1}{r} \frac{\partial u_z}{\partial \phi} + \frac{\partial u_\phi}{\partial z} & \\ \frac{4}{3} \frac{\partial u_z}{\partial z} - \frac{2}{3} \left(\frac{\partial u_r}{\partial r} + \frac{1}{r} \frac{\partial u_\phi}{\partial \phi} + \frac{u_r}{r} \right) & \end{pmatrix}. \quad (13)$$

The second term in the brackets on the left-hand side of Eq. (2) is a scalar product of the vector \mathbf{u} and

tensor $\nabla \mathbf{u}$, which is the same in Cartesian and curvilinear coordinates. The last term on the right-hand side of Eq. (2) is the divergence of the tensor $2\eta\tau_{ik}$, which is calculated using Eqs. (9) and (13). As a result we obtain the components of Eq. (2) in cylindrical coordinates:

$$\rho \left(\frac{\partial u_r}{\partial t} + u_r \frac{\partial u_r}{\partial r} + \frac{u_\phi}{r} \frac{\partial u_r}{\partial \phi} + u_z \frac{\partial u_r}{\partial z} - \frac{u_\phi^2}{r} \right) = -\frac{\partial P}{\partial r} + \rho g_r + \frac{2}{3} \frac{\partial}{\partial r} \left\{ \eta \left[\frac{2}{r} \frac{\partial (ru_r)}{\partial r} - \frac{1}{r} \frac{\partial u_\phi}{\partial \phi} - \frac{\partial u_z}{\partial z} \right] \right\} - 2 \frac{u_r}{r} \frac{\partial \eta}{\partial r} + \frac{1}{r} \frac{\partial}{\partial \phi} \left[\eta \left(\frac{\partial u_\phi}{\partial r} + \frac{1}{r} \frac{\partial u_r}{\partial \phi} - \frac{u_\phi}{r} \right) \right] - 2 \frac{\eta}{r^2} \frac{\partial u_\phi}{\partial \phi} + \frac{\partial}{\partial z} \left[\eta \left(\frac{\partial u_z}{\partial r} + \frac{\partial u_r}{\partial z} \right) \right]. \quad (14)$$

$$\rho \left(\frac{\partial u_\phi}{\partial t} + u_r \frac{\partial u_\phi}{\partial r} + \frac{u_\phi}{r} \frac{\partial u_\phi}{\partial \phi} + u_z \frac{\partial u_\phi}{\partial z} + \frac{u_r u_\phi}{r} \right) = -\frac{1}{r} \frac{\partial P}{\partial \phi} + \rho g_\phi + \frac{1}{r^2} \frac{\partial}{\partial r} \left[\eta r^3 \frac{\partial}{\partial r} \left(\frac{u_\phi}{r} \right) \right] + \frac{\partial}{\partial r} \left(\frac{\eta}{r} \frac{\partial u_r}{\partial \phi} \right) + \frac{2}{3r} \frac{\partial}{\partial \phi} \left\{ \eta \left[2 \left(\frac{1}{r} \frac{\partial u_\phi}{\partial \phi} + \frac{u_r}{r} \right) - \frac{\partial u_r}{\partial r} - \frac{\partial u_z}{\partial z} \right] \right\} + \frac{\partial}{\partial z} \left[\eta \left(\frac{1}{r} \frac{\partial u_z}{\partial \phi} + \frac{\partial u_\phi}{\partial z} \right) \right] + \frac{2\eta}{r^2} \frac{\partial u_r}{\partial \phi}. \quad (15)$$

$$\rho \left(\frac{\partial u_z}{\partial t} + u_r \frac{\partial u_z}{\partial r} + \frac{u_\phi}{r} \frac{\partial u_z}{\partial \phi} + u_z \frac{\partial u_z}{\partial z} \right) = -\frac{\partial P}{\partial z} + \rho g_z + \frac{1}{r} \frac{\partial}{\partial r} \left[\eta r \left(\frac{\partial u_z}{\partial r} + \frac{\partial u_r}{\partial z} \right) \right] + \frac{1}{r} \frac{\partial}{\partial \phi} \left[\eta \left(\frac{1}{r} \frac{\partial u_z}{\partial \phi} + \frac{\partial u_\phi}{\partial z} \right) \right] + \frac{2}{3} \frac{\partial}{\partial z} \left[\eta \left(2 \frac{\partial u_z}{\partial z} - \frac{\partial u_r}{\partial r} - \frac{1}{r} \frac{\partial u_\phi}{\partial \phi} - \frac{u_r}{r} \right) \right]. \quad (16)$$

The continuity equation for the disk flow is

$$\frac{\partial \rho}{\partial t} + \frac{\partial (\rho u_i)}{\partial x_i} = 0, \quad \text{or} \quad \frac{\partial \rho}{\partial t} + \nabla \cdot (\rho \mathbf{u}) = 0. \quad (17)$$

In cylindrical coordinates this equation becomes

$$\frac{\partial \rho}{\partial t} + \frac{\partial (r \rho u_r)}{r \partial r} + \frac{\partial (\rho u_\phi)}{r \partial \phi} + \frac{\partial (\rho u_z)}{\partial z} = 0. \quad (18)$$

2.3. Derivation of thin disk equations

For axisymmetric disk flows the ϕ -partial derivatives of the different scalar quantities vanish so that Eqs. (14)–(16) become

$$\begin{aligned} & \rho \left(\frac{\partial u_r}{\partial t} + u_r \frac{\partial u_r}{\partial r} + u_z \frac{\partial u_r}{\partial z} - \frac{u_\phi^2}{r} \right) \\ &= -\frac{\partial P}{\partial r} + \rho g_r \\ &+ \frac{2}{3} \frac{\partial}{\partial r} \left\{ \eta \left[\frac{2}{r} \frac{\partial(ru_r)}{\partial r} - \frac{\partial u_z}{\partial z} \right] \right\} \\ &- 2 \frac{u_r}{r} \frac{\partial \eta}{\partial r} + \frac{\partial}{\partial z} \left[\eta \left(\frac{\partial u_z}{\partial r} + \frac{\partial u_r}{\partial z} \right) \right], \end{aligned} \quad (19)$$

$$\begin{aligned} & \rho \left(\frac{\partial u_\phi}{\partial t} + u_r \frac{\partial u_\phi}{\partial r} + u_z \frac{\partial u_\phi}{\partial z} + \frac{u_r u_\phi}{r} \right) = \\ & \frac{1}{r^2} \frac{\partial}{\partial r} \left[\eta r^3 \frac{\partial}{\partial r} \left(\frac{u_\phi}{r} \right) \right] + \frac{\partial}{\partial z} \left(\eta \frac{\partial u_\phi}{\partial z} \right), \end{aligned} \quad (20)$$

$$\begin{aligned} & \rho \left(\frac{\partial u_z}{\partial t} + u_r \frac{\partial u_z}{\partial r} + u_z \frac{\partial u_z}{\partial z} \right) \\ &= -\frac{\partial P}{\partial z} + \rho g_z \\ &+ \frac{1}{r} \frac{\partial}{\partial r} \left[\eta r \left(\frac{\partial u_z}{\partial r} + \frac{\partial u_r}{\partial z} \right) \right] \\ &+ \frac{2}{3} \frac{\partial}{\partial z} \left[\eta \left(2 \frac{\partial u_z}{\partial z} - \frac{\partial u_r}{\partial r} - \frac{u_r}{r} \right) \right]. \end{aligned} \quad (21)$$

The continuity equation (18) takes the form

$$\frac{\partial \rho}{\partial t} + \frac{1}{r} \frac{\partial(r\rho u_r)}{\partial r} + \frac{\partial(\rho u_z)}{\partial z} = 0. \quad (22)$$

Many problems concerning thin accretion disks can be solved using the above equations in the equatorial plane or averaged over the thickness of the disk. The vertical structure of the disk is determined by the equilibrium of the pressure gradient and the vertical gravitational force g_z , which may include self-gravitation for sufficiently massive disks.

Problems connected with convective and meridional motion in disks need more detailed description with the full set of equations (14)–(18). A complete description requires including the magnetic force in the Navier–Stokes equations and the Maxwell equations for the field evolution (see Section 5).

In the equatorial plane of a thin disk, we have

$$u_z = 0, \quad g_z = \frac{\partial \rho}{\partial z} = \frac{\partial P}{\partial z} = \frac{\partial u_r}{\partial z} = \frac{\partial u_\phi}{\partial z} = 0, \quad (23)$$

where mirror symmetry about the equatorial plane is assumed. However, note that $\partial u_z / \partial z \neq 0$ even in this case. Neglecting u_z , g_ϕ and all z derivatives, we obtain the approximate equations

$$\begin{aligned} & \rho \left(\frac{\partial u_r}{\partial t} + u_r \frac{\partial u_r}{\partial r} - \frac{u_\phi^2}{r} \right) \\ &= -\frac{\partial P}{\partial r} + \rho g_r + \frac{4}{3} \frac{\partial}{\partial r} \left[\frac{\eta}{r} \frac{\partial(ru_r)}{\partial r} \right] \\ &- 2 \frac{u_r}{r} \frac{\partial \eta}{\partial r}, \end{aligned} \quad (24)$$

$$\rho r \left(\frac{\partial ru_\phi}{\partial t} + u_r \frac{\partial ru_\phi}{\partial r} \right) = \frac{\partial}{\partial r} \left[\eta r^3 \frac{\partial}{\partial r} \left(\frac{u_\phi}{r} \right) \right], \quad (25)$$

$$\rho g_z = \frac{\partial P}{\partial z}, \quad (26)$$

$$\frac{\partial \rho}{\partial t} + \frac{1}{r} \frac{\partial(r\rho u_r)}{\partial r} = 0. \quad (27)$$

Combining Eqs. (24) and (27) we get the radial equation in the form

$$\begin{aligned} & \frac{\partial \rho ru_r}{\partial t} + \frac{\partial \rho ru_r^2}{\partial r} - \rho r \left(\frac{u_\phi^2}{r} + g_r \right) = -r \frac{\partial P}{\partial r} \\ &+ \frac{4}{3} r \frac{\partial}{\partial r} \left[\frac{\eta}{r} \frac{\partial(ru_r)}{\partial r} \right] - 2u_r \frac{\partial \eta}{\partial r}. \end{aligned} \quad (28)$$

Following Shakura (1972), we write the viscosity coefficient η using the α -prescription,

$$\eta = \frac{2}{3} \alpha \rho_0 u_{s0} z_0, \quad (29)$$

where u_{s0} is a sound velocity in the equatorial plane ($z = 0$), and z_0 is half-thickness of the disk. Integrating Eqs. (25) and (27) over the thickness of the disk, we get an approximate set of equations describing the thin disk behavior, neglecting viscosity in the radial equation (24).

$$\frac{\partial u_r}{\partial t} + u_r \frac{\partial u_r}{\partial r} - \rho_0 (\Omega^2 r + g_r) + \frac{\partial P_0}{\partial r} = 0, \quad (30)$$

$$r \Sigma \frac{\partial j}{\partial t} + \frac{\dot{M}}{2\pi} \frac{\partial j}{\partial r} = \frac{2}{3} \alpha \frac{\partial}{\partial r} \left(\Sigma u_{s0} z_0 r^3 \frac{\partial \Omega}{\partial r} \right), \quad (31)$$

$$\frac{\partial \Sigma}{\partial t} + \frac{1}{2\pi r} \frac{\partial \dot{M}}{\partial r} = 0. \quad (32)$$

The average values, surface density Σ , accretion rate \dot{M} , and the values of the angular velocity Ω and specific angular momentum j are determined as follows

$$\Sigma = \int_{-z_0}^{z_0} \rho \, dz, \quad \dot{M} = 2 \pi r \int_{-z_0}^{z_0} \rho u_r \, dz = 2 \pi r \Sigma u_r,$$

$$\Omega = \frac{u_\phi}{r}, \quad j = r u_\phi. \quad (33)$$

Eqs. (30)–(32) determine the variables (Σ , \dot{M} , and j), where (u_r, Ω) are expressed from (33) with

$$u_r, \quad \dot{M} < 0. \quad (34)$$

The equation for vertical force balance (26) gives

$$u_{z0} = \left(\frac{\partial P_0}{\partial \rho_0} \right)_s^{1/2}, \quad z_0, \quad P_0, \quad (35)$$

as a functions of r , and Σ , when the equation of state is given in the form $P(\rho)$ (e.g., polytropic). Here, ρ_0, P_0 are the density and the pressure in the equatorial plane.

When the pressure P and velocity u_r derivatives are neglected in (30), the boundary conditions consist of the value of the mass flux and the Keplerian angular velocity at infinity; and of a condition on the angular velocity derivative near the accreting body (black hole, neutron star or other), determining the total angular momentum flux through the disk and zero density and pressure on the outer boundary of the disk.

$$\dot{M}(\infty) = \dot{M}_\infty, \quad \Omega(r \rightarrow \infty) = \left(\frac{GM}{r^3} \right)^{1/2}, \quad \rho(\pm z_0) = 0$$

$$\Omega(r_{in}) = \Omega_{in}, \quad \text{or} \quad \left(\frac{\partial \Omega}{\partial r} \right) (r_{in}) = \left(\frac{\partial \Omega}{\partial r} \right)_{in}, \quad (36)$$

where M is the mass of the star. If all terms are retained in Eq. (30), then an additional boundary condition is needed. It follows from the requirement that the flow solution u_r goes smoothly through the sonic (singular) point in the radial motion to the black hole or to the conditions at the outer boundary on the stellar equator. The stellar angular velocity may be much less than the Keplerian velocity of the accretion disk at that radius. In that case a boundary layer forms between the disk and the star, which needs to be treated separately (see Section 4.1).

In the case of a general equation of state $P(\rho, T)$, the temperature T appears as a new variable. Of course, T is connected with the heat flux F (ergs/

cm²/s), radiative or convective. Two additional equations for the energy balance over the disk and heat transfer to its outer boundary must be added together with boundary conditions for obtaining the full solution. These equations will be considered in later sections.

For solution of nonstationary accretion problems initial distributions are needed

$$\Sigma(r), \quad j(r), \quad \text{and} \quad \dot{M}(r), \quad (37)$$

in addition to the boundary conditions. In most cases the external force is represented by the gravity of the star, which may be treated as a point mass with a potential

$$\phi_g = - \frac{GM}{(r^2 + z^2)^{1/2}}. \quad (38)$$

The components of the gravitational acceleration g_i are written as

$$g_i = - \frac{\partial \phi_g}{\partial x_i} = \left(- \frac{GMr}{(r^2 + z^2)^{3/2}}, 0, \frac{GMz}{(r^2 + z^2)^{3/2}} \right). \quad (39)$$

For a thin disk we can use the expansion

$$g_i = \left\{ - \frac{GM}{r^2} \left(1 - \frac{3}{2} \frac{z^2}{r^2} \right), 0, - \frac{GMz}{r^3} \left(1 - \frac{3}{2} \frac{z^2}{r^2} \right) \right\}. \quad (40)$$

2.4. Structure of polytropic accretion disks

A polytropic equation of state has the form

$$P = K \rho^{1+1/n}. \quad (41)$$

Taking the main term in the gravitational force g_z from (40), we get the solution of Eq. (26) (Hōshi, 1977)

$$\rho = \rho_0 \left(1 - \frac{z^2}{z_0^2} \right)^n, \quad (42)$$

where the density in the equatorial plane ρ_0 is connected with r and z_0 by the relation

$$\rho_0 = \left[\frac{GM}{2K(n+1)} \right]^n \frac{z_0^{2n}}{r^{3n}}. \quad (43)$$

The physical quantities from (33)–(35) can be expressed in terms of r and ρ_0 .

$$z_0 = \left[\frac{2K(n+1)}{GM} \right]^{1/2} \rho_0^{1/n} r^{3/2} = \beta_{z_0} \rho_0^{1/n} r^{3/2}, \quad (44)$$

$$\Sigma = \sqrt{\pi} \frac{\Gamma(n+1)}{\Gamma\left(n + \frac{3}{2}\right)} \rho_0 z_0 = \beta_{\Sigma} \rho_0^{2n+1} r^{3/2}, \quad (45)$$

$$P_0 = K \rho_0^{1+\frac{1}{n}}, \quad u_{s,0} = \left(\frac{n+1}{n} K \right)^{1/2} \rho_0^{1/n} = \beta_{s,0} \rho_0^{1/n}, \quad (46)$$

where

$$\beta_{\Sigma} = \sqrt{\pi} \frac{\Gamma(n+1)}{\Gamma\left(n + \frac{3}{2}\right)} \left[\frac{2K(n+1)}{GM} \right]^{1/2}. \quad (47)$$

The isothermal case corresponds to $n \rightarrow \infty$,

$$P = K\rho, \quad (48)$$

and we have instead of (42)

$$\rho = \rho_0 \exp\left(-\frac{GMz^2}{2Kr^3}\right) = \rho_0 \exp\left(-\frac{z^2}{z_i^2}\right), \quad z_i = \left(\frac{2Kr^3}{GM}\right)^{1/2}. \quad (49)$$

Formally, an isothermal disk has infinite thickness z_0 , but the density falls exponentially with the characteristic height z_i from (49). Instead of (45)–(46) we have

$$\Sigma = \left(\frac{2\pi K}{GM}\right)^{1/2} \rho_0 r^{3/2}, \quad (50)$$

$$P_0 = K\rho_0, \quad u_{s,0} = \sqrt{K}. \quad (51)$$

We restrict our attention to stationary accretion disks with $\partial/\partial t = 0$. Then we have from (32)

$$\dot{M} = \text{const}, \quad (52)$$

and Eq. (31) can be integrated to give (Shakura, 1972)

$$\frac{\dot{M}}{2\pi} (j - j_0) = \frac{2}{3} \alpha \Sigma u_{s,0} z_0 r^3 \frac{d\Omega}{dr}. \quad (53)$$

The integration constant j_0 after multiplication by \dot{M} gives the total (advective plus viscous) flux of angular momentum within the accretion disk. A

positive value of j_0 corresponds to a negative total flux (due to a negative \dot{M}), which means that the central body accretes its angular momentum. When j_0 is negative the total angular momentum of the central body decreases, while its mass increases.

For a thin disk, neglecting u_r and \mathcal{P} , and taking only the main term for g_r from (40), we get from (30)

$$\Omega^{(0)} = \left(\frac{GM}{r^3}\right)^{1/2} = \Omega_K, \quad j^{(0)} = j_K = (GMr)^{1/2}. \quad (54)$$

The solution (54) is used outside the inner boundary of the accretion disk at $r = r_{\text{in}}$. The integration constant j_0 can be scaled by the Keplerian angular momentum $j_K(r_{\text{in}})$, so that

$$j_0 = \xi j_K(r_{\text{in}}) = \xi \sqrt{GM r_{\text{in}}} \quad (55)$$

Substituting (55) into (53) and taking account of (44)–(47), we get a relation for the density in the equatorial plane,

$$\rho_0^{(0)} = b_{\rho 0} \left[-\frac{\dot{M}}{r^3} \left(1 - \xi \sqrt{\frac{r_{\text{in}}}{r}}\right) \right]^{\frac{2n}{2n+3}}, \quad (56)$$

$$b_{\rho 0} = \left[\frac{1}{4\pi^{3/2} \alpha} \frac{\sqrt{n}}{(n+1)^{3/2}} \frac{\Gamma\left(n + \frac{3}{2}\right)}{\Gamma(n+1)} \frac{GM}{K^{3/2}} \right]^{\frac{2n}{2n+3}}. \quad (57)$$

Using (47), in (44)–(46) we get

$$z_0^{(0)} = b_{z_0} \left[-\dot{M} \left(1 - \xi \sqrt{\frac{r_{\text{in}}}{r}}\right) \right]^{\frac{1}{2n+3}} r^{\frac{3}{2} \frac{2n+1}{2n+3}}, \quad (58)$$

$$\Sigma^{(0)} = b_{\Sigma} \left[-\dot{M} \left(1 - \xi \sqrt{\frac{r_{\text{in}}}{r}}\right) \right]^{\frac{2n+1}{2n+3}} r^{-\frac{3}{2} \frac{2n-1}{2n+3}}, \quad (59)$$

$$P_0^{(0)} = b_{P_0} \left[-\frac{\dot{M}}{r^3} \left(1 - \xi \sqrt{\frac{r_{\text{in}}}{r}}\right) \right]^{\frac{2(n+1)}{2n+3}}, \quad (60)$$

$$u_{s,0}^{(0)} = b_{s,0} \left[-\frac{\dot{M}}{r^3} \left(1 - \xi \sqrt{\frac{r_{\text{in}}}{r}}\right) \right]^{\frac{1}{2n+3}}, \quad (61)$$

where

$$b_{z_0} = [2(n+1)]^{1/2} \times \left[\frac{1}{4\pi^{3/2}\alpha} \frac{\sqrt{n}}{(n+1)^{3/2}} \frac{\Gamma\left(n + \frac{3}{2}\right)}{\Gamma(n+1)} \right]^{\frac{1}{2n+3}} \times K^{\frac{n}{2n+3}} (GM)^{-\frac{2n+1}{2(2n+3)}} \quad (62)$$

$$b_{\Sigma} = [2\pi(n+1)]^{1/2} \frac{\Gamma(n+1)}{\Gamma\left(n + \frac{3}{2}\right)} \times \left[\frac{1}{4\pi^{3/2}\alpha} \frac{\sqrt{n}}{(n+1)^{3/2}} \frac{\Gamma\left(n + \frac{3}{2}\right)}{\Gamma(n+1)} \right]^{\frac{2n+1}{2n+3}} \times K^{-\frac{2n}{2n+3}} (GM)^{\frac{2n-1}{2(2n+3)}} \quad (63)$$

$$b_{P_0} = K b_{\rho_0}^{1+1/n}, \quad b_{s_0} = b_{\rho_0}^{1/2n} \left(K \frac{n+1}{n} \right)^{1/2}. \quad (64)$$

In the formula for the viscosity coefficient (29), z_0 must be replaced by z_i from (49) for the isothermal case,

$$\eta = \frac{2}{3} \alpha \rho u_{s_0} z_i \quad (65)$$

Then instead of (55)–(64) we get the solution

$$P_0^{(0)} = K \rho_0^{(0)} = \frac{GM}{4\pi^{3/2}\alpha K^{3/2}} \left(-\frac{\dot{M}}{r^3} \right) \left(1 - \xi \sqrt{\frac{r_{in}}{r}} \right), \quad (66)$$

$$\Sigma^{(0)} = \frac{\sqrt{GM}}{\alpha 2\pi K \sqrt{2}} \left(-\frac{\dot{M}}{r^{3/2}} \right) \left(1 - \xi \sqrt{\frac{r_{in}}{r}} \right). \quad (67)$$

The formulas for the values of z_i in (49) and u_{s_0} in (51) remain the same in all approximations for the isothermal case.

For accretion to a black hole in the presence of a free inner boundary with $\xi = 1$, the zero order approximation is not valid in the vicinity of r_{in} , where other terms in (30) must be taken into account. For accretion onto a slowly rotating star with angular velocity smaller than the Keplerian velocity on the equator, the drop of the angular velocity from Keplerian in the disk to that on the stellar equatorial happens in a thin boundary layer, which must be considered separately with proper account of the pressure term in (30).

2.5. Standard accretion disk model

2.5.1. Equilibrium equations

The small thickness of the disk in comparison with its radius $h \ll r$ indicates the small influence of the pressure gradient ∇P in comparison with gravity and inertia forces. This leads to a simple radial equilibrium where there is a balance between the gravitational and centrifugal accelerations. Thus, the angular velocity of the disk Ω is equal to the Keplerian value,

$$\Omega = \Omega_K = \left(\frac{GM}{r^3} \right)^{1/2}. \quad (68)$$

Note that just outside the last stable orbit around a black hole, and of course inside it, this suggestion fails, but in the “standard” accretion disk model the relation (68) is suggested to be fulfilled all over the disk, with an inner boundary at the last stable orbit.

The equilibrium equation in the vertical z -direction is determined by a balance between the gravitational force and pressure gradient

$$\frac{dP}{dz} = -\rho \frac{GMz}{r^3}. \quad (69)$$

For a thin disk this differential equation leads to algebraic one, determining the half-thickness of the disk as

$$h \approx \frac{1}{\Omega_K} \left(2 \frac{P}{\rho} \right)^{1/2}. \quad (70)$$

The ϕ -component of the Navier–Stokes equation has an integral which represents the conservation of angular momentum,

$$\dot{M}(j - j_{in}) = -2\pi r^2 2ht_{r\phi}, \quad t_{r\phi} = \eta r \frac{d\Omega}{dr}. \quad (71)$$

Here, $j = v_\phi r = \Omega r^2$ is the specific angular momentum, $t_{r\phi}$ is the (r, ϕ) component of the viscous stress tensor, and $\dot{M} > 0$ is the mass accretion rate. Here, j_0 is an integration constant. Multiplication of j_0 by \dot{M} gives the difference between the viscous and advective flux of angular momentum in the disk. For accretion to a black hole it is usually assumed that the viscous flux of angular momentum is zero at the inner disk radius (which corresponds to the radial gradient of the angular velocity being zero at the inner radius). In this case

$$j_{\text{in}} = \Omega_{\text{K}} r_{\text{in}}^2, \quad (72)$$

which is the Keplerian angular momentum of the matter on the last stable orbit. For accretion on to a slowly rotating star with angular velocity smaller than the Keplerian velocity on the inner edge of the disk, there is a maximum of the angular velocity close to its surface, where viscous flux is zero, and there is a boundary layer between this point and stellar surface. In this case (72) is also valid. The situation is different for accretion disks around rapidly rotating stars Keplerian speed on the equator (see Section 4). Note that in the pioneering paper of Shakura (1972), the integration constant j_{in} was found as in (72), but was taken zero in his subsequent formulae. The importance of using j_{in} in the form (72) was noticed by Novikov and Thorne (1973), and became a feature of the standard model.

2.5.2. Turbulent viscosity and instabilities

The choice of the viscosity coefficient is the most difficult and speculative aspect of accretion disk theory. In the laminar case of microscopic (atomic or plasma) viscosity, which is very small, a stationary accretion disk must be very massive and very thick, and before its formation matter is collected by disk leading to a small accretion rate to the central object. This contradicts observations of X-ray binaries where a considerable accretion rate is required. This can be explained only when the viscosity coefficient is much larger than the microscopic one. Shakura (1972) suggested that matter in the disk is turbulent and described by a viscous stress tensor parametrized as

$$t_{r\phi} = -\alpha \rho v_s^2 = -\alpha P, \quad (73)$$

where α is a dimensionless constant and v_s is the sound speed. This simple parameterization corresponds to a turbulent viscosity coefficient $\eta_t \approx \rho v_t \ell$ with an eddy velocity v_t and a length scale of the turbulent element ℓ . It follows from the definition of $t_{r\phi}$ in (71), when we take $\ell \approx h$ from (70)

$$t_{r\phi} = \rho v_t h r \frac{d\Omega}{dr} \approx \rho v_t v_s = -\alpha \rho v_s^2, \quad (74)$$

where the coefficient $\alpha < 1$ relates the turbulent and sound speeds, $v_t = \alpha v_s$. The representation of $t_{r\phi}$ in (73) and (74) are equivalent. Only when the angular

velocity differs significantly from the Keplerian one is the first relation, on the right-hand side of (74), preferable. Large departures from Keplerian flow do not occur in the standard theory, but may arise in advective dominated flows.

Development of turbulence in an accretion disk cannot be explained simply. A Keplerian disk is stable in the linear approximation to the development of axially symmetric perturbations, conserving the angular momentum. That is, the disks satisfy the Rayleigh criterion for stability. Ya.B. Zeldovich proposed that in presence of very large Reynolds number $Re = \rho v l / \eta$, the amplitude of perturbations at which nonlinear effects become important is very low so that turbulence may develop due to nonlinear instability even when the disk is linearly stable. Another source of $t_{r\phi}$ stress may arise from a magnetic field, but Shakura (1972) argued that the magnetic stress does not exceed the hydrodynamic stress.

Magnetohydrodynamic instability as a source of the turbulence in accretion disks has been studied extensively during the past several years (see review of Balbus and Hawley, 1998). They used an instability of a weak magnetic field in a differentially rotating disk discovered by Velikhov (1959) and Chandrasekhar (1981). The magnetic field is weak in the sense that the midplane Alfvén speed v_A must be less than the sound speed c_s in order for the instability to occur. This instability could be important in absence of any other source of the turbulence and if the magnetic fields were sufficiently weak. Stronger fields probably occur in actual disks. Magnetic field amplification by differential rotation can take place without instability (e.g., Bisnovatyi-Kogan and Lovelace, 2000). Coppi and Coppi (2000) have recently discovered unstable singular modes in a strongly magnetized ($v_A > c_s$) accretion disk, and this represents a promising area of future study.

A marco-scale hydrodynamic, Rossby wave instability has recently been shown to occur in non-magnetized disks which have non-monotonic profiles of surface density, pressure, and/or specific entropy (Lovelace et al., 1999a; Li et al., 2000). The instability has been found in 2D hydrodynamic simulations and has been shown to give rise to a small number ($m = 3-5$) of long lived Rossby

vortices which give outward transport of angular momentum (Li et al., 2001).

Bisnovaty-Kogan and Blinnikov (1976, 1977) showed that the inner regions of highly luminous accretion disks where radiation pressure dominates, are unstable to vertical convection. Development of this convection produces turbulence, needed for a high viscosity. Other regions of a standard accretion disk should be stable to development of vertical convection, and in those regions other mechanisms of a turbulence generation are needed.

In a Keplerian disk, the angular momentum per unit mass $j = \omega r^2 \sim r^{1/2}$ increases with distance. In this respect it is similar to the viscous flow between two rotating cylinders (a Taylor column) when the inner cylinder is not rotating. There are however important differences between these two problems. There are two boundaries on the surfaces of the cylinders with no slip boundary conditions, whereas the accretion disk has free boundaries. The radial equilibrium in the fluid between the cylinders has balance between centrifugal and pressure gradient forces, whereas in the disk there is a balance between centrifugal and gravitational forces. Finally, the fluid between cylinders in the laboratory experiments is usually strongly subsonic so that the flow is incompressible, whereas in the accretion disk the flow is highly supersonic. Nevertheless, it is thought that the fundamental theory tested in detail in the laboratory is relevant to astrophysical disks.

A phenomenological analysis of the Taylor experiment and the onset of turbulence in the “stable” case of the inner cylinder at rest was done by Zel’dovich (1981). There are two characteristic specific energies in the problem. One is the energy required to for the axisymmetric exchange over a small radial distance Δr of a rings or torii of fluid with conservation of angular momentum of each ring, $E_s = 2(\omega/r)(d(\omega r^2)/dr)(\Delta r)^2$. This energy is positive for Rayleigh stable conditions and negative in the unstable case. Another energy E_t corresponds to the merging the two rings with conservation of the total angular momentum, $E_t = (1/4)r(d\omega/dr)^2(\Delta r)^2$ is always positive. The ratio of these two energies was defined by Zel’dovich (1981) as the Taylor number

$$Ty = \frac{E_s}{E_t} = 4 \frac{d[(\omega r^2)^2]/dr}{r^5(d\omega/dr)^2}. \quad (75)$$

(Note that this is not the usual definition of the Taylor number.) The boundary $Ty = 0$ separate regions stable and unstable according to the Rayleigh criterion. In the case of closely spaced cylinders, $R_{out} - R_{in} \ll R = \frac{1}{2}(R_{in} + R_{out})$, we obtain from (75)

$$\omega_{out} \approx \omega_{in} \approx \omega, \quad R_{out} \approx R_{in} \approx R, \quad R_{out} - R_{in} \equiv t, \\ \frac{d}{dr} = \frac{1}{t}, \quad Ty \approx 8 \frac{t}{R}. \quad (76)$$

Note that $t \rightarrow 0$ corresponds to flat Couette flow which is formally stable at all Reynolds numbers (Schlichting, 1964) when dv/dr , is constant ($v = \omega r$ is the fluid velocity), in contradiction with the experiment. Account of the curvature of the streamlines, even if this is small, is very important here, and gives the instability, similar to the case with the free outer boundary, also corresponding to $Ty = 0$, when the instability starts at $Re = \rho vt/\eta \approx 2000$. Note, that account of the compressibility leads to instability even in the case of the flat Couette flow (Glatzel, 1989). The maximum of region of instability corresponds to Mach number $Ma \approx 4.9$, when instability first appears at $Re \approx 84$.

Taylor experiments with rotating cylinders has shown that for $Ty > 0$ the flow becomes turbulent for large enough Reynolds number Re . The value of Re for instability increases with increasing Ty . For the case of a Keplerian disk, $\omega \propto r^{-3/2}$, we have $Ty = 16/9$, formally corresponding to $t/R = 2/9 = 0.222$, and for this Ty the experimental number for the critical $Re \approx 2 \times 10^5$ (Zel’dovich, 1981). The experimental dependence of the critical value $Re = f(Ty)$ is characterized by the Couette-flow critical value $Re(0) = 2000$, and can be approximated by the dependence $Re \approx 10^4(Ty)^2$ for $Ty > 0.6$, $t/R > 0.075$. The last dependence was interpreted theoretically by Zel’dovich (1981) by introduction of the *split* regime for the turbulence between cylinders.

In the laminar viscous flow between cylinders, the exact solution (Schlichting, 1964) for $\omega_{in} = 0$ gives the velocity distribution

$$v(r) = \frac{R_{out}^2 \omega_{out}}{R_{out}^2 - R_{in}^2} \left(r - \frac{R_{in}^2}{r} \right) \approx \omega_{out} \frac{R}{t} (r - R_{in}) \\ = \omega_{out} \frac{q}{t} = \omega_{out} x, \quad q = r - R_{in}, \quad x = \frac{q}{t}. \quad (77)$$

Local values of Re' and Ty' numbers, defined by fluid parameters near the inner cylinder, have been introduced by Zel'dovich (1981) as

$$Re' = \frac{\rho v x}{\eta} = x^2 Re, \quad Ty' = 8 \frac{x}{R} = x Ty. \quad (78)$$

Zel'dovich (1981) proposed that turbulence between rotating cylinders is initiated when one of the following inequalities is fulfilled

$$\mathbf{a.} \quad Re = f(Ty) \quad \text{or} \quad \mathbf{b.} \quad Re' = f(Ty'). \quad (79)$$

If inequality (79b) is fulfilled first, and the global condition (79a) of instability is not reached, then turbulence arises in a local region near the inner cylinder. This was termed the “split” regime. Assuming that (79b) is fulfilled first we get

$$Re = \frac{Re'}{x^2} = \frac{f(Ty')}{x^2} = Ty^2 \frac{f(y)}{y^2}, \quad y = x Ty. \quad (80)$$

Suppose now, that the function $\phi(y) = f(y)/y^2$ has a minimum at

$$y = y_m, \quad \phi_m = \frac{f(y_m)}{y_m^2}. \quad (81)$$

Then, taking into account (77) we get the relation $Ty > y_m$, so

$$\phi(Ty) > \phi(y_m), \quad Re = Ty^2 \phi(y_m) < f(Ty), \quad (82)$$

the global criterion of the turbulence is not fulfilled, and the split regime is realized. Turbulence arises in the region $x < x_m = y_m/Ty$. Thus, the criterion for occurrence of the split regime has a quadratic dependence on Ty in accordance with the experimental results.

Zel'dovich (1981) noted that the boundary of the split regime of turbulence does not necessarily mean the beginning of the turbulence in an accretion disk, where inequality (79a) is probably needed. Two examples of functions are considered by Zel'dovich (1981). For the function

$$f(y) = A \left(1 - \frac{y}{y_0}\right)^{-1} \quad (83)$$

the absolute instability (79a) exist only at $Ty < y_0$, and the minimum is reached at

$$y = \frac{2}{3}y_0, \quad \phi_m = \frac{f(y_m)}{y_m^2} = \frac{27}{4} \frac{A}{y_0^2}. \quad (84)$$

From the flat Couette flow it follows that $A = 2000$, and from the Taylor experiments, assuming the split regime of turbulence and assuming (82), we get $\phi_m = 10^4$, $y_0 = 1.16$. Note that for the Keplerian accretion disk we have $Ty = 16/9 > 1.16$.

The second function considered by Zel'dovich (1981) is

$$f(y) = A \exp(y/y_0), \quad (85)$$

where $A = 2000$, similar to (83), and $y_0 = 0.3$ from the Taylor experiment. Here $Re = f(16/9) = 2000 \exp(1.78/0.3) \approx 8 \times 10^5$ for the beginning of absolute instability and the onset of turbulence.

The above discussion shows that the problem of the hydrodynamic instability of the Keplerian accretion disks is *far* from a full understanding. There are arguments, both experimental and theoretical, supporting the hydrodynamic origin of the accretion disk turbulence. A definite answer could be obtained from a full three-dimensional stability analysis of the Keplerian disk based on the Navier–Stokes equations. The calculation would be similar to the one made for viscous accretion tori by Klieber and Glatzel (1999) for a constant specific angular momentum distribution. Note that Reynolds numbers $\sim 10^6$ are well beyond the reach of present numerical simulations.

With the alpha-prescription for the viscosity, the equation of angular momentum conservation in the plane of the disk gives

$$\dot{M}(j - j_{in}) = 4\pi r^2 \alpha P_0 h. \quad (86)$$

If the angular velocity is far from Keplerian, the relation (71) is valid with a coefficient of a turbulent viscosity

$$\eta = \frac{2}{3} \alpha \rho_0 v_{s0} h, \quad (87)$$

where the subscripts “0” indicate evaluation at the midplane of the disk.

2.5.3. Heat balance

In the standard theory, the heat balance is local in the sense that all heat produced by viscosity in the disk between r and $r + dr$ is radiated through the sides of disk at the same r . The heat production rate Q_+ per unit area of the disk is

$$Q_+ = h t_{r\phi} r \frac{d\Omega}{dr} = \frac{3}{8\pi} \dot{M} \frac{GM}{r^3} \left(1 - \frac{j_{\text{in}}}{j}\right). \quad (88)$$

Heat loss from the disk depends on the optical depth. In the first standard disk model of Shakura (1972), the disk was assumed optically thick in the vertical direction. This implies an energy loss Q_- per unit area from the disk due to radiative transport. After substitution of the differential equation of a heat transfer by an algebraic relation one obtains

$$Q_- \approx \frac{4}{3} \frac{acT^4}{\kappa\Sigma}. \quad (89)$$

Here, a is the usual radiation energy–density constant, c is a speed of light, T is the midplane temperature of the disk, κ is the opacity, and the surface mass density is

$$\Sigma = 2\rho h. \quad (90)$$

Here, and subsequently, ρ, T , and P without the index “0” refer to values at the midplane of the disk.

The heat balance equation is

$$Q_+ = Q_-. \quad (91)$$

For stationary conditions the continuity equation gives radial velocity as

$$v_r = \frac{\dot{M}}{4\pi r h \rho} = \frac{\dot{M}}{2\pi r \Sigma}. \quad (92)$$

Eqs. (68), (70), (86), (90), (91), completed by an equation of state $P(\rho, T)$ and relation for the opacity $\kappa = \kappa(\rho, T)$ represent a full set of equations for the standard disk model. For power law equations of state of an ideal gas $P = P_g = \rho \mathcal{R} T$ (\mathcal{R} is a gas constant), or radiation pressure $P = P_r = aT^4/3$, and opacity in the form of electron scattering κ_e , or Kramers opacity κ_k , the solution of the standard disk accretion theory is obtained analytically (Shakura, 1972; Novikov and Thorne, 1973; Shakura and Sunyaev, 1973). Checking the assumption of a large optical thickness confirms the self-consistency of the model. One of the shortcomings of the analytical solutions of the standard model was the fact that the solutions for different regions of the disk (with

different equations of state and opacities) are not matched to each other.

2.5.4. Optically thin solution

A few years after the appearance of the standard model, it was found that in addition to the optically thick solution there is another branch of the disk structure with the same input parameters M, \dot{M} , and α which is also self-consistent and has a small optical thickness (Shapiro et al., 1976). For small optical thickness, a different equation of energy loss is required. It is determined by the volume emission

$$Q_- \approx q \rho h. \quad (93)$$

Due to the Kirchoff’s law the emissivity per unit volume q is connected with a Planckian averaged opacity κ_p by an approximate relation $q \approx acT_0^4 \kappa_p$. Note, that Kramers’ formulae for opacity is obtained after Rosseland averaging of the frequency dependent absorption coefficient. In the optically thin limit, the pressure is determined by the gas $P = P_g$. Analytical solutions are obtained here as well, from the same equations as before but with the volume energy loss and the pressure due only to the gas. In the optically thin solution, the thickness of the disk is larger then in the optically thick case and the density is lower.

While heating by viscosity is determined mainly by ions, and cooling is determined by electrons, the rate of the energy exchange between them is important for the thermal structure of the disk. The energy balance equations are written separately for ions and electrons. For small accretion rates and lower matter density the rate of energy exchange due to binary collisions is so slow that the ions become much hotter than the electrons. That also implies a large geometrical disk thickness and brings the standard accretion theory to the limit of its applicability.

Note that in the highly turbulent disk plasma, the energy exchange between ions and electrons may be strongly enhanced due to the presence of fluctuating electrical fields. Under such conditions the difference of temperatures of ions and electrons may be negligible. The theory of ion-electron energy exchange in a turbulent plasma is not completed, but there are indications of a large enhancement of the relaxation

in the presence of plasma turbulence, in comparison with the binary collisions (Quataert, 1998).

2.6. Accretion disk structure from equations describing continuously optically thin and thick conditions

In order to find equations for the disk structure valid in both limiting cases of optically thin and thick conditions, and smoothly describing the transition between them, we use the Eddington approximation for the heat flux and for the radiation pressure (Artemova et al., 1996). Suppose that disk is geometrically thin and has a constant density along the z -axis. Defining S_r to be the energy density of the radiation, F_{rad} the radiation flux in z -direction, P_{rad} the radiation pressure, we write momentum equations for averaged κ_p in the form (Bisnovaty-Kogan, 1989)

$$\frac{dF_{\text{rad}}}{dz} = -\rho c \kappa_p a T^4 \left(\frac{S_r}{a T^4} - 1 \right), \quad (94)$$

$$c \frac{dP_{\text{rad}}}{dz} = -\kappa_e \rho F_{\text{rad}}. \quad (95)$$

Consider the case where the scattering opacity κ_e is much larger than the absorption opacity κ_p , and assume that the heat production rate is proportional to the mass density ρ . Then, neglecting the flux in the radial direction we get

$$F_{\text{rad}} = 2 \frac{F_0}{\Sigma_0} \rho z, \quad (96)$$

where F_0 is the flux per unit area of the disk at $z = h$. Substituting (96) into (94) we get

$$S_r = 3P_{\text{rad}} = a T^4 \left(1 - \frac{2F_0}{c \kappa_p a T^4 \Sigma_0} \right). \quad (97)$$

Using (96) in (95) we get

$$c \frac{dP_{\text{rad}}}{dz} = -2\kappa_e \frac{F_0}{\Sigma_0} \rho^2 z. \quad (98)$$

Introducing the scattering optical depth

$$\begin{aligned} \tau &= \int_z^\infty \kappa_e \rho dz = \kappa_e \rho (h - z) = \tau_0 - \kappa_e \rho z, \quad \tau_0 \\ &= \kappa_e \rho h = \frac{1}{2} \kappa_e \Sigma_0, \end{aligned} \quad (99)$$

we rewrite (98) in the form

$$c \frac{dP_{\text{rad}}}{d\tau} = 2 \frac{F_0}{\Sigma_0} \frac{\tau_0 - \tau}{\kappa_e}. \quad (100)$$

We solve (100) with the following boundary condition

$$F_{\text{rad}}|_{\tau=0} = F_0 = \frac{c S_r|_{\tau=0}}{2} = \frac{3c P_{\text{rad}}|_{\tau=0}}{2}, \quad (101)$$

resulting in

$$c P_{\text{rad}} = F_0 \left(\frac{2}{3} + \tau - \frac{\tau^2}{2\tau_0} \right). \quad (102)$$

In the symmetry plane of the disk at $\tau = \tau_0$, we have

$$c P_{\text{rad},0} = F_0 \left(\frac{2}{3} + \frac{\tau_0}{2} \right). \quad (103)$$

Using (103) in (97) we get in the symmetry plane, where $T = T_0$

$$F_0 = c a T_0^4 \left(2 + \frac{3\tau_0}{2} + \frac{1}{\tau_{\alpha 0}} \right)^{-1}, \quad (104)$$

where the absorption optical depth

$$\begin{aligned} \tau_\alpha &= \int_z^\infty \kappa_p \rho dz = \kappa_p \rho (h - z) = \tau_{\alpha 0} - \kappa_p \rho z, \quad \tau_{\alpha 0} \\ &= \kappa_p \rho h = \frac{1}{2} \kappa_p \Sigma_0. \end{aligned} \quad (105)$$

Introducing the effective optical depth

$$\tau_* = (\tau_0 \tau_{\alpha 0})^{1/2}, \quad (106)$$

we finally get expressions for the vertical energy flux from the disk F_0 and the radiation pressure in the symmetry plane as

$$F_0 = \frac{2acT_0^4}{3\tau_0} \left(1 + \frac{4}{3\tau_0} + \frac{2}{3\tau_*^2} \right)^{-1}, \quad (107)$$

$$P_{\text{rad},0} = \frac{aT_0^4}{3} \frac{1 + \frac{4}{3\tau_0}}{1 + \frac{4}{3\tau_0} + \frac{2}{3\tau_*^2}}. \quad (108)$$

For $\tau_0 \gg \tau_* \gg 1$, we have (89) from (107). In the optically thin limit, $\tau_* \ll \tau_0 \ll 1$ we get

$$F_0 = acT_0^4\tau_{\alpha 0}, \quad P_{\text{rad},0} = \frac{2}{3}acT_0^4\tau_{\alpha 0}. \quad (109)$$

Using F_0 instead of Q_- and the equation of state $P = \rho\mathcal{R}T + P_{\text{rad},0}$, the equations for the accretion disk structure together with the equation

$$Q_+ = F_0, \quad (110)$$

with Q_+ from (88), have been solved numerically by Artemova et al. (1996). It is found that two solutions, optically thick and optically thin, exist separately when the luminosity is not very large. The two solutions intersect at $\dot{m} = \dot{m}_b$, where

$$\dot{m} = \frac{\dot{M}c^2}{L_{\text{Edd}}}, \quad L_{\text{Edd}} = \frac{4\pi cGM}{\kappa_e}, \quad (111)$$

and there is no global solution for the accretion disk for $\dot{m} > \dot{m}_b$ (see Fig. 2). It was concluded by Artemova et al. (1996), that in order to obtain a global, physically meaningful solution for $\dot{m} > \dot{m}_b$, account for the advective term in (110) is needed.

2.7. Accretion disks with advection

The standard accretion disk model gives somewhat nonphysical behavior near the inner edge of the accretion disk around a black hole. For high mass accretion rates, when the central region is radiation-dominated ($P \approx P_r$, $\kappa \approx \kappa_e$), the radial dependences are:

$$\begin{aligned} \rho &\sim r^{3/2} \mathcal{J}^{-2} \rightarrow \infty, & T &\sim r^{-3/8}, \\ h &\sim \mathcal{J} \rightarrow 0, & \Sigma &\sim r^{3/2} \mathcal{J}^{-1} \rightarrow \infty, \\ v_r &\sim r^{-5/2} \mathcal{J} \rightarrow 0 \end{aligned} \quad (112)$$

(Shakura and Sunyaev, 1973; Bisnovaty-Kogan, 1999a). The limits relate to the inner edge of the disk with $r = r_{\text{in}}$,

$$\mathcal{J} = 1 - \frac{j_{\text{in}}}{j} = 1 - \sqrt{\frac{r_{\text{in}}}{r}}. \quad (113)$$

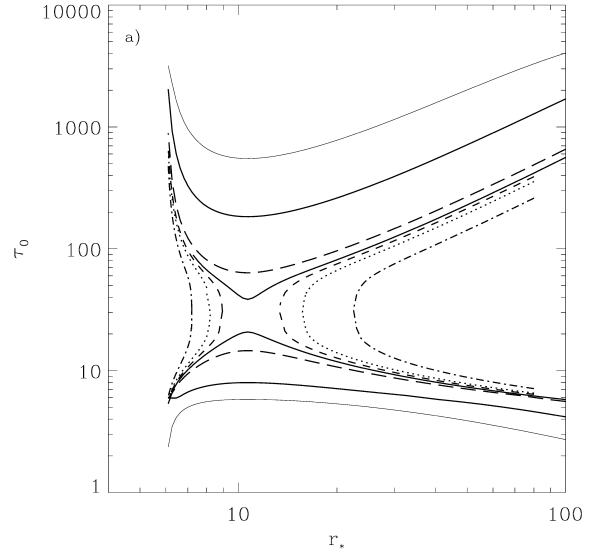


Fig. 2. The dependences of the optical depth τ_0 on radius, $r_* = r/r_g$, for the case $M_{\text{BH}} = 10^8 M_\odot$, $\alpha = 1.0$ and different values of \dot{m} . The thin solid, dot–triple dash, long dashed, heavy solid, short dashed, dotted and dot–dashed curves correspond to $\dot{m} = 1.0, 3.0, 8.0, 9.35, 10.0, 11.0,$ and 15.0 , respectively. The upper curves correspond to the optically thick family, while the lower curves correspond to the optically thin family.

At smaller \dot{M} , when near the inner edge $P \approx P_g$, $\kappa \approx \kappa_e$, there are different dependences,

$$\begin{aligned} \rho &\sim r^{-33/20} \mathcal{J}^{2/5} \rightarrow 0, & T &\sim r^{-9/10} \mathcal{J}^{2/5} \rightarrow 0, \\ h &\sim r^{21/20} \mathcal{J}^{1/5} \rightarrow 0, & \Sigma &\sim r^{-3/5} \mathcal{J}^{3/5} \rightarrow 0, \\ v_r &\sim r^{-2/5} \mathcal{J}^{-3/5} \rightarrow \infty. \end{aligned} \quad (114)$$

These dependences results from the local form of the equation of thermal balance (91). It is clear on physical grounds that when the local heat production due to viscosity goes to zero, the heat brought by radial motion of matter along the accretion disk becomes more important. In the presence of this advective heating (or cooling, depending on the radial entropy S gradient) we have

$$Q_{\text{adv}} = -\frac{\dot{M}}{2\pi r} T \frac{dS}{dr}. \quad (115)$$

The equation of a heat balance is modified to

$$Q_+ - Q_{\text{adv}} = Q_-. \quad (116)$$

In order to self-consistently describe the structure of the accretion disk, we also need an improved de-

scription of the radial force equilibrium of the disk. Including the pressure gradient and inertia terms we have

$$r(\Omega^2 - \Omega_K^2) = \frac{1}{\rho} \frac{dP}{dr} - v_r \frac{dv_r}{dr}. \quad (117)$$

Inclusion of the inertia term leads to transonic radial flow with a singular point. Conditions for the continuous passage of the solution through the critical point leads to a unique value of the integration constant j_{in} .

Paczyński and Bisnovaty-Kogan (1981) obtained simplified solutions for accretion disks including the advective terms in the vertically averaged disk equations. This approach with some modifications has been used by many researchers to study transonic accretion flows around black holes (Muchotrzeb and Paczyński, 1982; Matsumoto et al., 1984; Abramowicz et al., 1988; Beloborodov, 1998). The importance of the transonic nature of the flows on the disk structure has been emphasized by Hōshi and Shibazaki (1977); Liang and Thompson (1980) and Abramowicz and Zurek (1981), and later studied in more detail by Abramowicz and Kato (1989); see also Kato et al. (1998).

The problems of finding numerical solution of advective disk structure are connected with the possible non-uniqueness of global solutions for $\alpha > 0.01$, and the non-standard behavior at the singular point. Matsumoto et al. (1984) and Abramowicz et al. (1988) reported that in the case of viscosity prescription (68) the singular point changes its type from a saddle to a node as α increases. The presence of a nodal-type singular point leads to the possibility of multiple solutions as the authors have claimed.

Artemova et al. (2001) showed that the mentioned problems have been created by several inconsistencies in the preceding studies. Some problems are connected with an inaccurate averaging of the equations over the disk thickness, and another one appears due to the incomplete investigation of the singular points (Abramowicz et al., 1988). It was found that in the case of the viscosity prescription (73), a set of equations describing the vertically averaged advective accretion disks has *two* singular points, independent of α and of \dot{M} . Calculations of the advective disk structure was performed in the Paczyński–Wiita potential (Paczyński and Wiita, 1980)

$$\Phi(r) = - \frac{GM}{r - 2r_g}, \quad (118)$$

where M is the black hole mass and $2r_g = 2GM/c^2$ is the gravitational radius. The disk self-gravity is neglected. Note, that the multiplicity of singular points in solutions for accretion flows in the Paczyński–Wiita potential (118) was found by Fukue (1987), Chakrabarti and Molteni (1993), and Chakrabarti (1996) in a somewhat different context. Another type of accretion flow with multiple singular points was found by Dullemond and Turolla (1998); and Turolla and Dullemond (2000), who considered accretion disks having a phase transition. It was shown by Artemova et al. (2001), that for $\alpha < 0.01$, the inner and outer (with respect to the black hole location) singular points are of a saddle point type, and only one integral curve (“separatrix”) which crosses the inner point simultaneously crosses the outer one. This separatrix corresponds to the unique global solution which is determined by the two parameters, α and $\dot{m} = \dot{M}c^2/L_{\text{Edd}}$, for the given black hole mass. At larger $\alpha > 0.1$, the inner singular point changes its type to a node, while the outer point remains of a saddle point. There is still one integral curve which goes continuously through both the singular points providing a unique global solution.

In the case of the viscosity prescription in the first relation of (74)

$$t_{r\phi} = \eta r \frac{d\Omega}{dr} = \rho \nu r \frac{d\Omega}{dr}, \quad (119)$$

it was found that there is only one singular point which is always a saddle point. Only one physical solution passes through this point. Solutions which correspond to both forms of viscosity (73) and (119) are very close quantitatively in the low α limit, $\alpha < 0.1$.

Artemova et al. (2001) developed a numerical method to solve the set of equations describing vertically averaged advective accretion disks. The method is based on standard relaxation technique and explicitly uses conditions at the inner singular point and its vicinity. These conditions were obtained by expanding the solution in a power series around the singular point. Such a modification of the method allowed the construction of solutions which smoothly pass the singular points and satisfy the regularity

conditions at these points with high numerical precision for a wide range of parameters α and \dot{m} .

The equations describing the radial disk structure are written for the midplane density ρ , pressure P , radial velocity v and angular velocity Ω . They consist of the mass conservation equation,

$$\dot{M} = 4\pi r h \rho v, \quad (120)$$

$\dot{M} > 0$, and h is the disk half-thickness, which is expressed in terms of the isothermal sound speed $c_s = \sqrt{P/\rho}$ of gas,

$$h = \frac{c_s}{\Omega_K}. \quad (121)$$

The equations of motion in the radial direction is given by (117). The equation of motion in the azimuthal direction is

$$\frac{\dot{M}}{4\pi} \frac{dj}{dr} + \frac{d}{dr}(r^2 h t_{r\phi}) = 0, \quad (122)$$

where Ω_K is the Keplerian angular velocity, $\Omega_K^2 = GM/[r(r-2r_g)^2]$, $j = \Omega r^2$ is the specific angular momentum and $t_{r\phi}$ is the (r, ϕ) -component of the viscous stress tensor. Other components of the stress tensor are assumed to be negligibly small. The vertically averaged energy conservation equation is written in (115), (116)¹, with the advective term in the form

$$Q_{\text{adv}} = -\frac{\dot{M}}{2\pi r} \left[\frac{dE}{dr} + P \frac{d}{dr} \left(\frac{1}{\rho} \right) \right], \quad (123)$$

and

$$Q_+ = h t_{r\phi} r \frac{d\Omega}{dr}, \quad Q_- = \frac{2aT^4 c}{3\kappa \rho h}, \quad (124)$$

are the viscous dissipation rate and the cooling rate per unit area, respectively; T is the midplane temperature. The equation of state for the accreting gas–radiation mixture is

$$c_s^2 = \mathcal{R}T + \frac{1}{3} \frac{aT^4}{\rho}, \quad (125)$$

where \mathcal{R} is the gas constant. The specific energy of the mixture is

$$E = \frac{3}{2} \mathcal{R}T + \frac{aT^4}{\rho}. \quad (126)$$

Both prescriptions of viscosity (73) and (119) have been used in calculations with ν in the form

$$\nu = \frac{2}{3} \alpha c_s h. \quad (127)$$

Note that in the limit $\Omega \rightarrow \Omega_K$ both prescriptions (73) and (119) coincide. Integration of Eq. (122) gives

$$r^2 h t_{r\phi} = -\frac{\dot{M}}{4\pi} (j - j_{\text{in}}), \quad (128)$$

where the integration constant j_{in} is the specific angular momentum of accreting matter near the black hole horizon. The value of j_{in} is chosen to obtain a global transonic solution with the subsonic part at large radii and the supersonic part in vicinity of the black hole horizon. In the case of viscosity prescription (73) the expression (128) results in an algebraic equation, and the radial structure of the accretion disks is described by two first-order differential equations (117) and (116). In a general formulation, these two equations require two parameters to be fixed as boundary conditions in order to determine the solution. In the case of viscosity prescription (119), expression (128) results in an additional first order differential equation, so that we need to fix three parameters as boundary conditions.

We show here two examples of numerical results obtained by Artemova et al. (2001). Each calculated model is characterized by the unique value of j_{in} . Figs. 3 and 4 show the dependences of j_{in} on the accretion rate $\dot{m} = \dot{M} c^2 / L_{\text{Edd}}$ for three values of $\alpha = 0.01, 0.1$ and 0.5 in the case of viscosity prescription (73) and (119) respectively. At low $\dot{m} < 1$ the value of j_{in} is independent of \dot{m} and weakly varies with α . In the low α case, $\alpha = 0.01$ and 0.1 , the values of j_{in} are close to the minimum value of the Keplerian angular momentum, $(j_K)_{\text{min}} = 3.6742$. At high $\dot{m} > 0.1$ the values of j_{in} deviate from $(j_K)_{\text{min}}$ to larger or smaller values depending on α . In the case of $\alpha = 0.01$ and 0.1 one can see only minor differences

¹The vertical averaging in Eq. (116) have been made differently by different authors (compare e.g. Shakura and Sunyaev, 1973; and Abramowicz et al., 1988). Our choice of the coefficients in (123), (124), may be not the optimal one. A posteriori analysis had shown that using the factor 4 instead of 2 in the denominator of (123) would be more consistent choice, but this change has little influence on our numerical results.

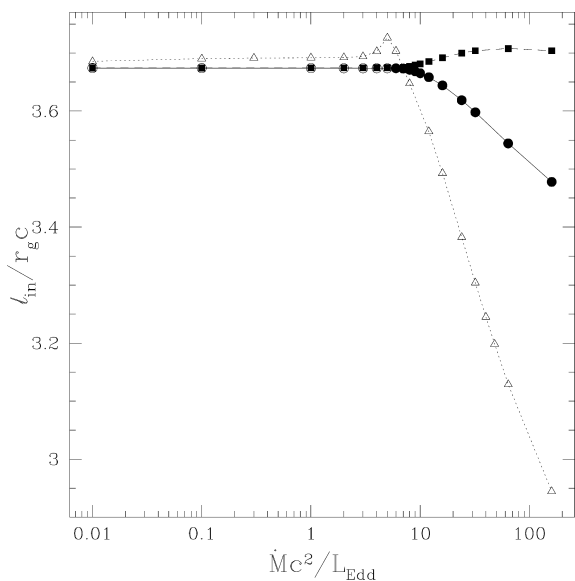


Fig. 3. Specific angular momentum $j_{\text{in}} \equiv \ell_{\text{in}}$ as a function of the mass accretion rate \dot{M} for different viscosity parameters $\alpha = 0.01$ (squares), 0.1 (circles) and 0.5 (triangles), corresponding to viscosity prescription (73). The solid dots represent models with a saddle-type inner singular points, whereas the empty dots correspond to a nodal-type point, from Artemova et al. (2001).

between models with different forms of viscosity. But, for large $\alpha = 0.5$ the difference in values of j_{in} increases.

Figs. 5 and 6 show locations of the inner singular points $(r_s)_{\text{in}}$ as a function of \dot{m} for different values of α and both viscosity prescriptions. Similar to the case of j_{in} discussed above the models at low \dot{m} show a weak dependence of $(r_s)_{\text{in}}$ on \dot{m} . In the low α models (squares and circles in Figs. 3–6) the values of $(r_s)_{\text{in}}$ are close to the location of the black hole last stable orbit at $r = 6r_g$. At high $\dot{m} > 0.1$ the values of $(r_s)_{\text{in}}$ are decreasing functions of \dot{m} in the case of low $\alpha = 0.01$ and 0.1, and non-monotonically behave in the case of $\alpha = 0.5$ (triangles in Figs. 3–6).

In the case of viscosity prescription (73), the solutions have the outer singular point in addition to the inner one. The change of value of $\beta = \mathcal{R}\mathcal{T}/c_s^2$ from 1 to 0 corresponds to a change of a state from gas pressure to radiative pressure dominated. The thin disks with $\beta \approx 1$ are locally stable, whereas parts of the disk in which $\beta \approx 0$ are thermally and viscously unstable (Pringle et al., 1973). For large

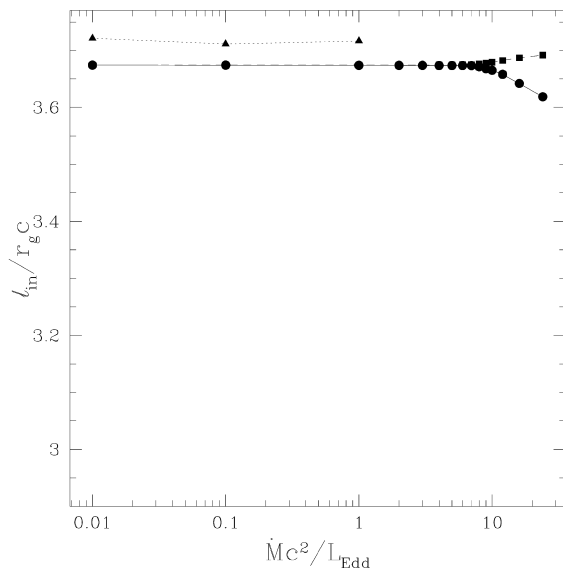


Fig. 4. Specific angular momentum $j_{\text{in}} \equiv \ell_{\text{in}}$ as a function of the mass accretion rate \dot{M} for different viscosity parameters $\alpha = 0.01$ (squares), 0.1 (circles) and 0.5 (triangles), corresponding to the viscosity prescription (119). The solid dots represent models with a saddle-type inner singular points, whereas the empty dots correspond to the nodal-type points, from Artemova et al. (2001).

$\dot{m} > 100$, the instability can be suppressed by advection (Abramowicz et al., 1988). It was shown by Artemova et al. (2001), that significant deviations of j_{in} and $(r_s)_{\text{in}}$ in Figs. 3–6 from a constant happens when β begins to deviate from unity. Analysis of the critical points shows that they are either saddle or nodal-type. In Figs. 3–6 the saddle-type points are indicated by the solid squares, circles and triangles. The nodal-type points are represented by the corresponding empty dots in the same figures. In the case of viscosity prescription (73) the inner singular points can be saddles or nodes depending on values of α and \dot{m} . Note that the change of critical point type from saddle to nodal one does not introduce new features in the solutions. The outer singular points are always saddle points. In the case of viscosity prescription (119), the solutions have only one (inner) singular point which is always of a saddle-type.

The models with $\dot{m} < 16$ and low $\alpha < 0.1$ have values of r_s and j_{in} which are very close to the location of the last stable orbit, $r_{\text{in}} = 6r_g$, and the value of $j_{\text{in}} = (j_{\text{K}})_{\text{min}}$ as assumed in the standard

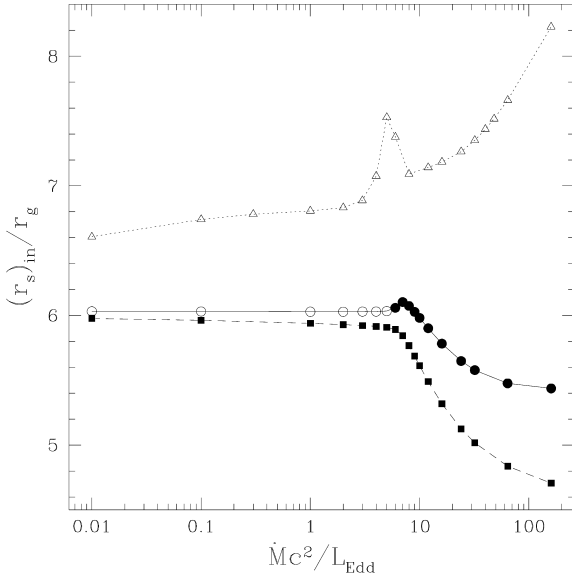


Fig. 5. Position of the inner singular points as a function of the mass accretion rate \dot{M} for different viscosity parameters $\alpha = 0.01$ (squares), 0.1 (circles) and 0.5 (triangles), corresponding to the viscosity prescription (73). The solid dots represent models with saddle-type inner singular points, whereas the empty dots correspond to the nodal-type point, from Artemova et al. (2001).

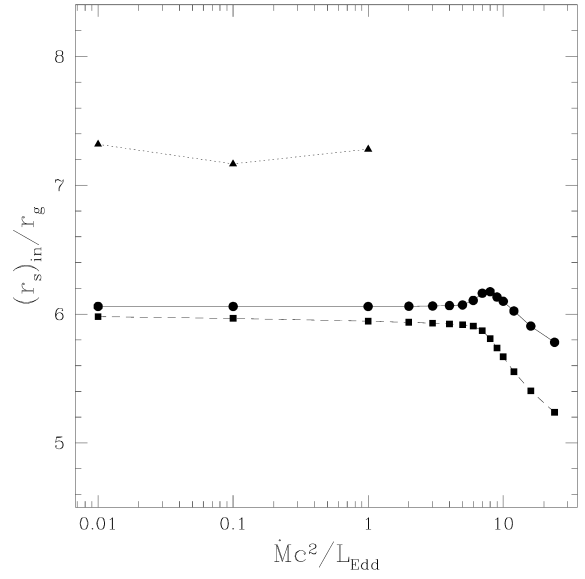


Fig. 6. Position of the inner singular points as a function of the mass accretion rate \dot{M} for different viscosity parameters $\alpha = 0.01$ (squares), 0.1 (circles) and 0.5 (triangles), corresponding to viscosity prescription (119). The solid dots represent models with saddle-type inner singular points, whereas the empty dots correspond to nodal-type points, from Artemova et al. (2001).

model (Shakura and Sunyaev, 1973). The radial structures of the models are also very close to the ones for the standard model in the same range of \dot{m} and α . Such a good coincidence means that the advective terms in Eqs. (116) and (117) are negligibly small in the considered models. However, the high α models show quite significant deviation from the standard model for all \dot{m} (see Figs. 3–6).

At high accretion rates, $\dot{m} > 16$, the effect of advection becomes significant, and at $\dot{m} = 100$ the advective part of the energy flux is ~ 2 times larger than the luminosity.

2.8. Convection in accretion disks

2.8.1. Vertical structure and convective instability in the radiation-dominated region of disks

Here, we consider in more detail the vertical structure of the accretion disk. Following Shakura (1972) and Shakura and Sunyaev (1973), we assume that the viscous heat production per unit mass in the disk is constant. This assumption was also made in Section 2.6. For variable vertical density the equation

of vertical heat flux is different from (96), and has a differential form with $F_0 \equiv Q_+$ from (88):

$$\frac{dF_{\text{rad}}}{dz} = 2F_0 \frac{\rho}{\Sigma_0} = \frac{3}{4\pi} \dot{M} \frac{GM}{r^3} \left(1 - \frac{j_{\text{in}}}{j}\right) \frac{\rho}{\Sigma_0}. \quad (129)$$

After integration this gives

$$F_{\text{rad}} = 2F_0 \frac{\Sigma}{\Sigma_0}. \quad (130)$$

Here, Σ is the mass in the layer $(0, z)$, so that $\Sigma(h) = \Sigma_0/2$, $d\Sigma = \rho dz$. The equation for vertical heat transport in the optically thick disk is

$$F_{\text{rad}} = -\frac{ac}{3\kappa\rho} \frac{dT^4}{dz} = -\frac{ac}{3\kappa} \frac{dT^4}{d\Sigma}. \quad (131)$$

We consider here only regions where electron scattering dominates so that $\kappa = \kappa_e$. Solving (131) together with (130) we obtain

$$T^4 = T_0^4 \left(1 - \frac{3\kappa F_0 \Sigma^2}{ac \Sigma_0 T_0^4}\right). \quad (132)$$

At the surface of the disk

$$\Sigma = \Sigma_0/2, \quad T = T_s, \quad F_0 = \frac{acT_s^4}{4}, \quad (133)$$

as in black-body radiation. Thus we obtain from (132)

$$T_0^4 = T_s^4 \left(1 + \frac{3\kappa\Sigma_0}{16} \right). \quad (134)$$

Assuming high optical depth $\Sigma_0\kappa \gg 1$, and using (134) in (132) we obtain the temperature distribution over the thickness of the disk in the form

$$T^4 = T_0^4 \left[1 - \left(\frac{2\Sigma}{\Sigma_0} \right)^2 \right]. \quad (135)$$

Note, that Eq. (89) follows from (134) at high optical depth, after using black-body connection between T_s and F_0 .

Consider now the z -dependence of the density the disk. In the radiation-dominated region where $P \approx P_r = aT^4/3$, we obtain from Eq. (69)

$$\frac{a}{3\rho} \frac{dT^4}{dz} = - \frac{GMz}{r^3}. \quad (136)$$

Using (130), (131), (136), we obtain

$$\Sigma = \frac{GMc\Sigma_0}{2r^3\kappa F_0} z. \quad (137)$$

After differentiating, we find that the density does not depend on the vertical coordinate z in a radiation-dominated disk.

$$\rho = \frac{GMc\Sigma_0}{2r^3\kappa F_0}. \quad (138)$$

Because the density is independent of z and the temperature decreases with z , the entropy,

$$S = \frac{4}{3} \frac{aT^3}{\rho}, \quad (139)$$

decreases with increasing z . The gravitational force g_z acts in the $-z$ direction. This corresponds to a convectively unstable situation as was first pointed out by Bisnovaty-Kogan and Blinnikov (1976, 1977).

For the outer regions of an accretion disk, where $P_g \gg P_r$ and $\kappa = \kappa_e$, there is no analytic solution for a vertical disk structure. We may however check the

convective stability in another way. In the gas-pressure dominated region the entropy

$$\begin{aligned} \frac{S}{\mathcal{R}} &= \log \left(\frac{T^{3/2}}{\rho} \right) + \text{const}, \quad \frac{dS}{\mathcal{R}} \\ &= \frac{3}{2} \frac{dT}{T} - \frac{d\rho}{\rho}. \end{aligned} \quad (140)$$

With $P = P_g = \mathcal{R}\rho T$ it follows from the vertical equilibrium equation (69) that

$$\frac{dT}{T} + \frac{d\rho}{\rho} = - \frac{GMz}{r^3 P} d\Sigma. \quad (141)$$

We obtain from (135)

$$\frac{dT}{T} = - \frac{1}{2} \frac{T_0^4 - T^4}{T^4} \frac{d\Sigma}{\Sigma}. \quad (142)$$

Using (141) and (142) in (140) we obtain

$$\begin{aligned} \frac{dS}{\mathcal{R}} &= - \frac{5}{2} \frac{dT}{T} + \frac{GMz}{r^3 P} d\Sigma \\ &= \left(\frac{GMz}{r^3 P} \Sigma - \frac{5}{4} \frac{T_0^4 - T^4}{T^4} \right) \frac{d\Sigma}{\Sigma}. \end{aligned} \quad (143)$$

It is easy to prove that entropy increases with z in the region near the equatorial plane $z \ll h$. Here we have $\Sigma \approx \rho_0 z \ll \Sigma_0$, and it follows from (135), (142), and (143) that

$$\frac{dS}{\mathcal{R}} \approx \left(\frac{GM\Sigma_0^2}{r^3 P_0 \rho_0} - 5 \right) \frac{\Sigma d\Sigma}{\Sigma_0^2}. \quad (144)$$

Calculating the last expression in brackets, using the solution of Shakura and Sunyaev (1973), we obtain

$$\frac{dS}{\mathcal{R}} = (8 - 5) \frac{\Sigma d\Sigma}{\Sigma_0^2} > 0,$$

which means stability against convection. Similarly, we can prove stability against convection in the region close to the disk surface, where $\Sigma = \Sigma_0/2$, $T = T_s$, $z = h$, $P = P_s$. From the theory of stellar atmospheres (see e.g. Bisnovaty-Kogan, 2001), we have the condition $P_s = 2g/(3\kappa)$ at the optical depth $\tau = 2/3$, where

$$g_z = - \frac{GMh}{r^3} \quad (145)$$

is the vertical gravitational acceleration at the disk

surface. Using these relations and (134) in (143) we get

$$\begin{aligned} \frac{dS}{\mathcal{R}} &\approx \left(\frac{GM\Sigma_0 h}{2r^3 P_s} - \frac{5}{4} \frac{T_0^4}{T_s^4} \right) \frac{d\Sigma}{\Sigma} \\ &= \left(\frac{GMh}{r^3 P_s \kappa} - \frac{15}{32} \right) \kappa d\Sigma = \left(\frac{3}{2} - \frac{15}{32} \right) \kappa d\Sigma \\ &> 0. \end{aligned}$$

Thus, the accretion disk in the standard model is convectively *unstable* in the radiation dominated region close to the black hole, whereas it is *stable* in the more distant gas pressure dominated regions. In the colder regions with incomplete ionization the behavior of the accretion disk becomes more complicated, with a non-unique solutions, and convective instability (Cannizzo et al., 1982).

2.8.2. Structure of convective accretion disk region

In the standard model with radiative heat conductivity in the vertical direction, the radiation-dominated region exists only when

$$\frac{L}{L_{\text{Edd}}} \geq \frac{1}{50} \left(\frac{\alpha M}{M_\odot} \right)^{-1/8} \quad (146)$$

(Shakura and Sunyaev, 1973). The appearance of convection changes the structure of the radiation-dominated region, and condition (146).

Let us estimate the part of the energy flux carried out by convection, using a mixing length model of the convection (Bisnovaty-Kogan and Blinnikov, 1976). The convective heat flow in the vertical direction is Q_{conv} (ergs/cm²/s), the convection velocity is v , and the excess of the temperature gradient above the adiabatic gradient is $\Delta\nabla T$. We take the mixing length l to be the half-thickness z_0 of the disk. The equations are

$$Q_{\text{conv}} = c_p \rho v (z_0/2) \Delta\nabla T, \quad (147)$$

where

$$\begin{aligned} c_p &= \mathcal{R} \left[\frac{5}{2} + 20 \frac{P_r}{P_g} + \left(\frac{4P_r}{P_g} \right)^2 \right], \\ v &= \left[\frac{Q_{\text{conv}} (1 + 4P_r/P_g)}{2\rho c_p T} \frac{GM}{r^3} \right]^{1/3} z_0^{2/3}, \end{aligned} \quad (148)$$

$$\Delta\nabla T = \left(\frac{4Q_{\text{conv}}}{\rho c_p} \right)^{2/3} \left[\frac{T}{(1 + 4P_r/P_g)GM} \right]^{1/3} r z_0^{-5/3}. \quad (149)$$

Hence we find that the excess $\Delta\nabla T$ in the temperature gradient is less than 20% of ∇T . The convection velocity is $v = 3 \times 10^8$ cm/s for $r = 10r_g$, which is close to the velocity v_s of the sound in this region. The heat flow is carried mainly by convection ($Q \approx Q_{\text{conv}}$), because of the high matter density, and the radiative flux is $\sim 20\%$ of the total flux. Convection acts to smooth out the entropy variation in the vertical direction, so that we may consider the entropy as a constant in the vertical direction with a precision $\sim 20\%$.

Bisnovaty-Kogan and Blinnikov (1977) obtained an analytic solution for the isentropic convective accretion disk in the radiation-dominated region. When $P_r \gg P_g$, the surface pressure at the photosphere with $\tau = 2/3$ is equal to

$$P_s = \frac{4g}{3\kappa} = \frac{4GMh}{3\kappa r^3}. \quad (150)$$

The effective temperature at the disk surface is connected with the surface radiative pressure in (150), and with the surface radiative flux in (88) as

$$\begin{aligned} \frac{aT_s^4}{3} = P_s &= \frac{4GMh}{3\kappa r^3}, \quad \frac{acT_s^4}{4} = Q_+ \\ &= \frac{3}{8\pi} \dot{M} \frac{GM}{r^3} \left(1 - \frac{j_{\text{in}}}{j} \right). \end{aligned} \quad (151)$$

The disk thickness is obtained from comparison of the two expressions in (151) as

$$h = \frac{3\kappa}{8\pi c} \dot{M} \left(1 - \frac{j_{\text{in}}}{j} \right). \quad (152)$$

In the radiative-dominated region the equation of state at constant entropy, using (139), is

$$P = \frac{aT^4}{3} = \left(\frac{3S^4}{256a} \right)^{1/3} \rho^{4/3} \equiv K_r \rho^{4/3}. \quad (153)$$

Integration of the equation of vertical equilibrium (69) gives

$$\rho^{1/3} = \rho_0^{1/3} - \frac{GMz^2}{8K_r r^3}. \quad (154)$$

Using the surface boundary condition

$$\rho_s \equiv \rho(h) = \left(\frac{P_s}{K_r}\right)^{3/4} = \left(\frac{4GMh}{3\kappa r^3 K_r}\right)^{3/4}$$

we determine the equatorial density ρ_0 from (154). Assuming $P_0 \gg P_s$ and $\rho_0 \gg \rho_s$, we obtain

$$\begin{aligned} \rho_0^{1/3} &= \frac{GMh^2}{8K_r r^3}, \quad P \\ &= K_r \left(\frac{GMh^2}{8K_r r^3}\right)^4 \left(1 - \frac{z^2}{h^2}\right)^4, \end{aligned} \quad (155)$$

or

$$\rho = \rho_0 \left(1 - \frac{z^2}{h^2}\right)^3, \quad P = P_0 \left(1 - \frac{z^2}{h^2}\right)^4.$$

The equatorial pressure is obtained from the angular momentum equation (71) and (152) as

$$P_0 = \frac{2c\Omega_K}{3\kappa\alpha}, \quad T_0^4 = \frac{2c\Omega_K}{a\kappa\alpha}, \quad (156)$$

and from the boundary condition (133) we obtain

$$P_s = \frac{4F_0}{3c}, \quad \frac{P_s}{P_0} = 2\alpha \frac{\Omega_K h}{c} \ll 1. \quad (157)$$

This equation justifies the previous assumption. We used here the relation following from (88) and (152)

$$F_0 = \frac{c\Omega_K}{\kappa} h. \quad (158)$$

Note, that we used here the exact angular momentum equation (71) in the plane of the disk, instead of the approximate equation obtained by averaging over the thickness, used by Bisnovatyi-Kogan and Blinnikov (1977). In this approach, Eqs. (156)–(158) are always valid in the radiation-dominated region, for either both radiative or convective conditions. The convection does not change the pressure and temperature distribution over the thickness of the disk or the disk thickness. It changes only the density distribution. In a radiative disk (135) (where ρ is independent of z), the distributions of temperature and pressure with z are the same as their distributions in a convective disk (155) (where ρ depends on z).

The density and surface density in the radiative disk are found from (133), (134), (156) and (158) as

$$\rho_0 = \frac{4c}{3\kappa\alpha} \frac{1}{\Omega_K h^2}, \quad \Sigma_0 = 2\rho_0 h = \frac{8c}{3\alpha} \frac{1}{\kappa\Omega_K h}. \quad (159)$$

In an isentropic convective disk, the density distribution is given in (155), the equatorial density ρ_0 , surface density Σ_0 , constant K and entropy S are found from (155) and (156) as

$$\begin{aligned} \rho_0 &= \frac{16c}{3\kappa\alpha} \frac{1}{\Omega_K h^2}, \quad \Sigma = \frac{32}{35} \rho_0 h = \frac{512c}{105\kappa\alpha} \frac{1}{\Omega_K h}, \\ K &= \left(\frac{3\alpha\kappa}{2c\Omega_K}\right)^{1/3} \frac{(\Omega_K h)^{8/3}}{16}, \\ S &= \left(\frac{a\alpha\kappa}{2c\Omega_K}\right)^{1/4} \frac{\Omega_K^2 h^2}{2}. \end{aligned} \quad (160)$$

It follows from (159) and (160) that in the equatorial plane the density of the convective disk is 4 times larger, than in the radiative disk, while the ratio of surface densities is 64/35. The increase of the density of the convective disk at the same temperature narrows the radiative-dominated region, which may exist now at luminosities ~ 2 times larger than in the radiative case (146).

2.8.3. Numerical simulations of convection in accretion disks

Two-dimensional numerical simulations have confirmed in general the conclusion about the isentropic vertical structure of the disk in convectively unstable regions. Fujita and Okuda (1998) found that the excess ΔT in the temperature gradient is less than $\sim 1\%$. This is even closer to the adiabatic structure than followed from estimations of Bisnovatyi-Kogan and Blinnikov (1976). It probably results from the fact that in the computations convective cells generally stretch from the disk mid-plane to the disk surface, increasing the efficiency of the convective mixing in the vertical direction, relative to the model of isotropic convection used in estimations. 2-D calculations by Agol et al. (2000) also show a satisfactory correspondence with the analytical solution of the isentropic convective disk structure of Bisnovatyi-Kogan and Blinnikov (1977).

2-D numerical simulations of accretion of highly viscous nonradiating gas have been done by Igumenshchev (2000) and Igumenshchev and Abramowicz (1999, 2000). An ideal gas with adiabatic

index γ was considered. Thus the pressure was connected with the density and specific internal energy ε as

$$P = (\gamma - 1)\rho\varepsilon. \quad (161)$$

Calculations were done for a range of viscous parameters, $\alpha = 0.01 - 1$, and for $\gamma = 4/3, 3/2$, and $5/3$. Convective instability or large scale circulation occurred at smaller α and γ . For $\gamma = 4/3$ all models with $\alpha \leq 0.3$ are unstable; for $\gamma = 3/2$ and $5/3$ instability takes place at $\alpha \leq 0.1$, and $\alpha \leq 0.03$ respectively. The calculations have been performed also with account of a turbulent heat conductivity, characterized by dimensionless Prandtl number

$$Pr = \frac{\nu}{\chi}, \quad (162)$$

where $\chi = \lambda/\rho$ is the thermometric conductivity or thermal diffusivity (cm^2/s), and ν is the kinematic turbulent viscosity given by (127). Stabilization of the flow had been obtained at $Pr = 1$ for all γ with $\alpha \geq 0.1$, and for $\alpha = 0.03$ at $\gamma = 5/3$.

The high-viscosity models at $\alpha = 1$ form powerful bipolar outflows. The pure inflow and large-scale circulation patterns occur in the moderate viscosity models $\alpha = 0.1-0.3$. All models with bipolar outflows and pure inflows are steady. The models with large scale circulation could be either steady or unsteady, depending on values of α and γ . All convective models are unsteady. The self-similar solution for accretion flows with bipolar outflows (advection-dominated inflows–outflows ADIOs) proposed by Blandford and Begelman (1999) have not been confirmed in the numerical simulations of Igumenshchev and Abramowicz (2000).

Three-dimensional numerical simulations of viscous non-radiating accretion flows made by Igumenshchev et al. (2000) have confirmed qualitatively and quantitatively those obtained in 2-D simulations. It was shown that convective eddies are nearly axisymmetric and transport angular momentum inward, tending to smooth out the angular momentum distribution. This is in contrast with a small scale turbulence, which acts as a viscosity, transporting angular momentum outward, and tending to smooth out the angular velocity distribution.

2.8.4. Hot corona and variability of Cyg X-1

In a convective disk the flow of acoustic energy

Q_{ac} in the vertical direction is given by Biermann and Lust (1960) as

$$Q_{ac} \approx \rho v^3 (v/v_s)^5 \approx 10^{21-22} \text{ erg}/(\text{cm}^2 \text{ s}), \quad (163)$$

where the numerical value is for a Mach number $v/v_s = 1$. Q_{ac} is of order of the total energy flux for characteristic parameters of Cyg X-1 (Bisnovatyi-Kogan and Blinnikov, 1976).

Acoustic waves generated in the convection zone escape into the optically thin layers, induce variable soft X-rays in the photosphere, and also give variable heating of the corona. Comptonization of the photospheric radiation by hot electrons under conditions where both temperature and density are variable should lead to flux variations in the hard range, $h\nu \geq 5$ keV. This X-ray fluctuation mechanism, involving the emergence of waves into transparent layers, evidently is of the same wave nature as the variability of the ultraviolet excess in stars experiencing intensive convection, such as T Tauri and UV Ceti.

The waves escaping into the transparent layers and producing variable radiation in the photosphere and corona occupy a rather narrow frequency band. Physically, the reason for this circumstance is the following. A medium with a high radiation pressure and a non-uniform distribution of plasma along the z -direction serve as efficient filters, picking out a characteristic frequency range from the broader spectrum generated by convection and turbulence. Waves of low frequencies with wavelengths exceeding the scale height of the atmosphere cannot escape but instead induce oscillations of the coronal atmosphere as a whole. On the other hand, under conditions where radiation pressure predominates, high-frequency waves experience a severe damping because of radiative friction, and their role in heating the corona will be insignificant.

The propagation of acoustic waves through a medium with strong radiation pressure, followed by their escape into the atmosphere was investigated in detail by Bisnovatyi-Kogan and Blinnikov (1978a,b, 1979), and by Agol and Krolik (1998) for MHD waves. Waves emerging into the transparent layers will have a phase and group velocity equal to the velocity of sound in gas, $v_g = (\gamma P_g/\rho)^{1/2} = (\gamma \mathcal{R}T)^{1/2}$, where $\gamma = 5/3$ or $\gamma = 1$ depending on whether scattering or absorption predominates, \mathcal{R} is the gas constant, and the temperature T of the

equilibrium atmosphere is approximately equal to the temperature T_s of the photosphere. The characteristic angular frequency ω_c of waves emerging into the atmosphere is given by the expression

$$\omega_c = \left(\frac{\gamma}{\mathcal{R}T} \right)^{1/2} g \left(1 - \frac{F}{F_c} \right) s^{-1}. \quad (164)$$

For the accretion disk model, the gravitational acceleration g at radius r is given by (145), and the characteristic thickness h is given by (152). The quantity $F/F_c = \kappa F/gc$ represents the ratio of the radiation pressure force to the gravity; κ is the opacity, including both absorption and scattering. In a spherically symmetric star of luminosity L and radius R we have $g = GM/R^2$, $F = L/(4\pi R^2)$, and $F/F_c = L/L_c$, where $L_c = 4\pi cGM/\kappa$ is the Eddington limiting luminosity.

Characteristic frequencies ω_c from (164) of fluctuations of Cyg X-1 in the convective accretion-disk model of Bisnovaty-Kogan and Blinnikov (1977) are in the range 5–40 ms for a black hole mass $M = 10 M_\odot$ and luminosity between $0.1L_c$ and $0.3L_c$ corresponding to the photospheric temperature T_s . For a corona with $T_{\text{cor}} \approx 10^2 T_s$, waves whose frequency is $\omega = \omega_c$ or even a little lower will be able to escape. This frequency range is in a good accord with the observed time-scales of variability (Boldt, 1977).

Due to strong radiative damping of the sound waves, only a small part of the acoustic energy flux, of order

$$Q_{\text{cor}} \sim (P_g/P_r) Q_{\text{ac}}, \quad (165)$$

is expended in heating the outer layers with an optical depth $\tau < 1$. Another mechanism is acting to heat these layers (Bisnovaty-Kogan and Blinnikov, 1977). A particle in a region near the surface of the disk that is transparent to radiation will be subject to the influence of radiation from the entire disk, and not just the local radiation pressure gradient. The radiation pressure force will accelerate particles in the transparent region above the disk. Calculations of the equations of motion for particles subject to radiative, centrifugal, and gravitational forces show that in the region with $\tau < 1$ the particles (protons and electrons) will acquire vertical velocities corre-

sponding to the temperatures $(1-8) \cdot 10^8$ K of protons for $L \approx 0.1L_c$. Turbulent relaxation of the particle motions in the corona will tend to equalize the mean energies of the ions and electrons and to form a quasi-Maxwellian particle velocity distribution. Thus the combined action of the two heating mechanisms we have described will produce around the accretion disk a hot corona with $T_e \approx 10^9$ K for $L \approx 0.1L_c$. The existence of an analogous corona was postulated phenomenologically by Price and Liang (1977).

Let us estimate the density ρ_{cor} of the corona and the amount of material it contains. Since the gas pressure varies continuously with transition from the photosphere to the corona, we readily find that at the base of the corona

$$\rho_{\text{cor}} \approx \rho_s T_s / T_{\text{cor}} \approx 10^{-2} \rho_s \approx 10^{-5} \text{ g/cm}^3, \quad (166)$$

where ρ_s and T_s are the density and temperature in the photosphere of the disk for the parameters of the source Cyg X-1 in the region of maximum energy release. The surface density of the corona is determined by the condition $\tau_{e_s} \approx 1$ and is $\approx 2 \text{ g/cm}^2$, which is more than an order of magnitude lower than the density of the opaque disk.

The existence of a hot corona can easily explain the peculiarities of the Cyg X-1 spectrum during its variations (Bisnovaty-Kogan and Blinnikov, 1976). The soft X-rays at $h\nu \leq 7$ keV, which comprise $\approx 70\%$ of the total flux, are formed in the photosphere of the opaque disk. Some of the radiation ($\approx 10\%$) passing through the hot corona, experience Comptonization and transforms into hard radiation up to $h\nu \approx 3kT_e \approx 200$ keV, which amounts to $\approx 30\%$ of the total flux. In Cyg X-1 the total luminosity varies around $L = 0.1L_c$.

The changes in the spectrum as the luminosity of Cyg X-1 varies (Holt et al., 1975) exhibit the following characteristic behavior. As the total energy flux rises, the radiation in the soft part of the spectrum ($h\nu \leq 7$ keV) increases, but in the hard range ($h\nu \geq 10$ keV) it remains almost constant, or perhaps may even decrease slightly. We shall assume that the variations in the luminosity are associated with variations in the mass accretion rate. As the mass accretion rate \dot{M} rises in the region with $P_r \gg P_g$ the fraction of the acoustic flow (165) used for heating of the corona decreases:

$$Q_{\text{cor}} = (P_g/P_r)Q_{\text{ac}} \sim \dot{M}^{-1}. \quad (167)$$

For $L \approx 0.1L_c$, when acoustic heating predominates, the rise in \dot{M} may cause some decrease in the heating of the corona and in the amount of hard radiation. At the same time the flux in the soft range is determined by the radiation of the disk photosphere and increases $\sim \dot{M}$. In strong bursts of luminosity, when L reaches about $0.3L_c$, the heating begins to be governed by radiation-pressure forces, so the temperature of the corona and thereby also the power of the hard radiation should increase along with the rise of \dot{M} and total energy flux. Similar explanation of spectral transitions in Cyg X-1 was considered by Poutanen et al. (1997).

Even if a corona with $T \approx 10^9$ K is present in the disk accretion model, radiation at $E_\gamma \geq 200$ keV cannot be produced, and more energetic electrons are needed. Radiation with energies E_γ up to 5 MeV was observed by CRGO from Cyg X-1 (McConnell et al., 2000). It was noted by Bisnovatyi-Kogan and Blinnikov (1976), that the hard X-ray and gamma radiation from Cyg X-1 points to the presence of a magnetic field in the accretion disk. Two processes for generating highly energetic electrons were considered. Both required the presence of a magnetic field in the disk. A magnetic field could exist in the disk either through twisting of the lines of force by differential rotation (Shakura and Sunyaev, 1973), or through infall onto the black hole of magnetized material having relatively small angular momentum (Bisnovatyi-Kogan and Ruzmaikin, 1976). In the latter case a poloidal magnetic field is generated. Eruption of small scale magnetic loops from the accretion disk owing to the Parker (1955) instability and analogous to the formation of magnetic loops in the corona of the Sun was discussed by Galeev et al. (1979).

In the binary system containing the source Cyg X-1, some of the material flowing from the giant star is dispersed in space near the system. The attraction of the black hole will not only produce an accretion disk, but also a small proportion of material having a low angular momentum will fall into the black hole and be decelerated in the disk. If this deceleration takes place at radii of $(10-30)r_g$ and if a thin collisionless shock wave is formed (as is very likely in the presence of an azimuthal magnetic field) wherein the kinetic energy is transformed into ther-

mal energy and $T_e \approx T_i$, then hot electrons with $T = 10^{10}-10^{12}$ K will appear. The inverse Compton mechanism of interaction of the disk radiation with these electrons can lead to the generation of hard radiation with $h\nu \approx 200-2000$ keV or even higher energies.

Another mechanism for producing fast particles is analogous to the pulsar process. If magnetized matter with low angular momentum falls into the black hole (in addition to the disk accretion), a strong poloidal magnetic field will arise (Bisnovatyi-Kogan and Ruzmaikin, 1976). By analogy with radio pulsars (Goldreich and Julian, 1969), the rotation gives rise to an electric field of strength $E \approx -(v/c)B$ in a non-rotating inertial frame. Electrons can be accelerated in this electric field to energies $\varepsilon \approx R(v/c)eB \approx 3 \cdot 10^4 [B/(10^7 \text{ G})] \text{ MeV}$ where $v/c \approx 0.1$ and $R \approx 10^7$ cm is the characteristic scale. In a field $B \approx 10^7$ G, such electrons will generate synchrotron radiation with energies up to $\approx 10^5$ keV. As for pulsars, electron-positron pairs may be formed and contribute to the synchrotron radiation.

3. Boundary layers between disks and rotating stars

3.1. Boundary layers

3.1.1. Structure of the boundary layer between a disk and star: fitting the disk solution

Inside the boundary layer (BL) between a disk and a rotating star the physical variables change considerably over the small thickness of the layer $H_b \ll r_{\text{in}}$. Matter has no space in which to accelerate in the radial direction so that the radial velocity term in (30) is negligible. However, the pressure term is comparable to the gravitational and centrifugal forces (Regev, 1983; Papaloizou and Stanley, 1986; Regev and Hougerat, 1988). The thickness H_b of the BL is smaller than its vertical size z_0 , which also remains small. The appropriate inequalities for the boundary layer parameters are

$$H_b \ll z_0 \ll r_*, \quad (168)$$

as will be confirmed by the following analysis. The radius of the star r_* differs from the radius, at which $\partial\Omega/\partial r = 0$, by the very small value H_b . In the

asymptotic analysis of the BL, we use r_* as an inner boundary for the disk solution

$$r_{in} = r_* . \tag{169}$$

The variable x

$$r = r_* + \delta x, \quad \delta \equiv \frac{H_b}{r_*} \ll 1 , \tag{170}$$

is used inside BL instead of r . The “inner” solution within the BL is sought in the region $0 < x < \infty$, while the “outer” solution (55)–(60) is valid for $r_* < r < \infty$. According to the method of matched asymptotic expansion (MAE) (see Nayfeh, 1973) the inner and outer solutions are fitted so that the values for the outer solution at $r = r_*$ are equal to the corresponding values of the inner solution at $x = \infty$. This condition is valid asymptotically at $\delta \rightarrow 0$.

Consider a stationary accretion disk BL where Eqs. (30), (52), and (53) are valid with the integration constant ξ_b for ξ in (55). The thickness of the disk remains small in the boundary layer so that relations (41)–(47) for the polytropic case and (48)–(51) for the isothermal case are valid. Accounting only for the main terms in the asymptotic expansion inside BL, we get the equations from (30) and (53) (Regev, 1983)

$$\frac{dP_0}{dx} = -\Omega_{K*}^2 H_b \rho_0 (1 - \omega^2) , \tag{171}$$

$$\frac{d\omega}{dx} = -\frac{\dot{M}H_b}{2\pi\Sigma\nu_b r_*^2} (\xi_b - \omega) , \tag{172}$$

where

$$\omega = \frac{\Omega}{\Omega_{K*}} , \quad \Omega_{K*}^2 = \frac{GM}{r_*^3} . \tag{173}$$

Eq. (171) was obtained from the exact equation of radial equilibrium (30), instead of the approximate equation averaged over the disk thickness used originally by Regev (1983). In the MAE approximation these two equations are identical (Shorokhov, 2000). In the case of an advective disk the difference is essential, and the exact equation (30) should be used. The viscosity η is expressed in the BL through the coefficient of kinematical viscosity ν_b

$$\eta = \rho_0 \nu_b . \tag{174}$$

While the radial extent of the BL, H_b , is much less

then its vertical size z_0 the formula (29) cannot be used for a viscosity coefficient approximation. Inside BL we thus use the α approximation in the form

$$\nu_b = \alpha_b u_{s0} H_b . \tag{175}$$

3.1.2. Polytropic case

This case was investigated by Bisnovatyi-Kogan (1994). It is convenient to use the variables (Σ, ω) in Eqs. (171) and (172). We get from (45)–(46)

$$\rho_0 = d_{\rho 0} \Sigma^{\frac{2n}{2n+1}} , \quad P_0 = d_{P 0} \Sigma^{\frac{2(n+1)}{2n+1}} , \tag{176}$$

$$u_{s0} = d_{s0} \Sigma^{\frac{1}{2n+1}} , \tag{177}$$

$$d_{\rho 0} = \left[\frac{1}{\sqrt{2\pi}} \frac{\Gamma\left(n + \frac{3}{2}\right)}{\Gamma(n+1)} \right]^{\frac{2n}{2n+1}} \left[\frac{GM}{r_*^3 K(n+1)} \right]^{\frac{n}{2n+1}} ,$$

$$d_{P 0} = K d_{\rho 0}^{\frac{n+1}{n}} , \tag{178}$$

$$d_{s0} = \left[\frac{n+1}{n} K \right]^{1/2} d_{\rho 0}^{1/2n}$$

$$= \left(\frac{n+1}{n} K \right)^{1/2} \left[\frac{1}{\sqrt{2\pi}} \frac{\Gamma\left(n + \frac{3}{2}\right)}{\Gamma(n+1)} \right]^{\frac{1}{2n+1}}$$

$$\times \left[\frac{GM}{r_*^3 K(n+1)} \right]^{\frac{1}{2(2n+1)}} . \tag{179}$$

Note that the dimensions of d_{s0} are

$$[d_{s0}] = [v][\rho r]^{-\frac{1}{2n+1}} . \tag{180}$$

For the matching conditions of MAE we need to get the Keplerian angular velocity $\Omega = \Omega_{K*}$, $\omega = 1$ from the inner solution at $x \rightarrow \infty$ in order to fit the outer solution (54) at the inner boundary $r = r_*$. This implies $\xi_b = 1$ for the constant in (172). We get after transition to the variable Σ in (171) and (172)

$$\frac{d\Sigma}{dx} = -\frac{d_{\rho 0}}{d_{P 0}} \frac{2n+1}{2(n+1)} \Omega_{K*}^2 H_b (1 - \omega^2) \Sigma^{\frac{2n-1}{2n+1}} , \tag{181}$$

$$\frac{d\omega}{dx} = -\frac{\dot{M}}{2\pi\alpha_b r_*^2 d_{s0}} (1 - \omega) \Sigma^{-2\frac{n+1}{2n+1}} . \tag{182}$$

Dividing (181) by (182) we get

$$D_b \frac{d\Sigma}{d\omega} = -(1 + \omega) \Sigma^{\frac{4n+1}{2n+1}} , \tag{183}$$

with

$$D_b = -\frac{2(n+1)}{2n+1} \frac{d_{p0}}{d_{\rho0} d_{s0}} \frac{\dot{M}}{2\pi\alpha_b H_b} \frac{1}{r_*^2 \Omega_{K*}^2}. \quad (184)$$

The solution of (183) must fit the boundary condition on the stellar surface $\Sigma = \Sigma_*$ at $\omega = \omega_*$. Taking into account that the surface density grows rapidly inward towards the star, we may put with sufficient accuracy $\Sigma_* = \infty$ and obtain the solution, using (179), (178), and (184) in the form

$$\Sigma = d_\Sigma \frac{\sqrt{K\Omega_{K*}^{\frac{1}{n}}}}{(\Omega_{K*} r_*)^{\frac{2n+1}{n}}} \left(-\frac{\dot{M}}{\alpha_b H_b} \right)^{\frac{2n+1}{2n}} \times \left[(\omega - \omega_*) \left(1 + \frac{\omega + \omega_*}{2} \right) \right]^{-\frac{2n+1}{2n}}, \quad (185)$$

where

$$d_\Sigma = \sqrt{n+1} n^{-\frac{2n+1}{4n}} (2\pi)^{-\frac{4n+3}{4n}} \left[\frac{\Gamma\left(n + \frac{3}{2}\right)}{\Gamma(n+1)} \right]^{\frac{1}{2n}}. \quad (186)$$

For fitting the inner BL solution and the outer solution for the accretion disk we must make the surface densities (185) at $\omega = 1$ and (58) at $r = r_{in}$ equal. This fitting uniquely determines the outer integration constant ξ . After some algebraic calculations with account of (62) and (186) we get

$$1 - \xi = d_n \alpha_b^{-\frac{2n+3}{2n}} \left(\frac{r_*}{H_b} \right)^{\frac{2n+3}{2n}} \times \left[-\frac{\dot{M}K^n}{r_*^2 (\Omega_{K*} r_*)^{2n+1}} \right]^{\frac{3}{2n}} \times [(1 - \omega_*)(3 + \omega_*)]^{-\frac{2n+3}{2n}}, \quad (187)$$

where

$$d_n = 2^{\frac{4n+3}{2n}} \sqrt{\pi} (2\pi)^{-\frac{2n+9}{4n}} n^{-\frac{4n+3}{4n}} \times (n+1)^{3/2} \left[\frac{\Gamma\left(n + \frac{3}{2}\right)}{\Gamma(n+1)} \right]^{3/2n}. \quad (188)$$

The value of H_b is still not determined. It must be found from Eq. (182), where Σ is substituted from the solution (185). Before doing this we estimate the

order of magnitudes of the values of u_{s0}/u_K from (43) and u_r/u_K from (53),

$$u_K = \Omega_K r, \quad \frac{u_{s0}}{u_K} \sim \frac{z_0}{r},$$

$$\frac{u_r}{u_K} \sim \alpha \left(\frac{z_0}{r} \right)^2 \left(1 - \xi \sqrt{\frac{r_{in}}{r}} \right)^{-1}. \quad (189)$$

Eq. (182) contains a nonphysical logarithmic divergence owing to the MAE method. For an estimation of the value of H_b , we use the characteristic distance of the ω variation. Using the definition (170) for this, the following relation may be written

$$-\frac{2\pi\alpha_b r_* d_{s0}}{\dot{M}} \Sigma^{2\frac{n+1}{2n+1}} \Big|_{\omega=1} = 1. \quad (190)$$

With the help of (179), (185), and (186), we obtain from (190),

$$\frac{H_b}{r_*} \approx d_H \alpha_b^{-1/n+1} \left[-\frac{\dot{M}K^n}{r_*^2 (\Omega_{K*} r_*)^{2n+1}} \right]^{1/n+1} \times [(1 - \omega_*)(3 + \omega_*)]^{-1}, \quad (191)$$

$$d_H = 2(2\pi)^{-\frac{3}{2(n+1)}} n^{-\frac{2n+1}{2(n+1)}} \times (n+1)^{\frac{n}{n+1}} \left[\frac{\Gamma\left(n + \frac{3}{2}\right)}{\Gamma(n+1)} \right]^{\frac{1}{n+1}}. \quad (192)$$

Using (191) and (192) in (187), we finally get the expression for $(1 - \xi)$,

$$1 - \xi \approx d_\xi \alpha_b^{-\frac{2n+3}{2(n+1)}} \left[-\frac{\dot{M}K^n}{r_*^2 (\Omega_{K*} r_*)^{2n+1}} \right]^{\frac{1}{2(n+1)}}, \quad (193)$$

$$d_\xi = d_n d_H^{-\frac{2n+3}{2n}} = 2\sqrt{\pi} (2\pi)^{-\frac{2n+5}{4(n+1)}} n^{\frac{1}{4(n+1)}} (n+1)^{\frac{n}{2(n+1)}} \times \left[\Gamma\left(n + \frac{3}{2}\right) \Gamma(n+1) \right]^{\frac{1}{2(n+1)}}. \quad (194)$$

Estimating the order of magnitude of the values, with account of (189) and combining (191) and (193), we get

$$(1 - \xi) \sim \frac{\alpha}{\alpha_b} \frac{z_0}{r}, \quad (195)$$

$$\frac{H_b}{r_*} \sim \frac{1}{1 - \omega_*} \left(\frac{z_0}{r} \right)^2. \tag{196}$$

Thus we obtain a complete analytical solution for the boundary layer of a disk near a star for a viscosity inside the layer from (175) and a polytropic equation of state everywhere. Analytical solutions for boundary layer of disks with simplifying assumptions about the viscosity coefficient and temperature distribution were obtained directly without expansions by Colpi et al. (1991) and Glatzel (1992). The MAE method introduced by Regev (1983) for the solution of the accretion disk BL problem permits the derivation of a self-consistent analytical solution for the boundary layer of a disk for a viscosity coefficient in the usual α representation.

3.1.3. Isothermal case

For an isothermal disk with the same viscosity (175), using (48)–(50), (171) and (172), we get

$$\frac{d\rho_0}{d\rho} = \frac{1}{K}, \quad \frac{d\Sigma}{dx} = -\frac{\Omega_{K*}^2}{K} H_b \Sigma (1 - \omega^2), \tag{197}$$

$$\frac{d\omega}{dx} = -\frac{\dot{M}(1 - \omega)}{2\pi\alpha_b \sqrt{K}\Sigma r_*^2}. \tag{198}$$

Dividing the last two equations, and using the approximate boundary condition $\Sigma_* = \infty$, we get the solution (Shakura and Sunyaev, 1988)

$$\Sigma = \left(-\frac{\dot{M}\sqrt{K}}{2\pi\alpha_b H_p} \right) \frac{1}{r_*^2 \Omega_{K*}^2} \times \left[(\omega - \omega_*) \left(1 + \frac{\omega + \omega_*}{2} \right) \right]^{-1}. \tag{199}$$

From (190), (199), and (198), we obtain the characteristic scale, which we identify with H_b ,

$$\frac{H_b}{r_*} \approx \frac{2K}{r_*^2 \Omega_{K*}^2} [(1 - \omega_*)(3 + \omega_*)]^{-1}. \tag{200}$$

Matching (66) and (199) with account of (200) as for a polytrope, we get an expression for the integration constant

$$1 - \xi = \frac{\sqrt{2K}}{r_* \Omega_{K*}} \frac{\alpha}{\alpha_b}. \tag{201}$$

Comparing (200) and (201) with (195) and (196),

we see that the order of magnitude estimates for the polytropic case become exact for the isothermal case apart from numerical coefficients close to unity.

In the isothermal case there is a simple solution of Eq. (198) when (199) is substituted for Σ ,

$$(1 - \omega)^{-2} (\omega - \omega_*)^{\frac{3 + \omega_*}{1 + \omega_*}} (2 + \omega + \omega_*)^{-\frac{1 - \omega}{1 + \omega_*}} = \exp \left[2 \frac{H_b r_*}{K} \Omega_{K*}^2 x (1 - \omega_*) (3 + \omega_*) \right]. \tag{202}$$

We can see from (202) that the scale (200) naturally appears in the exponent. It is clear that this solution makes physical sense only over this characteristic scale — the thickness of BL — where $0 < x < r_*$. Nayfeh (1973) proved that the region of applicability of the inner and outer solutions obtained by the MAE method do overlap and the formula, constructed from the inner (i) and outer (e) solutions, gives a good interpolation also for the intermediate region. The formula, describing physical variable f in the whole region, has the structure

$$f = f_i + f_e - (f_i)_e. \tag{203}$$

Here, $(f_i)_e$ is the value of the inner solution on the outer edge [equal to the value of the outer solution on the inner edge $(f_e)_i$]. The solution for $\Sigma(r)$ is constructed using $\Sigma^{(0)}(r)$ from the relation (45) for the outer solution, and the solution of Eq. (181) with account of (170), (185), and (186) for $\Sigma_i(r)$. The choice of ξ from (193) gives the equality $(\Sigma_i)_e = (\Sigma_e)_i$. The solution for $\Omega(r)$ is constructed using $\Omega_K(r)$ from (54) for the external solution, and the solution of (182), with account of (170), (173), and (185) for the internal solution $\Omega_i(r)$. It is clear from these considerations that $(\Omega_i)_e = (\Omega_e)_i = \Omega_{K*}$.

The existence of overlapping regions where both solutions, internal and external, are valid was first proved by Prandtl (1905), cited by Nayfeh (1973) for the problem of the boundary layer near a solid body in the high Reynolds number flow of a viscous fluid. Prandtl invented the MAE method. The interpolation formulae of the type (203) were introduced by Vasil'eva (1959) (cited by Nayfeh, 1973), and represent a uniformly valid approximation in the whole region due to existence of the overlapping regions. The direct proof of the validity of (203), for the cases where general analytic solutions exist can be found in the books of Nayfeh (1981) and

Zwillinger (1992). These books, as well as Nayfeh (1973), contain examples of applications of the MAE method, including quasi-linear equations of the type (52) and (53), and also references to many other applications of the MAE method.

Using the relation $\dot{M} = 2\pi r_* \Sigma u_r$ for the estimation of the radial velocity u_r in the boundary layer, we obtain from (176)–(178), (185), and (191) for a polytropic boundary layer [or from (199) and (200) for the isothermal case], the estimation

$$u_r/u_{s0} \sim \alpha_b. \tag{204}$$

This means that the solution obtained neglecting the radial velocity is valid only for sufficiently small viscosity, that is, $\alpha_b \ll 1$.

3.1.4. Boundary layers with account of thermal processes: heat production in the boundary layer

Rapid braking of the rotational velocity in the boundary layer in disk accretion on to a slowly rotating star leads to strong heating and a large energy release. As a result, matter in the boundary layer is hotter than in the disk, and the boundary layer emits radiation at a higher effective temperature. The equations for the heat balance in the boundary layer are different from the heat equations in a thin accretion disk (115), (116), and (124). The component of the stress tensor should be written on the form (119) only, because in the boundary layer Ω deviates strongly from the Keplerian value. The turbulent viscosity coefficient should be scaled by the smaller value of the boundary layer thickness H_b , instead of the disk thickness h , as in (174) and (175). Due to the narrow radial width of the boundary layer, the radial heat flux inside it must be taken into account. The radial flux is usually more important than the losses through the sides of the disk Q_- in (124). From (124) and (119), and using the momentum conservation Eq. (128), we obtain an expression for the viscous heat production rate in the half-thickness of the boundary layer per unit disk surface area,

$$Q_+ = ht_{r\phi} r \frac{d\Omega}{dr} = h\eta \left(r \frac{d\Omega}{dr} \right)^2 \approx \frac{GMM}{4\pi r_*^2} (\omega - 1) \frac{d\omega}{dr}. \tag{205}$$

Here, as in the previous section, we take in the boundary layer $\xi_b = 1$, $r = r_*$, $\omega = \Omega/\Omega_{K*}$.

Inside the boundary layer we define

$$Q_t = 4\pi r Q_+ \approx 4\pi r_* Q_+ = \frac{GMM}{r_*} (\omega - 1) \frac{d\omega}{dr}, \tag{206}$$

which determines the heat production by viscosity in the entire ring of the boundary layer per unit of its radial extent in the accretion disk. The radiative heat conductivity in the radial direction is the main term in the heat balance of the boundary layer. The radial heat flux through the optically thick boundary layer is

$$\Phi = - \frac{4acT^3}{3\kappa\rho} \frac{dT}{dr} 4\pi rh, \tag{207}$$

The heat balance equation is

$$\frac{d\Phi}{dr} = Q_t = \frac{GMM}{r_*} (\omega - 1) \frac{d\omega}{dr}. \tag{208}$$

Integrating this equation, we obtain

$$\Phi = \frac{GMM}{r_*} \left(\omega - \frac{\omega^2}{2} - \omega_A + \frac{\omega_A^2}{2} \right) = \frac{GMM}{r_*} (\omega - \omega_A) \left(1 - \frac{\omega}{2} - \frac{\omega_A}{2} \right). \tag{209}$$

Consider the boundary layer at $\omega = \omega_A$, where the temperature has a maximum, so that the radial heat flux is zero at this point. The heat fluxes have opposite directions on the two sides of this layer. The position of this layer should be found from time-dependent evolutionary calculation of the boundary layer structure. If, for example, accretion is started to a cold neutron star, then a heat wave is started from the accretion disk and propagates inward to the neutron star, heating it. In this case the level with $\omega = \omega_A$ moves with time to the boundary of the star. For longer times, when the whole star becomes almost isothermal, this level coincides with the star boundary. If accretion is going on to a hot neutron star, then heat production in the boundary layer may be comparable with the heat flux from the star, which is equal to Φ_* on the star surface with $\omega = \omega_*$. Then we obtain instead of (209), the solution

$$\Phi = \Phi_* + \frac{GM\dot{M}}{r_*}(\omega - \omega_*) \left(1 - \frac{\omega}{2} - \frac{\omega_*}{2}\right). \quad (210)$$

It follows from (210), taking into account that the angular velocity is Keplerian at the outer edge of the boundary layer $\omega_{\text{out}} = 1$, that the total energy flux from the boundary layer due to heating by viscosity Q_{bl} is equal to

$$Q_{\text{bl}} = \frac{GM\dot{M}}{2r_*}(1 - \omega_*)^2, \quad (211)$$

(Popham and Narayan, 1995).

The relation (211) can also be obtained from the conservation laws. When a mass dm crosses the boundary layer, the change of its energy is

$$dE_m = \frac{1}{2}dm\Omega_{K*}^2 r_*^2 (1 - \omega_*^2). \quad (212)$$

From angular momentum conservation, the angular momentum lost by the accreting matter is

$$dJ_m = dm\Omega_{K*} r_*^2 (1 - \omega_*). \quad (213)$$

This is absorbed by the star, so that

$$dJ_* = I_* \Omega_{K*} d\omega_* = dJ_m. \quad (214)$$

From the last two equations, $I_* d\omega_* = dm r_*^2 (1 - \omega_*)$, so that the kinetic energy absorbed by the star is

$$dE_* = I_* \Omega_{K*}^2 \omega_* d\omega_* = dm \Omega_{K*}^2 r_*^2 \omega_* (1 - \omega_*). \quad (215)$$

The heat produced in the boundary layer is

$$dE_{\text{bl}} = dE_m - dE_* = \frac{1}{2}dm\Omega_{K*}^2 r_*^2 (1 - \omega_*)^2, \quad (216)$$

which gives (211) with account of

$$Q_{\text{bl}} = \frac{dE_{\text{bl}}}{dt}, \quad \dot{M} = \frac{dm}{dt}, \quad \Omega_{K*}^2 = \frac{GM}{r_*^3}. \quad (217)$$

3.1.5. Explicit models of accretion disks with boundary layers

The set of equations describing a stationary accretion disk together with its boundary layer have been solved numerically by several authors. The equations of radial and azimuthal motion, and the continuity equation coincide with the corresponding equations the structure of an advective disk (117) and (71) with the Ω -derivative description of the viscosity, and a continuity equation (120). In contrast with the

structure of an advective disk around a black hole where there is transonic radial motion, an accretion disk around a star with a boundary layer always has subsonic radial velocity (204) with a Mach number $\sim \alpha_b$, where α_b characterizes the viscosity in the boundary layer [see (174) and (175)].

The viscosity coefficient continuously describing the disk and boundary layer should include a transition from the thickness scale h in the disk to the smaller boundary layer radial thickness H_b . An expression having these properties was used by Popham and Narayan (1995),

$$\nu = \frac{2}{3} \left[\frac{1}{(\alpha h)^2} + \frac{(2 dP_0/dr)^2}{(3\alpha_b P_0)^2} \right]^{-1/2}. \quad (218)$$

The coefficient (2/3) is included two times in (218) in order to make a continuous transition to (127) in the disk where $h \ll H_b = P_0/(dP_0/dr)$, and to (175) in the boundary layer where $h \gg H_b$. The equation for thermal balance should include the radiative heat transfer Φ in the radial direction from (207), which is larger than all other cooling sources inside the boundary layer. Taking Q_+ and Q_- from (124), advective heating Q_{adv} from (115), and Φ from (207), we obtain the equation of the heat balance valid in the whole disk, including the boundary layer

$$Q_+ = Q_- + Q_{\text{adv}} + \frac{1}{4\pi r} \frac{d\Phi}{dr}. \quad (219)$$

This may also be written as

$$\dot{M} T \frac{dS}{dr} = \frac{d\Phi}{dr} + \dot{M}(j - j_{\text{in}}) \frac{d\Omega}{dr} + \frac{2aT^4 c}{3\kappa\rho h} 4\pi r. \quad (220)$$

The thickness of the disk h is everywhere determined by the vertical equilibrium equation (70). Popham and Narayan (1995) used somewhat more complicated equations of heat transfer. Instead of Q_- and Φ from above, they considered expressions following from a simplified solution of the radiative transfer equation with account of absorption and scattering opacities, similar to the approach of Section 2.6, which is valid also in the optically thin case. The equation of state $P = P_g + P_r$ takes into account deviations of the radiation pressure P_r from the equilibrium value, similar to (108).

The boundary conditions used by Popham and

Narayan (1995) required the angular velocity to be equal to the stellar one Ω_* at the inner edge of the boundary layer at the stellar radius r_* , and to the Keplerian angular velocity at the outer boundary, specified at $R_{\text{out}} = 100R_*$. The boundary conditions for the vertical heat flux is equivalent to the Q_- energy losses from (124). The radial heat flux from the star $\Phi_* > 0$ was specified on its surface, which is equivalent to the situation described by (210).

Calculations have been performed for cataclysmic binaries where disk accretion goes to a white dwarf star. Other similar calculations (Popham et al., 1996; Collins et al., 1998) considered white dwarfs or pre-main-sequence stars. Boundary layers of accretion disks around neutron stars were not considered in explicit calculations, but this case can be treated analytically or by the MAE method (Regev, 1983). Calculations of Popham and Narayan (1995) revealed the existence of a dynamical boundary layer, where there is a rapid drop of the angular velocity and of a velocity of the radial motion, inside the thermal boundary layer. There is a strong radial acceleration of matter when the flow approaches the dynamical boundary layer, and the density is rapidly increasing inside this layer. The heat flux from the boundary layer is propagating radially into the accretion disk and is radiated vertically on the scale of the order of the disk thickness.

Time-dependent calculations for accretion disks with boundary layers around pre-main-sequence stars have been performed in the 1-D (r) approximation by Godon (1996a,b), using a zero heat flux boundary condition, $dT/dr = 0$ at $r = r_*$, which corresponds to $\Phi_* = 0$ in (210). The results of 1-D calculations are qualitatively in accordance with the stationary model of Popham and Narayan (1995). The thermal boundary condition used above does not take into account possible important heat flux out of or into the star. It is more consistent to use the following simplified thermal boundary condition,

$$\frac{dT_*}{dt} = -\frac{\Phi_*}{C_*}, \quad (221)$$

where C_* is the heat capacity of a star, and Φ_* is the heat flux on the star boundary from (207), which may be positive or negative, depending on the temperature T_* . In the case of a neutron star or a white dwarf, the heat capacity C_* may be estimated

from the existing models of their structure. The heat capacity of an isothermal star can be taken as a rough approximation.

Time-dependent 2-D simulations have been done by Kley (1991). These calculations show temporal oscillations of the luminosity the amplitude of which depends on the choice of input parameters. These oscillations could be excited by instabilities, but numerical effects cannot be excluded.

3.1.6. Models of accretion disks with boundary layers constructed by MAE method

The matched asymptotic expansion (MAE) method was used for description of boundary layers in hydrodynamics (Prandtl, 1905), and was first applied for accretion disks by Regev (1983). The structure of an accretion disk and boundary layer with a polytropic equation of state was solved analytically by Bisnovaty-Kogan (1994) using the MAE method, and is described in Section 3.1.2. Account of thermal processes with the equation of state $P(\rho, T)$ makes the problem more complicated and analytic solutions have not been found. The equilibrium equations describing the outer solution for the disk may be taken from the standard model without advection with $\Omega = \Omega_K$, valid inward to the inner boundary of the outer solution at $r = r_*$. In contrast with the standard model, where the integration constant j_{in} was taken as $j_{\text{in}} = \xi \Omega_{K*} r_*^2$ with $\xi = 1$, in the outer MAE solution for the disk the constant ξ is slightly less than unity, and should be found from matching of the inner and outer solutions, as in the polytropic case (see Section 3.1.2).

The thermal equations in the disk may be taken in the form (220), where the advective term may be neglected, and (207). The term with Φ in this equation should take into account the heat flux coming from the boundary layer into the accretion disk, which is given by the boundary value $\Phi(r_*) = \Phi_{\text{bl}}$. The constant Φ_{bl} should be found from the matching to the inner solution. The second boundary condition for solving the two differential Eqs. (220) and (207) comes from the approach of the solution at large r to the standard one with a very small $\Phi(r)$. It is possible to write the thermal balance equation in the disk in a simpler way. It is evident from the physical model, and also is confirmed by calculations of Popham and Narayan (1995), that the heat flux

from the boundary layer Φ_{bl} coming into the disk is radiated from the disk on the scale of the order of the disk thickness h_* near the boundary layer. Instead of solving the differential equation, we can model the radiation flux from the boundary layer by an additional heating term, which is distributed over a distance h_* from the inner boundary with the profile

$$\frac{d\Phi}{dr} \approx \frac{\Phi_{bl}}{h_*} \exp\left(-\frac{r-r_*}{h_*}\right). \quad (222)$$

Integration of (222) over the radii between r_* and ∞ gives the additional energy emitted by the disk due to the heat flux from the boundary layer equal to Φ_{bl} . This flux is emitted in the region $\delta r \sim h_*$ adjacent to the boundary layer. In this description there is one additional matching condition defining Φ_{bl} , in comparison with the polytropic case.

To obtain the inner MAE solution, we should solve the equilibrium equations (171) and (172) together with the equations for heat production and heat transfer. The constant $\xi_b = 1$ here, as in the polytropic case from the matching condition for $\omega = 1$ at $x = \infty$, equal to the inner Keplerian value of the outer solution. Matching the densities of the inner and outer solutions determines the integration constant ξ of the outer solution. Application of MAE to the solution for a boundary layer including thermal processes meets with a definite problem. Using (209) in (207), we can write the equation of heat transfer in the boundary layer as

$$\Phi = -4\pi r h \frac{4acT^3}{3\kappa\rho} \frac{dT}{dr} = \frac{GM\dot{M}}{2r_*} [(1 - \omega_\Lambda)^2 - (1 - \omega)^2]. \quad (223)$$

It follows from (223) that the heat flux in the boundary layer consists of the constant value Φ_0 in the first term to the left, and a variable part $\sim (1 - \omega)^2$. The presence of the constant flux leads to unphysical behavior of the temperature at large x in the MAE method which gives an unlimited fall of the temperature. Therefore, in the papers of Regev (1983) and Regev and Bertout (1995), the solution was obtained for $\Phi_0 = 0$, which means that all heat produced in the boundary layer heats the star and does not go outward into the accretion disk. This is opposite to the condition used by Popham and

Narayan (1995). As was mentioned above, the maximum of the temperature may correspond to an intermediate position in the boundary layer, and heat flux from it may heat simultaneously the star and the disk. In direct calculations, this corresponds to changing of the boundary conditions, but was not realized. A MAE solution cannot be obtained directly for non-zero Φ_0 . Modifications of the MAE method are needed for its account.

Note, that large deviations of ξ from unity, $\xi = 0.61$, obtained by Regev (1983) for $\omega_* = 0.3$ could indicate that one is in the region where the asymptotic expansion is no longer valid. When the stellar angular velocity approaches a critical value, the boundary layer becomes thick [see (191)] and the MAE method fails.

3.2. Accretion disks around rapidly rotating stars

Investigations of low-mass X-ray binaries (LMXB) containing a neutron star have led to the conclusion that the accreting object can rotate rapidly with a surface angular velocity close to the Keplerian value. The question of accretion onto a rapidly rotating star also arises in cataclysmic variables where the primary is a white dwarf. When the stellar angular velocity reaches its critical value, the difference in the angular velocity across the boundary layer may be small. Disk accretion on to a rapidly rotating star, with Keplerian angular velocity at its equator, was investigated by Popham and Narayan (1991); Paczynski (1991); and Colpi et al. (1991). A self-consistent solution for a maximally rotating star was found by Bisnovatyi-Kogan (1993a). In this solution, the star continues to rotate rapidly during the accretion process.

3.2.1. Self-consistent model

When a star reaches the critical rotation rate at which the surface angular velocity is Keplerian, the flux of angular momentum into the star leads to differential rotation inside the star. It is clear that disk properties at large distances from the star do not change when the star reaches its critical rotation rate. Thus the disk remains Keplerian. The properties of the transition layer between the star and the disk are

determined by the stellar rotational law, but we do not need to know the detailed properties of this transition zone in order to build a self-consistent model. We only have to know that during accretion onto a rapidly rotating star, the transition layer is smooth, all variables change monotonically, and there is no enhanced heat production in this layer. This is in contrast with the case of a boundary layer between an accretion disk and a slowly rotating star.

The evolution of a star undergoing mass accretion may be characterized by the evolution of two quantities, its mass M and total angular momentum J , and by one function, $j(r)$, which describes the angular momentum distribution within the star. Note that $j(r)$ is determined by the viscosity law inside the star. For a given mass accretion rate \dot{M} , determined by conditions far from the star, the star gradually increase its mass and angular momentum. When the stellar rotation is small compared with the Keplerian value, the specific angular momentum of matter accreting onto the star is approximately equal to $\dot{M}v_{\text{Ke}}R_{\text{se}}$, ($v_{\text{Ke}} = (GM/r^3)^{1/2}$ is the Keplerian velocity, R_{se} is the stellar equatorial radius, and the subscript “e” refers to values at the stellar equator). When the stellar equatorial rotational velocity is smaller than the Keplerian value, the angular velocity of the disk has a maximum near R_{se} . At this point, the viscous flux of angular momentum is zero and the total angular momentum flux is determined by the convective term $\dot{M}j_e$, $j = rv_\phi$. The maximum of the rotational velocity disappears when the star’s rotation is close to the critical velocity and the (negative) viscous momentum flux becomes important.

The requirement of self-consistency during accretion onto a rapidly rotating star may be formulated as the condition that *the star absorb the accreted matter with a specific angular momentum such that the star remains in the state of critical rotation*. Depending on the viscosity law, a critically rotating star may have different distributions $j(r)$ and in general, the structure of the star gradually changes with time. If the viscosity inside the star is high, the star rotates almost rigidly; this case has been considered in the above-mentioned papers. If the star-disk system can be described by a polytropic equation of state, there is a self-similar solution for such a system which does not depend on mass.

3.2.2. Self-similar solution for a polytropic star-disk system in the case of a rigidly rotating star

The equations describing the structure of a rotating star with a polytropic equation of state (41) the equilibrium equations in spherical coordinates are

$$\frac{1}{\rho} \frac{\partial P}{\partial r} + \frac{\partial \Phi}{\partial r} - \Omega^2 r(1 - \mu^2) = 0, \quad (224)$$

$$\frac{1}{\rho} \frac{\partial P}{\partial \mu} + \frac{\partial \Phi}{\partial \mu} + \Omega^2 r^2 \mu = 0, \quad (225)$$

(Chandrasekhar, 1989). The equation for the gravitational potential Φ is

$$\frac{1}{r^2} \frac{\partial}{\partial r} \left(r^2 \frac{\partial \Phi}{\partial r} \right) + \frac{1}{r^2} \frac{\partial}{\partial \mu} \left((1 - \mu^2) \frac{\partial \Phi}{\partial \mu} \right) = 4\pi G \rho. \quad (226)$$

Here, $\mu = \cos \theta$ and Ω is the angular velocity of the stellar matter. In general Ω is not constant inside the star. For a equilibrium polytropic star Ω depends only on the cylindrical radius $r \sin \theta$. Eliminating Φ from Eqs. (224)–(226), we get

$$\frac{1}{r^2} \frac{\partial}{\partial r} \left(\frac{r^2}{\rho} \frac{\partial P}{\partial r} \right) + \frac{1}{r^2} \frac{\partial}{\partial \mu} \left(\frac{1 - \mu^2}{\rho} \frac{\partial P}{\partial \mu} \right) + 4\pi G \rho - \frac{1}{x} \frac{d}{dx} (x^2 \Omega^2) = 0, \quad (227)$$

where $x = r \sin \theta = r\sqrt{1 - \mu^2}$, $\Omega = \Omega(x)$.

Dimensionless polytropic variables,

$$\xi = r/r_*, \quad \Theta^n = \rho/\rho_c, \quad \omega = \Omega/\Omega_*, \quad (228)$$

are useful in view of the fact that $P = K\rho^{1+1/n}$. Here, ρ_c is the central density of the star, and

$$r_* = \left(\frac{(n+1)K\rho_c^{\frac{1}{n}-1}}{4\pi G} \right)^{1/2}, \quad \Omega_* = \sqrt{2\pi G\rho_c}. \quad (229)$$

In terms of these dimensionless variables (228)–(229) and Eq. (227) for $\Omega = \text{const.}$ can be written in the form

$$\frac{1}{\xi^2} \frac{\partial}{\partial \xi} \left(\xi^2 \frac{\partial \Theta}{\partial \xi} \right) + \frac{1}{\xi^2} \frac{\partial}{\partial \mu} \left((1 - \mu^2) \frac{\partial \Theta}{\partial \mu} \right) + \Theta^n - \omega^2 = 0 \quad (230)$$

The solution of (230) is uniquely determined by the boundary conditions

$$\Theta = 1, \quad \frac{\partial \Theta}{\partial \xi} = 0 \quad \text{at} \quad \xi = 0, \tag{231}$$

$$\sqrt{1 - \mu^2} \frac{\partial \Theta}{\partial \mu} = 0 \quad \text{at} \quad \mu = 0, \quad \mu = \pm 1,$$

and by the value of ω . One also requires that the solution satisfies the original equilibrium, (224) and (225). The latter condition results from the fact that Eqs. (224) and (225) were differentiated in order to obtain (230), so that a solutions of (230) do not necessarily satisfy (224) and (225). It is in fact necessary to find a gravitational potential Φ from (226) which, when written in dimensionless form $\phi = \Phi/(4\pi G\rho_c r_*^2)$, satisfies the scaling conditions of the self-similar solution. For compressible matter with $n > 0$, a solution exists only for $\omega < \omega_c$. For $\omega = \omega_c$, the centrifugal force on the equatorial boundary of the star exactly balances gravity. The proof of this is given by Bisnovatyi-Kogan and Blinnikov (1981). Numerical calculations have been done to obtain the structure of rotating polytropic stars for different values of ω up to the critical value ω_c (James, 1964; Blinnikov, 1975; Ipser and Managan, 1981; see also Tassoul, 1978).

For a given n , the structure of a critically rotating star does not depend on its mass. The mass M and the total angular momentum J are given by

$$M = 2\pi\rho_c r_*^3 \int_{-1}^1 d\mu \int_0^{\xi_{\text{out}}(\mu)} \Theta^n(\xi, \mu) \xi^2 d\xi, \tag{232}$$

$$J = 2\pi\rho_c r_*^5 \omega \sqrt{2\pi G\rho_c} \times \int_{-1}^1 (1 - \mu^2) d\mu \int_0^{\xi_{\text{out}}(\mu)} \Theta^n(\xi, \mu) \xi^4 d\xi. \tag{233}$$

Introducing dimensionless values of the mass \mathcal{M}_n and of the total angular momentum \mathcal{J}_n defined as

$$\mathcal{M}_n = \frac{1}{2} \int_{-1}^1 d\mu \int_0^{\xi_{\text{out}}(\mu)} \Theta^n(\xi, \mu) \xi^2 d\xi, \tag{234}$$

$$\mathcal{J}_n = \frac{\omega}{2} \int_{-1}^1 (1 - \mu^2) d\mu \int_0^{\xi_{\text{out}}(\mu)} \Theta^n(\xi, \mu) \xi^4 d\xi. \tag{235}$$

The dimensional values, M and J are thus

$$M = 4\pi\rho_c r_*^3 \mathcal{M}_n, \tag{236}$$

$$J = 4\pi\rho_c r_*^5 \sqrt{2\pi G\rho_c} \mathcal{J}_n. \tag{237}$$

The average specific angular momentum of the star j_s and the derivative along the critical states $j_a = (dJ/dM)_c$ are written, using (229) and (236), as

$$j_s = J/M = r_*^2 \sqrt{2\pi G\rho_c} \mathcal{J}_n / \mathcal{M}_n,$$

$$j_a = \frac{5 - 2n}{3 - n} j_s. \tag{238}$$

Using (236) one can write ρ_c and r_* , which appear in (229), as a function of M

$$\rho_c = \left(\frac{4\pi G}{(n+1)K} \right)^{\frac{3n}{3-n}} \left(\frac{M}{4\pi\mathcal{M}_n} \right)^{\frac{2n}{3-n}},$$

$$r_* = \left(\frac{4\pi G}{(n+1)K} \right)^{\frac{n}{n-3}} \left(\frac{M}{4\pi\mathcal{M}_n} \right)^{\frac{1-n}{3-n}}. \tag{239}$$

The specific angular momentum of matter j_e at the stellar equator r_e can be written as

$$j_e = \Omega r_e^2 = r_*^2 \sqrt{2\pi G\rho_c} \xi_e^2 \omega,$$

$$\xi_e = r_e / r_* = \xi_{\text{out}}(\pi/2). \tag{240}$$

From a comparison of (238) and (240), it follows that the ratio

$$\frac{j_a}{j_e} = \frac{5 - 2n}{3 - n} \frac{j_s}{j_e} = \frac{5 - 2n}{3 - n} \frac{\mathcal{J}_n}{\mathcal{M}_n \xi_e^2 \omega} \tag{241}$$

does not depend on the stellar mass M , and is a function only of n and ω .

Table 1 gives the dimensionless values of the angular velocity ω_c , the equatorial radius $\xi_{\text{out}}(\theta = \pi/2) = \xi_e$, the mass \mathcal{M}_n , the momentum of inertia around the rotational axis $\mathcal{I}_n = \mathcal{J}_n / \omega_c$, the average specific angular momentum of the star ζ_s , the dimensionless derivative ζ_a ,

$$\zeta_s = j_s / (r_*^2 \sqrt{2\pi G\rho_c}) = \mathcal{J}_n / \mathcal{M}_n,$$

$$\zeta_a = \frac{5 - 2n}{3 - n} \zeta_s, \tag{242}$$

and the specific angular momentum of matter on the stellar equator

$$\zeta_e = j_e / (r_*^2 \sqrt{2\pi G\rho_c}) = \xi_e^2 \omega_c \tag{243}$$

for several polytropic indices n in the state of critical rotation. These values are based on calculations by

Table 1
Parameters of non-rotating and critically rotating polytropic stars

n	ξ_{n0}	\mathcal{M}_{n0}	\mathcal{J}_{n0}	ω_c	ξ_e	ξ_e/ξ_p	\mathcal{M}_n	\mathcal{J}_n	ζ_s	$\beta = \zeta_a/\zeta_e$
0.5	2.7528	3.7871		0.389 (0.367)		2.51				
0.6				0.362 (0.354)		2.29				
0.808				0.326	4.7652	1.917	5.0248	24.43	1.585	0.3304
1.0	π	π	8.104	0.289	4.8265	1.792	4.289	18.73	1.262	0.2805
1.5	3.65375	2.71406	7.413	0.209	5.36	1.626	3.2138	12.18	0.792	0.176
2.0	4.35287	2.41105	7.074	0.147	6.307	1.555	2.6518	9.62	0.533	0.0894
2.5	5.35528	2.18720	7.013	0.09965	7.7623	1.522	2.30563	8.49	0.367	0.0
3.0	6.89685	2.01824	7.234	0.0639	10.123	1.535	2.0743	8.125	0.250	$-\infty$

James (1964); Blinnikov (1975); and Ipser and Managan (1981). The ratio of the equatorial and polar radii ξ_e/ξ_p and the nondimensional parameters for nonrotating polytropes (outer radius ξ_{0n} , mass \mathcal{M}_{0n} and momentum of inertia around the symmetry axis \mathcal{J}_{0n} , Chandrasekhar, 1957; James, 1964; Blinnikov, 1975) are also given.

In dimensionless variables it is obvious that the derivative ζ_a of the angular momentum of the star along the sequence of critically rotating states is always smaller than the equatorial value ζ_e . ζ_e is equal to the Keplerian value of a critically rotating non-spherical star. The viscous flux of specific angular momentum in the accretion disk around a critically rotating star j_v is therefore negative. Near the surface of the star, j_v is equal to

$$j_v = j_a - j_e, \quad (244)$$

as one requires that the total angular momentum flux into the star is equal to $\dot{M}j_a$ for self-consistency. In a self-consistent model of an accretion disk around a rapidly rotating polytropic star, the value of the constant ξ in the formulae of Section 2.4 should be taken equal to ζ_a from Table 1.

3.2.3. General, non-polytropic case of disk accretion on to a rapidly rotating star

In realistic cases, thermal processes are very important in the disk and the polytropic approximation is inadequate. Equations for the thermal balance from Section 2.5.3 need to be taken into account. The transition to a rapidly rotating star is accompanied by a substantial change of the integra-

tion constant in Eqs. (71) and (88) which leads to important observational consequences.

The total luminosity of the accretion disk is equal to

$$L = \int_{r_i}^{\infty} 4\pi Fr dr = \left(\frac{3}{2} - \beta\right) \frac{GMM}{r_i}. \quad (245)$$

When $\beta = 1$, the star accretes matter with Keplerian angular momentum, and only half of the gravitational energy of the accreted matter is radiated from the disk, according to the virial theorem. The fate of the remaining half is different. In the case of a black hole, it is absorbed by the black hole, increasing the mass and angular momentum of the black hole without any significant radiation. Note however that matter falling from the last stable orbit to the horizon still emits radiation (Bisnovatyi-Kogan and Ruzmaikin, 1974).

In the case of accretion on to a slowly rotating neutron star there are several possibilities. If the radius of the neutron star r_s is smaller than $3r_g$, then $r_i = 3r_g$ and the disk luminosity is the same as in the case of a black hole, and the remaining gravitational energy, including the part gained during free fall onto the neutron star surface, is emitted close to the neutron star surface. If $r_s > 3r_g$, then $r_i = r_s$, the disk luminosity is $GMM/2r_s$ and an equal amount of energy is emitted in the boundary layer near the stellar surface, where the accreting matter converts its kinetic energy into heat.

The situation changes gradually as the central object absorbs angular momentum. The black hole moves from a Schwarzschild to an extreme Kerr

solution. The radius of the last stable orbit decreases from $3r_g$ to r_g , and the radius of the horizon changes from r_g to $r_g/2$. The efficiency of the disk energy emission increases from 5.7 to 42% (Novikov and Thorne, 1973). The changes go in an opposite direction when a neutron star accelerates its rotation. Let us consider only the case $r_s > 3r_g$. The luminosity of the disk decreases because the stellar radius increases. The fraction of energy emitted by the neutron star also decreases. It changes from $GMM/2r_s$ in the case of a nonrotating star to the difference between rotational energy of matter in the disk and at the stellar surface.

A rapid change in the efficiency of energy release and disk luminosity happens when the rotation of the star reaches its maximum, critical value. The energy emitted near the stellar surface tends to zero, but the luminosity of the disk undergoes a drastic change. The star no longer absorbs all of the angular momentum coming from the disk, but absorbs only the fraction required to maintain the star in a critically rotating state. The specific angular momentum of matter accreted by the star is equal to $(dJ/dM)_c$ and the remaining part is carried away in the disk by the viscous stress (see Section 2). Viscosity carries not only angular momentum, but also energy, so that the energy production and luminosity of the disk rapidly increase, from the value corresponding to $\beta = 1$ to the value corresponding to $\beta = j_a/j_e$ according to (245). For polytropic stars the values of β are given in the last column of Table 1. This implies a rapid increase of the total luminosity by a factor 2–3, depending on the stellar structure. This rapid increase is easy to understand if one remembers that when a star increases its rotation rate, part of the gravitational energy is converted into rotational energy without heat production. When a star reaches its limiting rotation rate, the growth rate of its rotational energy strongly diminishes and a correspondingly larger fraction of gravitational energy is transformed into heat. The minimum of luminosity of an accreting neutron star is reached when the stellar angular velocity is slightly below the critical value. A rapid increase in luminosity must be accompanied by a corresponding hardening of the emitted spectrum because the energy release is increased, raising the effective temperature in the inner part of the disk. Such events may occur in objects such as LMXB or cataclysmic variables.

Note, that whereas the standard solution for an accretion disk (Shakura, 1972; Shakura and Sunyaev, 1973; Novikov and Thorne, 1973) is not valid in regions close to the inner edge in the case of a black hole (see Paczyński and Bisnovatyi-Kogan, 1981), the self-consistent solution for accretion on to a rapidly rotating star, may be used down to the stellar radius, which is the inner edge of the disk.

4. Accretion flows in presence of magnetic field

4.1. Magnetic field amplification in quasi-spherical accretion

Matter flowing into a black hole from a companion star or from the interstellar medium is very likely to be magnetized. Due to the more rapid increase of the magnetic energy density in comparison with any other energy densities, the dynamical and heating role of the magnetic field becomes more and more important closer to the central object. Schwartzman (1971) was the first to emphasize the importance of the magnetic field for an energy release during accretion to a black hole. He showed that due to the more rapid growth of magnetic energy with decreasing r , its energy density E_M increases up to the point where it equals the kinetic energy density E_k of the flow. He proposed that for smaller distances, *equipartition* results with $E_M \approx E_k$. At the smaller distances $E_M \approx E_k$ is maintained by the annihilation of the magnetic field. This hypothesis is usually accepted in the modern picture of accretion (see e.g. Narayan and Yi, 1995). Schwartzman (1971) considered an averaged quasi-stationary picture with local equipartition. Another variant of magnetic accretion is where equipartition and magnetic field annihilation is accompanied by the formation of shock waves. This was considered by Bisnovatyi-Kogan and Sunyaev (1972) and also by Chang and Ostriker (1985). A more accurate account of heating of the plasma by magnetic field annihilation was made by Bisnovatyi-Kogan and Ruzmaikin (1974) where an exact nonstationary solution for the field amplification in a radial accretion flow was also obtained.

Consider the general problem of the field amplification in the accretion flow where gas has an angular momentum and field annihilation is approximated by a finite “turbulent” conductivity. This approach

should reproduce a smooth averaged flow, considered by Schwartzman. In the known stationary velocity field $v(r, \theta)$ the magnetic field \mathbf{B} is described by Maxwell equations in the MHD approximation (without the displacement current), with a finite conductivity

$$\nabla \times \mathbf{B} = \frac{4\pi}{c} \mathbf{j}, \quad \nabla \times \mathbf{E} = -\frac{1}{c} \frac{\partial \mathbf{B}}{\partial t}, \quad \nabla \cdot \mathbf{B} = 0, \quad \mathbf{j} = \sigma \left(\mathbf{E} + \frac{1}{c} \mathbf{v} \times \mathbf{B} \right), \quad (246)$$

where σ is the plasma conductivity, \mathbf{j} is the electrical current density, and \mathbf{E} is the electrical field strength. Consider an axisymmetric situation in spherical coordinate system r, θ, ϕ where all ϕ derivatives are zero, but all vectors $v, \mathbf{B}, \mathbf{E}, \mathbf{j}$ may have all three components non-zero. An equation containing only the magnetic field follows from (246)

$$\frac{\partial \mathbf{B}}{\partial t} = \nabla \times [\mathbf{v} \times \mathbf{B}] + \frac{c^2}{4\pi\sigma} \nabla^2 \mathbf{B}. \quad (247)$$

These equations are completed by the condition of zero divergence of the magnetic field, which for the chosen case is

$$\frac{1}{r^2} \frac{\partial}{\partial r} (r^2 B_r) + \frac{1}{r \sin \theta} \frac{\partial}{\partial \theta} (\sin \theta B_\theta) = 0. \quad (248)$$

4.1.1. Time-dependent amplification of a magnetic field in spherical accretion

For spherical accretion with $v = (v_r, 0, 0)$, Eq. (247) reduces to

$$\begin{aligned} \frac{\partial B_r}{\partial t} = & \frac{1}{r \sin \theta} \frac{\partial}{\partial \theta} (\sin \theta v_r B_\theta) + \frac{c^2}{4\pi\sigma} \\ & \times \left[\frac{1}{r^2} \frac{\partial}{\partial r} \left(r^2 \frac{\partial B_r}{\partial r} \right) + \frac{1}{r^2 \sin \theta} \frac{\partial}{\partial \theta} \left(\sin \theta \frac{\partial B_r}{\partial \theta} \right) \right. \\ & \left. - \frac{2B_r}{r^2} - \frac{2}{r^2 \sin \theta} \frac{\partial}{\partial \theta} (\sin \theta B_\theta) \right], \quad (249) \end{aligned}$$

$$\begin{aligned} \frac{\partial B_\theta}{\partial t} = & -\frac{1}{r} \frac{\partial}{\partial r} (rv_r B_\theta) \\ & + \frac{c^2}{4\pi\sigma} \left[\frac{1}{r^2} \frac{\partial}{\partial r} \left(r^2 \frac{\partial B_\theta}{\partial r} \right) \right. \\ & + \frac{1}{r^2 \sin \theta} \frac{\partial}{\partial \theta} \left(\sin \theta \frac{\partial B_\theta}{\partial \theta} \right) \\ & \left. - \frac{B_\theta}{r^2 \sin^2 \theta} + \frac{2}{r^2} \frac{\partial B_r}{\partial \theta} \right], \quad (250) \end{aligned}$$

$$\begin{aligned} \frac{\partial B_\phi}{\partial t} = & -\frac{1}{r} \frac{\partial}{\partial r} (rv_r B_\phi) \\ & + \frac{c^2}{4\pi\sigma} \left[\frac{1}{r^2} \frac{\partial}{\partial r} \left(r^2 \frac{\partial B_\phi}{\partial r} \right) + \frac{1}{r^2 \sin \theta} \frac{\partial}{\partial \theta} \left(\sin \theta \frac{\partial B_\phi}{\partial \theta} \right) \right. \\ & \left. - \frac{B_\phi}{r^2 \sin^2 \theta} \right]. \quad (251) \end{aligned}$$

An analytical solution can be obtained for the initial nonstationary stage of field amplification, when the field dissipation is negligible (Bisnovatyi-Kogan and Ruzmaikin, 1974). From (249) with account of (248), and from (250), (251) we get

$$\frac{d(r^2 B_r)}{dt} = 0, \quad \frac{d(rv_r B_\theta)}{dt} = 0, \quad \frac{d(rv_r B_\phi)}{dt} = 0, \quad (252)$$

where the total or convective derivative is

$$\frac{d}{dt} = \frac{\partial}{\partial t} + v_r \frac{\partial}{\partial r}. \quad (253)$$

A solution of (252)–(253) is determined by 4 first integrals of the characteristic equations,

$$\begin{aligned} C_1 = & t - \int \frac{dr}{v_r}, \quad C_2 = r^2 B_r, \quad C_3 = rv_r B_\theta, \\ C_4 = & rv_r B_\phi. \quad (254) \end{aligned}$$

For the case of free fall with $v_r = -\sqrt{2GM}/r$, we get

$$C_1 = t + \frac{2}{3} \frac{r^{3/2}}{\sqrt{2GM}}. \quad (255)$$

The initial value problem from $t = 0$ is solved separately for poloidal and toroidal field components. For an initial field which is uniform, $B_{r0} = B_0 \cos \theta$, $B_{\theta0} = -B_0 \sin \theta$, we obtain the integrals

$$\begin{aligned} C_1 = & \frac{2}{3} \frac{r^{3/2}}{\sqrt{2GM}}, \quad C_2 = r^2 B_0 \cos \theta, \\ C_3 = & \sqrt{2GM} r B_0 \sin \theta. \quad (256) \end{aligned}$$

The relation between the integrals found at $t = 0$, after excluding $r(C_1)$, is valid at any time, so finally we get from (254) the solution (Bisnovatyi-Kogan and Ruzmaikin, 1974)

$$B_r = \frac{B_0 \cos \theta}{r^2} \left(r^{3/2} + \frac{3}{2} t \sqrt{2GM} \right)^{4/3},$$

$$B_\theta = -\frac{B_0 \sin \theta}{\sqrt{r}} \left(r^{3/2} + \frac{3}{2} t \sqrt{2GM} \right)^{1/3}. \quad (257)$$

The radial component of the field grows most rapidly. It is $\propto r^{-2}$ for sufficiently long times, and it is $\propto t^{4/3}$ at given sufficiently small radii. It grows with time everywhere.

For an initial dipole field, $B_{r,0} = B_0 \cos \theta / r^3$, $B_{\theta,0} = -B_0 \sin \theta / (2r^3)$, we obtain the following solution

$$B_r = \frac{B_0 \cos \theta}{r^2} \left(r^{3/2} + \frac{3}{2} t \sqrt{2GM} \right)^{-2/3},$$

$$B_\theta = -\frac{B_0 \sin \theta}{2\sqrt{r}} \left(r^{3/2} + \frac{3}{2} t \sqrt{2GM} \right)^{-5/3}. \quad (258)$$

Here the magnetic field is decreasing everywhere with time, tending to zero. That describes the compression of the dipole magnetic field onto the stellar surface. The toroidal stellar magnetic field is confined inside the star. When the outer layers of the star are compressed at free-fall speed, then for an initial field distribution $B_{\phi,0} = B_0 r^n f(\theta)$ the change of magnetic field with time is described by a relation

$$B_\phi = -\frac{B_0 f(\theta)}{\sqrt{r}} \left(r^{3/2} + \frac{3}{2} t \sqrt{2GM} \right)^{1/3+n}. \quad (259)$$

4.1.2. Amplification of magnetic field in rotating accretion flows

In a quasi-spherical accretion flow of a perfectly conducting plasma, $d(\mathbf{B} \cdot d\mathbf{S})/dt = 0$, where $d\mathbf{S}$ is a surface area element and d/dt is the derivative following the flow ($v = v_r \hat{\mathbf{r}} + v_\phi \hat{\boldsymbol{\phi}}$, in spherical coordinates). With $d\mathbf{S} = r^2 d\Omega \hat{\mathbf{r}}$, $v_r \approx v_r(|\mathbf{r}|)$, and $d\Omega$ a fixed solid angle increment, one finds that $B_r \propto 1/r^2$ independent of the toroidal velocity v_ϕ . Writing $B_r = B_0 (r_{\text{out}}/r)^2$, the radius at which $\rho v_K^2/2 = B_r^2/(8\pi)$ is

$$r_{\text{equi}} = \left(\frac{g B_0^2 r_0^4}{\sqrt{GM}} \right)^{2/3}, \quad (260)$$

where $v_K \equiv (GM/r)^{1/2}$ and the accretion speed is assumed $v_r = -g v_K$, with $g = \text{const} < \sim 1$. For example, for a black hole mass $M = 10^6 M_\odot$, $\dot{M} = 0.1 M_\odot/\text{yr}$, $B_0 = 10^{-5}$ G, $r_0 = 1$ pc, and $g = 0.1$, we find $r_{\text{equi}} \approx 6 \times 10^{14}$ cm, which is much larger than the Schwarzschild radius, $r_s \approx 3 \times 10^{11}$ cm. Thus the

magnetic field resulting from flux-freezing is dynamically important in quasi-spherical accretion flows (Schwartzman, 1971), and this is independent of dynamo processes or MHD instabilities. Further accretion for $r < r_{\text{equi}}$ is possible *only* if magnetic flux is destroyed by reconnection and the magnetic energy is dissipated. Fig. 7 shows a sketch of the *instantaneous* poloidal magnetic field configuration.

For example, for a flow with time-averaged velocity $v = v_r \hat{\mathbf{r}} + v_\phi \hat{\boldsymbol{\phi}}$, an approximate solution for the *time-averaged* magnetic field for infinite conductivity can readily be obtained in the vicinity of the equatorial plane. In this region it is reasonable to assume $\mathbf{B} = B_r \hat{\mathbf{r}} + B_\phi \hat{\boldsymbol{\phi}}$; that is, B_θ is neglected. Thus

$$\nabla \cdot \mathbf{B} = 0 = \frac{1}{r^2} \frac{\partial}{\partial r} (r^2 B_r) + \frac{1}{r \sin \theta} \frac{\partial}{\partial \phi} (B_\phi).$$

Near the equatorial plane, $\sin \theta \approx 1$. This equation is then satisfied by taking

$$B_r = \frac{\text{const}}{r^2} \exp \left(i \int dr k_r + im\phi \right), \quad (261)$$

$$B_\phi = f(r) \exp \left(i \int dr k_r + im\phi \right), \quad (262)$$

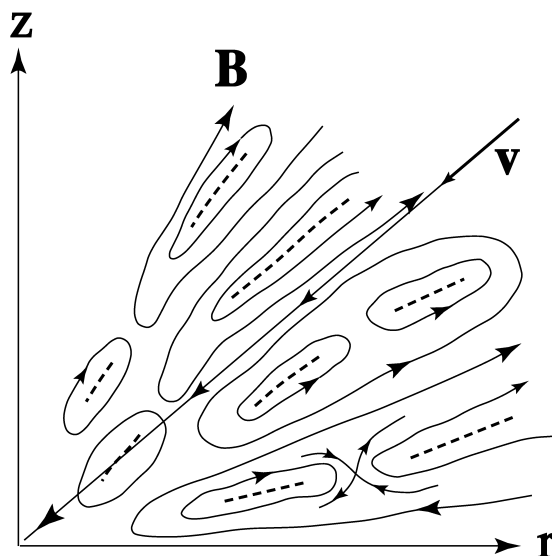


Fig. 7. Poloidal projection of the instantaneous magnetic field in an accretion flow.

with the actual fields given by the real parts and with

$$\mathbf{k} \cdot \mathbf{B} = k_r B_r + k_\phi B_\phi = 0, \quad (263)$$

where $\mathbf{k} \equiv \hat{\mathbf{r}}k_r + \hat{\boldsymbol{\phi}}k_\phi$, $k_\phi \equiv m/r$ is the azimuthal wavenumber, and $m = \pm 1, \pm 2$, etc. The stationary magnetic field satisfies $\nabla \times (\mathbf{v} \times \mathbf{B}) = 0$, and this requires

$$\mathbf{v} \times \mathbf{B} = \hat{\boldsymbol{\theta}}(v_\phi B_r - v_r B_\phi) = 0, \quad \text{or} \quad B_\phi = (v_\phi/v_r) B_r.$$

That is, $v \propto \mathbf{B}$ and $\mathbf{k} \cdot \mathbf{v} = 0$. Owing to Eq. (3),

$$k_r = -(v_\phi/v_r)k_\phi. \quad (264)$$

In ADAF accretion models, $v_\phi/v_r = \text{const}$, so that $k_r \propto 1/r$. Thus, $|B_r| = |v_r/v_\phi||B_\phi| \propto 1/r^2$, and $f(r) \propto 1/r^2$.

The nature of the field is most easily obtained from the flux function rA_θ (with \mathbf{A} the vector potential), where

$$B_r = -\frac{1}{r^2} \frac{\partial(rA_\theta)}{\partial\phi}, \quad B_\phi = \frac{1}{r} \frac{\partial(rA_\theta)}{\partial r},$$

for $\sin\theta \approx 1$. Note that $(\mathbf{B} \cdot \nabla)(rA_\theta) = 0$. Thus the frozen-in field is described by

$$rA_\theta = \text{const} \exp\left(im \left[\left| \frac{v_\phi}{v_r} \right| \ln r + \phi \right] \right), \quad (265)$$

where it is assumed that $v_\phi > 0$, $v_r < 0$, and $v_\phi/v_r = \text{const}$. The fact that $|rA_\theta| = \text{const}$ corresponds to the conservation of the ingoing or outgoing flux in a given tube. A given field line satisfies

$$r = \text{const} \exp\left(-\phi \left| \frac{v_r}{v_\phi} \right| \right). \quad (266)$$

Fig. 8 shows the nature of the equatorial field for $m = 2$.

Consider now the problem of magnetic field amplification in an accretion flow which is *not* infinitely conducting. The flow is described by the magnetohydrodynamics (MHD) equations,

$$\begin{aligned} \rho \frac{d\mathbf{v}}{dt} &= -\nabla p + \rho \mathbf{g} + \frac{1}{c} \mathbf{J} \times \mathbf{B} + \eta \nabla^2 \mathbf{v}, \\ \nabla \times \mathbf{B} &= \frac{4\pi}{c} \mathbf{J}, \quad \nabla \times \mathbf{E} = -\frac{1}{c} \frac{\partial \mathbf{B}}{\partial t}, \\ \mathbf{J} &= \sigma(\mathbf{E} + \mathbf{v} \times \mathbf{B}/c), \end{aligned} \quad (267)$$

where v is the flow velocity, \mathbf{B} the magnetic field, p the plasma pressure, σ the plasma conductivity, η

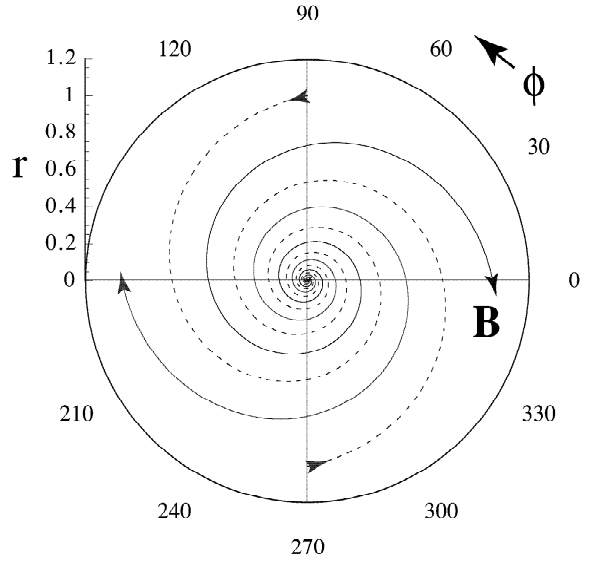


Fig. 8. Equatorial projection of the magnetic field given by Eq. (265) for an infinitely conducting accretion flow.

the dynamic viscosity (with $\nu = \eta/\rho$ the kinematic viscosity), \mathbf{J} the current density, and \mathbf{E} the electric field. These equations can be combined to give the induction equation,

$$\begin{aligned} \frac{\partial \mathbf{B}}{\partial t} &= \nabla \times (\mathbf{v} \times \mathbf{B}) - \nabla \times (\eta_m \nabla \times \mathbf{B}), \\ &\approx \nabla \times (\mathbf{v} \times \mathbf{B}) + \eta_m \nabla^2 \mathbf{B}, \end{aligned} \quad (268)$$

where $\eta_m \equiv c^2/(4\pi\sigma)$ is the magnetic diffusivity, and the approximation involves neglecting $\nabla\eta_m$.

In Eqs. (267) and (268) both the viscosity ν and the magnetic diffusivity η_m have the same units and both are assumed to be due to turbulence in the accretion flow. Thus, it is reasonable to express both transport coefficients using the ‘‘alpha’’ prescription of Shakura (1972) and Shakura and Sunyaev (1973),

$$\nu = \alpha c_s \ell_t, \quad \eta_m = \alpha_m c_s \ell_t, \quad (269)$$

where ℓ_t is the outer scale of the turbulence, and $c_s = \sqrt{p/\rho}$ is the isothermal sound speed. Bisnovatyi-Kogan and Ruzmaikin (1976) introduced α_m and proposed that $\alpha_m \sim \alpha$. Note that α and α_m characterize a turbulent MHD flow in which there is a Kolmogorov cascade of energy from large scales (ℓ_t) to much smaller scales where the actual (microscopic) dissipation of energy occurs.

We obtain stationary \mathbf{B} field solutions for accretion flows with time-averaged flow $v = \hat{\mathbf{r}}v_r + \hat{\boldsymbol{\phi}}v_\phi$ and with finite diffusivity η_m in the form of Eqs. (261) and (262), but with k_r complex, $k_r = k_r^R + ik_r^I$. Eq. (262) still applies, but (264) does not. In its place we have from Eq. (268),

$$0 \approx i\mathbf{k} \times (\mathbf{v} \times \mathbf{B}) - \eta_m \mathbf{k}^2 \mathbf{B}, \quad (270)$$

where the approximation involves neglect of terms of order $1/(|\mathbf{k}|r) \ll 1$ or smaller. Solution of (270) gives

$$k_r^R v_r + k_\phi v_\phi \approx 0, \quad \text{and} \quad k_r^I \approx -\frac{\eta_m \mathbf{k}^2}{|v_r|}, \quad (271)$$

where in this equation $\mathbf{k}^2 = (k_r^R)^2 + k_\phi^2$. Consistent with the first part of (12), we take $k_r^R = n_r/r$, where $n_r = \text{const}$. For the ADAF flows, we write the second part of (269) as $\eta_m = \alpha_m c_s r$. The second part of (271) then gives

$$k_r^I = -\left(\frac{\alpha_m c_s}{|v_r|}\right) \frac{n_r^2 + m^2}{r}, \quad (272)$$

where the quantity $\alpha_m c_s / |v_r| = \text{const}$.

The imaginary part of k_r gives an additional radial dependence of B_r and B_ϕ (and rA_θ), multiplying the earlier expressions (261), (262), and (265) by a factor r^δ , where $\delta = (\alpha_m c_s / |v_r|)(n_r^2 + m^2)$. For radial distances $r < r_{\text{equi}}$, we have equipartition with magnetic energy density $E_m \propto r^{-5/2}$ so that $|\mathbf{B}_p| \propto r^{-5/4}$. This requires $\delta = 3/4$ so that $|rA_\theta| \propto r^{3/4}$, which corresponds to the flux within a given tube decreasing as r decreases. The accretion speed is

$$|v_r| = \frac{4}{3}(n_r^2 + m^2)\alpha_m c_s. \quad (273)$$

Note that for the present solution the accretion depends on the magnetic diffusivity η_m but not the viscosity ν ; more general solutions have v_r dependent on both viscosity and diffusivity. Validity of this solution requires $|k_r^I|/|\mathbf{k}| = (3/4)/\sqrt{n_r^2 + m^2} \ll 1$. The field line pattern is similar to that in Fig. 8, but the number of field lines in a tube $\propto r^{3/4}$.

The magnitude of the magnetic field follows from the requirement that the inflow of angular momentum carried by the matter, $\dot{L}_{\text{mech}} = 4\pi r^3 < \sin \theta > \rho v_r v_\phi \approx 4\pi r^3 \rho v_r v_\phi < 0$, equal the outflow carried by the field, $\dot{L}_{\text{mag}} = -r^3 B_r B_\phi > 0$, which gives $\rho v_r^2 \approx$

$B_r^2/4\pi$. More generally, turbulent viscosity carries away part of the angular momentum in which case the magnetic field strength is reduced. For $r \leq r_{\text{equi}}$, we have $B_r = B_0(r_{\text{equi}}/r)^{5/4}$, and zero angular momentum flux gives

$$B_0 = \left(\frac{4(n_r^2 + m^2)\alpha_m(c_s/v_\phi)\sqrt{GM\dot{M}}}{3r_{\text{equi}}^{5/2}} \right)^{1/2}. \quad (274)$$

This gives $B_0 \approx 55$ G for $r_{\text{equi}} = 10^{15}$ cm, $M = 10^6 M_\odot$, $\dot{M} = 0.1 M_\odot/\text{yr}$, $\alpha_m = 0.1$, $c_s/v_\phi = 0.1$, and $n_r^2 + m^2 = 10^2$.

4.2. Stationary picture of the magnetic field distribution in quasi-spherical accretion: turbulence, equipartition and field annihilation; two-temperature advective disks

In an optically thin accretion disk at low mass accretion rates, the density of the matter is low and energy exchange between electrons and ions due to binary collisions is slow. In this situation, due to different mechanisms of heating and cooling for electrons and ions, they may have different temperatures. This situation was first discussed by Shapiro et al. (1976) where advection was not included in the heat equation. Narayan and Yi (1995) (see also Ichimaru, 1977), pointed out that advection in this case may be extremely important. It may carry the main energy flux into the black hole, resulting in a low radiative efficiency of the accretion of the order of 10^{-3} – 10^{-4} . These are termed advective dominated accretion flows (ADAFs). This conclusion of low radiative efficiency is valid only when the effects connected with magnetic field annihilation and heating of matter due to it are neglected.

In the ADAF solution, the ion temperature is of the order of the virial temperature $kT_i \sim GMm_i/r$. This means that even when matter is supplied with high angular momentum, the disk becomes very thick, forming a quasi-spherical accretion flow. It is connected also with an ‘‘alpha’’ prescription of viscosity. At high ion temperatures, which result from strong viscous heating, the ion pressure becomes high, making the viscosity very effective. Thus, in this situation where energy losses by the ions are low, the ‘‘alpha’’ viscosity prescription gives a kind of a ‘‘thermo-viscous’’ instability.

Heating increases the viscosity, and viscosity increases the heating. Development of this instability leads to formation of ADAF.

A full account of the the presence of a magnetic field in the flow changes considerably the picture of ADAF. As mentioned above, Schwartzman (1971) showed that the radial component of the magnetic field increases so rapidly in the spherical flow that equipartition between magnetic and kinetic energy is reached in the flow far from the black hole horizon. In the region where the main energy production occurs, there is equipartition. In the presence of an equipartition magnetic field, the efficiency of radiation during accretion to a black hole increases enormously from $\sim 10^{-8}$ up to ~ 0.1 (Schwartzman, 1971) due to the efficiency of a magneto-bremstrahlung radiation. Thus the possibility of spherical ADAF accretion flows was noticed long ago. Equipartition is maintained in the flow by continuous magnetic field reconnection/annihilation. The field annihilation of course heats the plasma by Ohmic heating.

Bisnovatyi-Kogan and Ruzmaikin (1974) showed that due to Ohmic heating the efficiency of spherical accretion to a black hole may become as high as $\sim 30\%$. As a consequence of equipartition, the rate of Ohmic heating is

$$T \frac{dS}{dr} = -\frac{3}{2} \frac{B^2}{8\pi r}. \quad (275)$$

In a supersonic radial accretion flow, equipartition between magnetic and kinetic energy was suggested by Schwartzman (1971) as

$$\frac{B^2}{8\pi} \approx \frac{\rho v_r^2}{2} = \frac{\rho GM}{r}. \quad (276)$$

For the disk accretion, where there is more time for a field dissipation, near equipartition between magnetic and turbulent energy was suggested by Shakura (1972). For the “alpha” viscosity prescription, this gives

$$\frac{B^2}{8\pi} \sim \frac{\rho v_i^2}{2} \approx \alpha_m^2 P, \quad (277)$$

where α_m characterizes the magnetic viscosity in a way similar to the turbulent α viscosity. Bisnovatyi-Kogan and Ruzmaikin (1976) first proposed the

relationship between viscous and magnetic Reynolds numbers, or between turbulent and magnetic viscosity coefficients

$$Re = \frac{\rho v l}{\eta}, \quad Re_m = \frac{\rho v l}{\eta_m}, \quad (278)$$

where the turbulent magnetic viscosity η_m is connected with a turbulent conductivity σ

$$\sigma = \frac{\rho c^2}{4\pi\eta_m}. \quad (279)$$

Taking $\eta_m = (\alpha_m/\alpha)\eta$, we get a turbulent conductivity

$$\sigma = \frac{c^2}{4\pi\alpha_m h v_s}, \quad v_s^2 = \frac{P_g}{\rho} \quad (280)$$

where the second formula neglects the radiation pressure. For spherical accretion, the turbulent conductivity may involve the typical size of a turbulent eddy ℓ_r , and turbulent viscosity v_t in (280) instead of h and v_s . In ADAF solutions, where the ion temperature is of the order of the virial one the two suggestions (276) and (277) almost coincide at $\alpha_m \sim 1$.

The heating of matter due to Ohmic dissipation may be obtained from Ohm’s law for radial accretion in the form

$$\begin{aligned} T \frac{dS}{dr} &= -\frac{\sigma \mathcal{E}^2}{\rho v_r} \approx -\frac{\sigma v_E^2 B^2}{\rho v_r c^2} \\ &= -\frac{B^2 v_E^2}{4\pi\rho\alpha_m v_r v_s l_t}. \end{aligned} \quad (281)$$

This coincides with (275) when $\alpha_m = 4rv_E/(3v_r l_t)$, or $l_t = 4rv_E^2/(3v_r v_s \alpha_m)$. Here, the electric field strength in a highly conducting plasma is of the order of $\mathcal{E} \sim v_E B/c$, $v_E \sim v_t \sim \alpha v_s$ for the radial flow.

Separate equations are required for the radial variation of the energy of the ions and that of the electrons,

$$\frac{dE_i}{dt} - \frac{P_i}{\rho^2} \frac{d\rho}{dt} = \mathcal{H}_{\eta_i} + \mathcal{H}_{B_i} - Q_{ie}, \quad (282)$$

$$\frac{dE_e}{dt} - \frac{P_e}{\rho^2} \frac{d\rho}{dt} = \mathcal{H}_{\eta_e} + \mathcal{H}_{B_e} + Q_{ie} - \mathcal{C}_{\text{brem}} - \mathcal{C}_{\text{cyc}}, \quad (283)$$

(Bisnovatyi-Kogan and Lovelace, 1997, 2000). Here, $d/dt = \partial/\partial t + v_r \partial/\partial r$. The rate of viscous heating of ions \mathcal{H}_{η_i} is obtained from (88) as

$$\begin{aligned}\mathcal{H}_{\eta_i} &= \frac{2\pi r}{\dot{M}} Q_+ = \frac{3}{2} \alpha \frac{v_K v_s^2}{r}, \\ \mathcal{H}_{\eta_e} &\leq \sqrt{\frac{m_e}{m_i}} \mathcal{H}_{\eta_i}.\end{aligned}\quad (284)$$

The equality in the last equation is related to binary collisions. Combining (70), (92), (86), and (90), we get

$$\begin{aligned}v_r &= \alpha \frac{v_s^2}{v_K \mathcal{F}}, \quad h = \sqrt{2} \frac{v_s}{v_K} r, \\ \rho &= \frac{\dot{M}}{4\pi\alpha\sqrt{2}} \frac{v_K^2 \mathcal{F}}{r^2 v_s^3},\end{aligned}\quad (285)$$

where $v_K = r\Omega_K$, $\mathcal{F} = 1 - (j_{\text{in}}/j)$. The rate of the energy exchange between ions and electrons due to binary collisions was obtained by Landau (1937) and Spitzer (1940) as

$$Q_{ie} \approx \frac{4(2\pi)^{1/2} n e^4}{m_i m_e} \left(\frac{T_e}{m_e} + \frac{T_i}{m_i} \right)^{-3/2} [\ell n \Lambda] (T_i - T_e), \quad (286)$$

with $\ell n \Lambda = \mathcal{O}(20)$ the Coulomb logarithm. Thermodynamic functions must take into account a possible relativistic effects for electrons the energy of which may exceed $m_e c^2$. Neglecting pair formation for an low density accretion disk, the pressure is

$$\begin{aligned}P_g &= P_i + P_e = n_i k T_e + n_e k T_p \\ &= n_e k (T_e + T_i).\end{aligned}\quad (287)$$

An approximate expression for the energy,

$$E_g = E_e + E_i \approx \frac{3}{2} \frac{m_e c^2 + 3kT_e}{m_e c^2 + kT_e} \frac{kT_e}{m_p} + \frac{3}{2} \frac{kT_i}{m_p}, \quad (288)$$

gives a smooth interpolation between nonrelativistic and relativistic electrons.

The electron bremsstrahlung $\mathcal{E}_{\text{brem}}$ and magneto-bremsstrahlung \mathcal{E}_{cyc} cooling of Maxwellian, semi-relativistic electrons, with account of free-bound radiation in the nonrelativistic limit, may be written as

$$\mathcal{E}_{\text{brem}} \approx \frac{2 \times 10^{30} m_e c^2 + 3 \times 10^{32} (kT_e)^{3/2}}{m_e c^2 + kT_e} (kT_e)^{1/2}, \quad (289)$$

$$\mathcal{E}_{\text{cyc}} \approx \frac{1.7 \times 10^{16} m_e c^2 + 1.7 \times 10^{22} (kT_e)^2}{m_e c^2 + kT_e} kT_e B^2. \quad (290)$$

by interpolation of limiting cases (Bisnovatyi-Kogan and Ruzmaikin, 1976).

Effects of the cyclotron self-absorption may be important for nonrelativistic electrons, where radiation itself is low. With increasing of the electron temperature self-absorption effects decrease, because the black-body emission increase with a temperature ($\sim T^4$) more rapidly then magneto-bremsstrahlung volume losses. The theory of the self-absorption of cyclotron emission has been developed by by Trubnikov (1958, 1973).

In the case of disk accretion there are several characteristic velocities, v_K , v_r , v_s , and $v_t = \alpha v_s$, all of which may be used for determining the “equipartition” magnetic energy density. There is one characteristic length, h . Consider the three possible choices with $v_B^2 = v_K^2$, v_r^2 , and v_t^2 for scaling $B^2 = 4\pi\rho v_B^2$. (Note that the choice of cross products of different velocities and of v_s is also possible.) We get the following expressions for the magnetic field strengths in different cases,

$$\begin{aligned}\text{a. } v_B &= v_K, \quad \frac{B^2}{8\pi} = \frac{\rho v_K^2}{2}, \quad B = \left(\frac{\dot{M}}{\alpha\sqrt{2}} \frac{v_K^4 \mathcal{F}}{r^2 v_s^3} \right)^{1/2}, \\ \text{b. } v_B &= v_r, \quad \frac{B^2}{8\pi} = \frac{\rho v_r^2}{2}, \quad B = \left(\frac{\dot{M}\alpha}{\sqrt{2}\mathcal{F}} \frac{v_s}{r^2} \right)^{1/2}, \\ \text{c. } v_B &\sim v_t, \quad \frac{B^2}{8\pi} = \frac{\alpha_m^2 \rho v_t^2}{\alpha^2 2}, \\ &B = \alpha_m \left(\frac{\dot{M}}{\alpha\sqrt{2}} \frac{v_K^2 \mathcal{F}}{r^2 v_s} \right)^{1/2},\end{aligned}\quad (291)$$

with account of (285).

Expressions for the Ohmic heating in a turbulent accretion disk can also be written in different ways, using different velocities v_E in the expression for the scale of the electrical field,

$$\mathcal{E} = v_E B / c. \quad (292)$$

Self-consistency of the model requires that expressions for the magnetic heating \mathcal{H}_B , obtained from the condition of stationarity of the flow (275), and from Ohm's law (281) be identical. That gives restrictions on the choice of a characteristic velocity in (292). Comparison of (275) and (281) with account of (280) and (285) shows the identity of these two expressions for

$$\frac{\alpha}{\mathcal{J}\alpha_m} \frac{v_E^2}{v_r^2} = \frac{3\sqrt{2}}{4}. \quad (293)$$

This implies $v_E \sim v_r \sim \alpha v_s^2 / (v_K \sqrt{\mathcal{J}}) \approx v_i v_s / (v_K \sqrt{\mathcal{J}}) < v_i$. Thus the model is self-consistent for a reasonable choice of the parameters. Note, that in the ADAF models, \mathcal{J} is replaced by another function which is not zero at the inner edge of the disk. The heating due to magnetic field reconnection \mathcal{H}_B in Eqs. (282) and (283), obtained from (275) and (291), can be written with account of (284) as

$$\mathcal{H}_B = \frac{3}{16\pi} \frac{B^2}{r\rho} v_r = \frac{1}{2\mathcal{J}} \mathcal{H}_{\eta_i} \left(\frac{v_B}{v_K} \right)^2. \quad (294)$$

Thus for $v_B = v_K$ the expressions for viscous and magnetic heating are almost equal. The partition of the magnetic heating between electrons and ions has a critical influence on the model. Bisnovaty-Kogan and Lovelace (2000) have argued that the Ohmic heating goes mainly into heating the electrons. Thus, viscous heating of ions is expected to be comparable to Ohmic heating of electrons. Observations of magnetic field reconnection events in the Solar corona (Tsuneta, 1996) indicate that electron heating is dominant in a majority of events. A further effect acting to heat electrons is the ion-electron energy exchange which may be greatly enhanced over the binary collision rate (286) owing to plasma turbulence in the presence of a magnetic field.

It follows from the physical picture of magnetic field reconnection that transformation of the magnetic energy into heat is connected with the destruction of magnetic flux and the generation of rotational electrical field. This electric field has an outer scale-length of the order of the turbulent eddy size and it varies rapidly. The forces on the electrons and the protons in this field are identical, but the accelerations differ by a factor ~ 2000 . Consequently, during a sufficiently short time of the turbulent

fluctuations, the electrons may gain much more energy than the protons.

Bisnovaty-Kogan and Lovelace (1997) solved Eqs. (282) and (283) in the approximation of nonrelativistic electrons, $v_B = v_K$, which allowed the combination of viscous and magnetic heating into a unique formula. The combined heating of electrons and ions is

$$\mathcal{H}_e = (2 - g)\mathcal{H}_{\eta_i}, \quad \mathcal{H}_i = g\mathcal{H}_{\eta_i}. \quad (295)$$

In the expression for a cyclotron emission, self-absorption was taken into account according to Trubnikov (1973). The results of calculations for $g = 0.5-1$ show that almost all energy of the electrons is radiated, so the relative efficiency of the two-temperature, optically thin disk accretion cannot become less than 0.25. Note again that accurate account of plasma turbulence for ion-electron energy exchange may increase Q_{ie} sufficiently so that the relative efficiency is of order unity. Thus the radiative efficiency of the ADAF solutions including a magnetic field may be comparable to that of optically thick disks.

Studies of the solar corona have led to the general conclusion that the energy build up in the chaotic coronal magnetic field by slow photospheric driving is released by magnetic reconnection events or flares on a wide range of scales and energies (Benz, 1997). The observations support the idea of "fast reconnection," not limited to a rate proportional to an inverse power of the magnetic Reynolds number (Parker, 1979, 1990). The data clearly show the rapid acceleration of electrons (e.g., hard X-ray flares, Tsuneta, 1996) and ions (e.g., gamma ray line events and energetic ions, Reames et al., 1997), but the detailed mechanisms of particle acceleration are not established.

An essential aspect of the coronal heating is the continual input of energy to the chaotic coronal magnetic field due to motion of the photospheric plasma. As emphasized here, there is also a continual input of energy to the chaotic magnetic in a quasi-spherical accretion flow due to compression of the flow. The fact that the ratio of the plasma to magnetic pressures is small in the corona but of order unity in the accretion flow may of course affect the details of the plasma processes.

In magnetic field reconnection plasma flows into

the neutral layer from above and below with a speed of the order of the turbulent velocity v_t . Magnetic flux is destroyed in this layer as required for the reasons discussed earlier. Consequently, there is an electric field in the z -direction $\mathcal{E}_z = -(1/c)\partial A_z/\partial t = \mathcal{O}(v_t B_0/c)$, where B_0 is the field well outside of the neutral layer. This is the same as the estimate of the electric field given by Bisnovatyi-Kogan and Lovelace (1997). In the vicinity of the neutral layer ($|y| \ll \ell_t$) this electric field is typically much larger than the Dreicer electric field for electron runaway $E_D = 4\pi e^3(n_e/kT_e) \ln \Lambda$ (Parail and Pogutse, 1965), and this leads to streaming motion of electrons in the z -direction. Note that it is much more difficult to have ion runaway because of the large gyro radii of ions (Bisnovatyi-Kogan and Lovelace, 1997; Lesch, 1991; Romanova and Lovelace, 1992). Of course, in the almost uniform magnetic field assumed by Quataert (1998) there may be no runaway of particles.

The streaming of the electrons can give rise to a number of different plasma instabilities the growth of which gives an anomalous resistivity. Galeev and Sagdeev (1983) discuss the quasi-linear theory for such conditions and derive expressions for the rate of heating of electrons,

$$\frac{dT_e}{dt} = \frac{1}{n} \int \frac{d^3k}{(2\pi)^3} \gamma_k W_k \frac{\mathbf{k} \cdot \mathbf{u}_e}{\omega_k}, \quad (296)$$

and ions,

$$\frac{dT_i}{dt} = \frac{1}{n} \int \frac{d^3k}{(2\pi)^3} \gamma_k W_k, \quad (297)$$

where W_k is the wavenumber energy spectrum of the turbulence, γ_k is the linear growth rate of the mode with real frequency ω_k , n is the number density, and \mathbf{u}_e is the electron drift velocity. If the quantity $\mathbf{k} \cdot \mathbf{u}_e/\omega_k$ is assumed constant and taken out of the integral sign in (19), then the ratio of heating of electrons to that of ions is

$$\frac{dT_e}{dT_i} = \frac{u_e}{(\omega/k)}. \quad (298)$$

This result is independent of the instability type. Galeev and Sagdeev (1983) point out that for most instabilities, relation (29) predicts faster heating of electrons than ions. Earlier, Lesch (1991), Field and

Rogers (1993) and Di Matteo et al. (1998) emphasized the role of reconnection in accelerating electrons to relativistic energies in accretion flows of AGNs.

5. Accretion on to magnetized stars

5.1. Disk accretion on to a rotating star with an aligned dipole B-field

5.1.1. Introduction

The problem of matter accretion on to magnetized stars has been of continued interest since the discovery of X-ray pulsars in binary systems (Giacconi et al., 1971; Schreier et al., 1972; Tananbaum et al., 1972). The X-ray pulsars were interpreted as magnetized neutron stars, accreting matter from a companion star (Pringle and Rees, 1972; Davidson and Ostriker, 1973; Lamb et al., 1973; Rappaport and Joss, 1977). Of the more than 40 of known X-ray pulsars, most are in high-mass ($M_{\text{tot}} > 15$) binary systems, while only few are in low-mass ($M_{\text{tot}} < 3$) binary systems (see, for example, review by Nagase, 1989).

From the early observations, many X-ray pulsars were found to show secular decreases of pulse period (spin-up of the neutron star rotation) with relatively large rates of change of $-P/P = 10^{-2} - 10^{-6} \text{ yr}^{-1}$ (Gursky and Schreier, 1975; Schreier and Fabbiano, 1976; Rappaport and Joss, 1983). The long-term monitoring of X-ray pulsars during the last two decades have shown a wide variety of pulse-period evolution on different time-scales. Some X-ray pulsars show a steady spin-up evolution during many years which rapidly changes to a steady spin-down evolution (e.g., GX 1+4, SMC X-1, 4U 1626-67). Others show the wavy variations of P on time-scales of a few years on a background of systematic spin-up or spin-down (e.g., Cen X-3, Her X-1, Vela X-1) (Nagase, 1989; Sheffer et al., 1992; Bildsten et al., 1997).

Short-term fluctuations of pulse-period on time-scales of days to months, including clear evidence of spin-down episodes, were found for a number of sources, for example, Her X-1 (Giacconi, 1974), Cen X-3 (Fabbiano and Schreier, 1977), Vela X-1 (Nagase et al., 1984). Detailed observations of Vela X-1

with Hakucho and Tenma satellites, and with HEAO-1 have revealed fluctuations of large amplitude with time-scales about 3–10 days, which were estimated to be random in both amplitude and sign (Nagase, 1981). BATSE observations have shown that in some cases (Cen X-3, Her X-1) the timescale of fluctuations is less than 1 day with the change of sign from spin-up to spin-down and vice-versa (Bildsten et al., 1997). Note that some X-ray pulsars (usually the long-period ones) show no evidence of regular spin-up or spin-down (for example, 4U 0115+63, GX 301-2).

In some cases, like Her X-1, the existence of an accretion disk is indicated from various observations in the X-ray and optical bands (for example, Middleditch and Nelson, 1976; Bisnovaty-Kogan et al., 1977; Middleditch et al., 1985). In several other cases, such as Cen X-3, SMC X-1, GX 1+4 (Chakrabarty et al., 1997; Cui, 1997), and 4U 1626-67, there are also different kinds of evidence, that matter from companion star forms a disk (for example, Tjemkes et al., 1986; Nagase, 1989). Most of these are short-period pulsars with period about several seconds or less (excluding GX 1+4 with period 122 s). However, most of long-period pulsars, are supposed to be powered by the capture of stellar wind from companion. However if the companion is the star of Be type with slow rate of outflow, then it is probable that once again the disk first forms, opposite to the case when the companion star is of O–B kind with high speed of matter outflow (see review of Nagase, 1989).

Some aspects of matter accretion by magnetized neutron stars were considered for the first time by Bisnovaty-Kogan and Friedman (1969); and by Schwartzman (1971). Ideas on the spinning-up of pulsars by accretion were first proposed in the case of disk-fed pulsars by Pringle and Rees (1972); Lamb et al. (1973); and Lynden-Bell and Pringle (1974), and for wind-fed pulsars by Davidson and Ostriker (1973); and Illarionov and Sunyaev (1975) (see also Lipunov, 1993). The spin-down of a rapidly rotating magnetized star due to “propellar” action of the magnetosphere was suggested by Schwartzman (1971) and Illarionov and Sunyaev (1975), but a detailed model has not been worked out. Pringle and Rees (1972) considered matter accretion from a viscous disk to a magnetized rotating neutron star.

Their theory considered the idealized case of an aligned rotator where the magnetic moment of pulsar is aligned parallel or anti-parallel with the pulsar’s spin-axis and the normal to the plane of the accretion disk. They supposed that accreting matter stops at the point where the magnetic pressure of the magnetosphere becomes equal to pressure of matter. At this distance, matter transfers its angular momentum to the star through a thin boundary layer. Another idea regarding the width of the transition zone between the unperturbed accretion disk and magnetosphere, was considered in series of papers by Ghosh and Lamb (1978, 1979a,b). They assumed that magnetic field of the neutron star threads the accretion disk at different radii in a broad “transition” zone, in spite of predominance of the disk stress compared with magnetic stress in this region. Their work is based on the idea of anomalous resistivity connected with the supposed fast reconnection of toroidal component of the magnetic field lines across the disk.

Lovelace et al. (1995) (hereafter LRBK95) and Li and Wickramasinghe (1997) proposed an essentially different picture for disk accretion onto a star with an aligned dipole magnetic field. The idea is based on the fact that when there is a large difference between the angular velocity of the star and that of the disk, the magnetic field lines threading the star and the disk undergo a rapid inflation so that the field becomes open with separate regions of field lines extending outward from both the star and the disk. As a result, the magnetosphere consists of an open field line region far from the star and a closed region approximately corotating close to the star. This is shown schematically in Fig. 9. The LRBK95 model does not assume an anomalous resistivity, but rather a turbulent magnetic diffusivity proposed by Bisnovaty-Kogan and Ruzmaikin (1976), analogous to the turbulent α viscosity of Shakura (1972) and Shakura and Sunyaev (1973). This corresponds to a resistivity about 10^4 times smaller than that assumed by Ghosh and Lamb (1978, 1979a,b). Campbell (1992) has earlier discussed closed field line models of disk accretion onto an aligned dipole star assuming a magnetic diffusivity comparable to the turbulent α viscosity.

The existence of an open magnetic field region of the disk leads to the possibility of magnetically

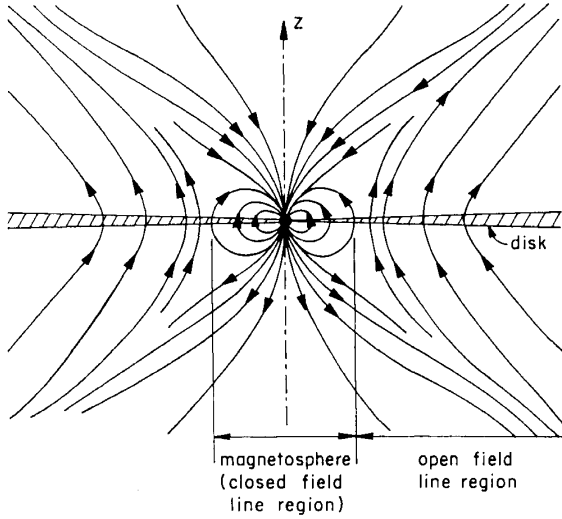


Fig. 9. Schematic drawing of the magnetic field configuration considered by LRBK95. The magnetosphere consists of an inner part, where the magnetic field lines are closed and an outer part where the field lines are open. The outer region where open field lines thread the disk gives rise to a MHD wind from the disk.

driven outflows. LRBK95 developed a model for magnetohydrodynamic (MHD) outflows and their back influence on the disk using the work on MHD outflows and magnetized disks by Blandford and Payne (1982); Lovelace et al. (1991); Lovelace et al. (1993); and Lovelace et al. (1994). In Sections 5.1.1–5.1.8 we review the arguments of LRBK95. In Section 5.2 we discuss the magnetic propeller regime of accretion first considered by Illarionov and Sunyaev (1975) and more recently by Lovelace et al. (1999a); hereafter LRBK99).

5.1.2. Theory

The basic equations for an assumed stationary plasma configuration are

$$\begin{aligned} \nabla \cdot (\rho \mathbf{v}) &= 0, \quad \nabla \times \mathbf{B} = \frac{4\pi}{c} \mathbf{J}, \\ \nabla \cdot \mathbf{B} &= 0, \quad \nabla \times \mathbf{E} = 0, \\ \mathbf{J} &= \sigma_e (\mathbf{E} + \mathbf{v} \times \mathbf{B}/c), \\ \rho (\mathbf{v} \cdot \nabla) \mathbf{v} &= -\nabla p + \rho \mathbf{g} + \frac{1}{c} \mathbf{J} \times \mathbf{B} + \mathbf{F}^{vis}. \end{aligned} \quad (299)$$

Here, v is the flow velocity, ρ is the density, σ_e is the effective electrical conductivity, \mathbf{F}^{vis} is the

viscous force density, $p = \rho k_B T/m$ is the gas pressure (with k_B the Boltzmann constant, m the mean particle mass, and with the radiation pressure assumed negligible), and \mathbf{g} is the gravitational acceleration. Outside of the disk, dissipative effects are considered to be negligible ($\sigma_e \rightarrow \infty, \mathbf{F}^{vis} = 0$, etc.). We neglect the self-gravity of the disk and relativistic effects so that $\mathbf{g} = -\nabla \Phi_g$ with $\Phi_g = -GM/(r^2 + z^2)^{1/2}$, where M is the mass of the central star. Eqs. (299) are supplemented later by an equation for the conservation of energy in the disk.

A general axisymmetric \mathbf{B} -field can be written as $\mathbf{B} = \mathbf{B}_p + \hat{\phi} B_\phi$, where $\mathbf{B}_p = \nabla \times (\hat{\phi} \Psi/r)$ is the poloidal field, B_ϕ is the toroidal field, and Ψ is the flux function (see, for example, Mestel, 1968, or Lovelace et al., 1986). We use a non-rotating cylindrical coordinate system so that $\mathbf{B}_p = (B_r, 0, B_z)$. Notice that $\Psi(r, z) = \text{const}$ labels a poloidal field line, $(\mathbf{B}_p \cdot \nabla) \Psi = 0$, or a flux-surface if the poloidal field line is rotated about the z -axis. For the present problem, the \mathbf{B}_p field can be represented as $\Psi = \Psi_* + \Psi'$, with Ψ_* the star's field-assumed to be a dipole $\Psi_* = \mu r^2 (r^2 + z^2)^{-3/2}$ and with Ψ' due to the non-stellar toroidal currents.

5.1.3. Inflation and opening of coronal \mathbf{B} -field

Fig. 10 shows the poloidal projections of two nearby field lines connecting the star and the disk. Because $\partial/\partial t = 0$, the \mathbf{E} field is electrostatic and the poloidal plane line integral of \mathbf{E} around the loop, $1 \rightarrow 2 \rightarrow 3 \rightarrow 4 \rightarrow 1$, is zero. Because of axisymmetry and the fact that $\mathbf{E} + \mathbf{v} \times \mathbf{B}/c = 0$ outside of the disk, the line integrals of \mathbf{E} along the two curved segments in Fig. 10 vanish separately. That is, the electrostatic

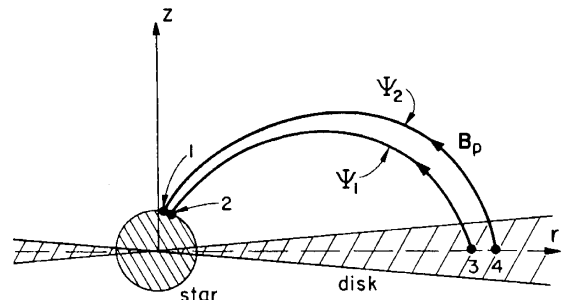


Fig. 10. This shows two poloidal field lines used in the derivation of Eq. (300).

potential is a constant on any given flux surface (see, for example, Lovelace et al., 1986). The potential difference between the points (1,2) on the star's surface is $-\delta\mathbf{r}_{12} \cdot \mathbf{E}_* = \omega_* \delta\Psi/c$, with $\delta\Psi \equiv \Psi_1 - \Psi_2$, where we have assumed that the star is perfectly conducting [$\mathbf{E}_* = -(\mathbf{v} \times \mathbf{B})_*/c$], and where ω_* is the angular rotation rate of the star. Thus, we have $\delta r_{34}(E_r)_d = -\omega_* \delta\Psi/c = -\omega_* r B_z(r, 0) \delta r_{34}/c$, where the path element δr_{34} is in the mid plane of the disk, and the “d” subscript indicates that the quantity is evaluated in the disk. In turn, we have $E_r|_d = (J_r/\sigma_e - v_\phi B_z/c)_d$. From Ampère's law, $J_r = -(c/4\pi)(\partial B_\phi/\partial z)$, the fact that B_ϕ is necessarily an odd function of z , and the approximation $\partial B_\phi/\partial z = (B_\phi)_h/h$, we have $J_r \alpha \approx -(c/4\pi)(B_\phi)_h/h$, where h is the half-thickness of the disk, and the notation $(\cdot \cdot \cdot)_h$ indicates that the quantity is evaluated at $z = h$. Combining these results gives for stationary conditions

$$(B_\phi)_h(r) = -\frac{hr}{\eta_t} [\omega_d(r) - \omega_*] B_z(r), \quad (300)$$

where $\eta_t = c^2/(4\pi\sigma_e)$ is the magnetic diffusivity of the disk, and ω_d is the angular rotation rate of the disk. The fractional variation in B_z between the midplane and surface of the disk is negligible [$O(h/r)$] if the disk is thin in the sense that $h/r \ll 1$. For the conditions of interest here, it follows from (70) that $h/r \leq c_s/v_K$, where $c_s \equiv (k_B T/m)^{1/2}$ the Newtonian sound speed based on the mid-plane temperature of the disk, and $v_K = (GM/r)^{1/2}$ is the Keplerian velocity at r . Campbell (1992) has independently derived equation (300) but does not place any limit on the ratio $|B_\phi/B_z|$.

In contrast with the work of Ghosh and Lamb (1978, 1979a,b), we assume that the magnetic diffusivity of the disk η_t is of the order of magnitude of the disk's effective viscosity (see Bisnovatyi-Kogan and Ruzmaikin, 1976; Parker, 1979; Campbell, 1992). Additionally, we assume that the disk viscosity is the turbulent viscosity as formulated by Shakura (1972) and Shakura and Sunyaev (1973), $\nu_t = (2/3)\alpha c_s h$, where α is a dimensionless quantity less than unity. In this work, we assume that α is in the range 10^{-1} to 10^{-2} . The possible contribution to the turbulent momentum flux due to small-scale magnetic field fluctuations is assumed included in α (Eardley and Lightman, 1975; Coroniti, 1981; Bal-

bus and Hawley, 1992; Kaisig et al., 1992; Rastätter and Schindler, 1999). We write $\eta_t = D\nu_t$ where D is dimensionless and of order unity.

With η_t the turbulent diffusivity, Eq. (300) gives $|(B_\phi)_h/B_z| = (3/2)r|\omega_d(r) - \omega_*|/(\alpha D c_s)$. This ratio is a measure of the twist of the \mathbf{B} field between the star and the disk. For the outer part of the disk $\omega_d(r)$ is expected to be close to the Keplerian value $\omega_K = (GM/r^3)^{1/2}$. Thus, it would appear that the twist $|(B_\phi)_h/B_z|$ can be very much larger than unity, say, > 10 . We argue here that such large values of the twist do not occur.

For a discussion of the limitation on the twist $|(B_\phi)_h/B_z|$ we consider that the plasma outside of the disk is force-free, $\mathbf{J} \times \mathbf{B} = 0$, which is the coronal plasma limit of Gold and Hoyle (1960). This limit is valid under conditions where the kinetic energy density of the plasma is much less than $\mathbf{B}^2/8\pi$. The general response of force-free coronal magnetic field loops to stress (differential twisting) applied to the loop foot points (in the solar photosphere) has been studied intensely by Aly (1984, 1991); Sturrock (1991); and Porter et al. (1992). The conclusion of these studies is that a closed field loop with a small twist evolves into an open field-line configuration as the twist is increased. The related problem of the twisting of a force free magnetic field configuration with foot points at different radii in a Keplerian disk has been studied by Newman et al. (1992); and Lynden-Bell and Boily (1994). The twisting due to the differential rotation of the disk acts to increase the total magnetic energy of the coronal field and this in turn acts to “inflate” the field.

An alternative measure of the field twist between the star and the disk is simply the difference in the azimuthal location, $\Delta\phi$, of the stellar and disk foot points of a given flux tube. We have $r d\phi/dl_p = B_\phi(r, z)/|B_p(r, z)|$, where dl_p is the length element along a poloidal field line $\Psi(r, z) = \text{const}$. Because $rB_\phi(r, z)$ depends only on Ψ in a force-free plasma, we have

$$\Delta\phi = [r(B_\phi)_h]_{\text{disk}} \int_{\text{star}}^{\text{disk}} \frac{dl_p}{r|\nabla\Psi|}. \quad (301)$$

For small $\Delta\phi$ (say, < 1), the poloidal field is close to that of a dipole, and the integral gives $\Delta\phi = C_t [(B_\phi)_h/B_z]_d$ with $C_t = 8/15$. For increasing $\Delta\phi$, the value of C_t increases because of the longer path

length and the smaller value of $|\nabla\Psi|$. The present situation is analogous to a current-carrying plasma column with a longitudinal B field. For the plasma column there is the well-known Kruskal–Shafranov stability condition (see, for example, Bateman, 1980) on the twist $\Delta\phi$ of the field (at the column's surface) over the length of the column. This condition, $\Delta\phi < 2\pi$, is required for stability against symmetry changing kink perturbations. A related, non-axisymmetric instability may accompany the above-mentioned inflation and opening of the star/disk field in response to increasing $\Delta\phi$.

LRBK95 argued that there is a definite upper limit on the twist $\Delta\phi$ of any field lines connecting the star and the disk. This limit implies a corresponding limit on $|(B_\phi)_h/B_z|_d$ in Eq. (300). If $\Delta\phi$ is larger than this limit, then the field is assumed to be open as indicated in Fig. 9.

5.1.4. Equations for disk

The flow velocity in the disk is $v(r) = -u(r)\hat{r} + v_\phi(r)\hat{\phi}$, where u is the accretion speed. The surface density of the disk is σ . The main equations are:

1. Mass conservation:

$$\dot{M} = 2\pi r\sigma u, = \text{const.} \quad (302)$$

We assume that the change of \dot{M} with r due to possible MHD outflows is small.

2. Radial force balance:

$$\frac{\sigma v_\phi^2}{r} = \frac{GM\sigma}{r^2} - \frac{(B_r B_z)_h}{2\pi} + \frac{d}{dr} \int_{-h}^h dz p. \quad (303)$$

3. Angular momentum conservation:

$$\frac{d}{dr}(\dot{M}F) = -r^2(B_\phi B_z)_h, \quad (304)$$

$$F \equiv r^2\omega + \frac{r^2 v_t}{u} \frac{d\omega}{dr},$$

where $\omega = v_\phi/r$. The term $-r^2(B_\phi B_z)_h$ represents the outflow of angular momentum from the $\pm z$ surfaces of the disk (that is, a torque on the disk). We assume that the angular momentum carried by the matter of the outflow is small compared with that carried by the field. If the B field at r is open as discussed in Section 5.1.3, then the angular momentum outflow from the disk is carried to infinity. On

the other hand, if the field is closed, then the angular momentum outflow from (or inflow to) the disk is carried by the coronal B field to (or from) the star.

4. Energy conservation:

$$\sigma v_t \left(r \frac{d\omega}{dr} \right)^2 + \frac{4\pi}{c^2} \int_{-h}^h dz \eta_t \mathbf{J}^2 = \frac{4acT^4}{3\kappa\sigma} \quad (305)$$

$$\equiv 2\sigma_B T_{\text{eff}}^4.$$

The first term is the viscous dissipation, the second is the Ohmic dissipation, while the third term is the power per unit area carried off by radiation (in the $\pm z$ directions) from the disk which is assumed optically thick. Here, κ is the opacity assumed due to electron scattering, a and $\sigma_B = ac/4$ are the usual radiation constants, T is the midplane temperature of the disk, and T_{eff} is disk's effective surface temperature.

5. Conservation of magnetic flux for a general time-dependent disk:

$$\frac{\partial}{\partial t}(rB_z) = \frac{\partial}{\partial r} \left[rB_z u - \frac{\eta_t r}{h} (B_r)_h \right],$$

where the generally small radial diffusion of the B_z field has been neglected (see LRN). The first term inside the square brackets represents the advection of the field while the second term represents the diffusive drift. In a stationary state,

$$\beta_r(r) \equiv \frac{(B_r)_h}{B_z} = \frac{uh}{\eta_t}. \quad (306)$$

6. Vertical hydrostatic equilibrium: The z -component of the Navier–Stokes equation (30) gives the condition for vertical hydrostatic balance which can be written as

$$\left(\frac{h}{r} \right)^2 + b \left(\frac{h}{r} \right) - \left(\frac{c_s}{v_K} \right)^2 = 0, \quad (307)$$

where c_s is the Newtonian sound speed based on the midplane temperature of the disk, and $b \equiv r[(B_r)_h^2 + (B_\phi)_h^2]/(4\pi\sigma v_K^2)$ (Wang et al., 1988). Radiation pressure is negligible for the conditions of interest. For $b \ll 2c_s/v_K$, this equation gives the well-known relation $h/r = c_s/v_K$ (Shakura and Sunyaev, 1973), while for $b \gg 2c_s/v_K$ it gives $h/r = b^{-1}(c_s/v_K)^2$

which is smaller than c_s/v_K owing to the compressive effect of the magnetic field external to the disk (Wang et al., 1988) It is useful to write $b = \epsilon \beta^2$, where $\epsilon \equiv rB_z^2(r, 0)/(2\pi\sigma v_K^2)$ and $\beta^2 \equiv [(B_r)_h^2 + (B_\phi)_h^2]/(2B_z^2)$. In Section 5.1.6, we discuss that $\beta = O(1)$ in order to have outflows from the disk, and $\beta \leq 1$ with no outflows. Thus, the Alfvén speed in the midplane of the disk is $v_A = v_K \epsilon^{1/2} (h/r)^{1/2}$. We may term the magnetic field as weak if $\epsilon < c_s/v_K \approx h/r$. In this limit, $v_A/c_s \approx (\epsilon r/h)^{1/2} \leq 1$, and the magnetic compression of the disk is always small. In the opposite, strong field limit, $\epsilon > c_s/v_K$. If at the same time $\beta = O(1)$, then the disk is magnetically compressed, and for $\epsilon \gg c_s/v_K$, $v_A/c_s = 1/\beta$.

Note that with the magnetic field terms neglected these equations give the Shakura and Sunyaev (1973) solution for region “b”.

5.1.5. Magnetically driven outflows

Consider the outer region of the disk where the value of the field twist $\Delta\phi$ given by Eq. (301) [or $|(B_\phi)_h/B_z|$ of Eq. (300)] is larger than a critical value. In this region the B field threading the disk is open as discussed in Section 5.1.3. The angular momentum flux carried by the disk is $\dot{M}F$. If the angular rotation of the disk is approximately Keplerian, $\omega(r) \approx \omega_K(r)$, then the viscous transport contribution to F is $r^2(v/u)(d\omega/dr) \approx -(3/2)r^2\omega[h/(\beta_r r)]$. As discussed in detail below a necessary condition for MHD outflows is that $\beta_r = O(1)$. Consequently, the viscous contribution to F in Eq. (304) is smaller than the bulk transport term by the small factor $h/r < 1$, and $F \approx \omega r^2$.

In Eq. (304) we therefore have $d(\dot{M}F)/dr \approx \dot{M}\omega_K r/2$. In Eq. (304) we let $(B_\phi)_h = -\beta_\phi B_z(r, 0)$. Studies of MHD outflows (Blandford and Payne, 1982, LBC, LRC) indicate that $\beta_\phi = \text{const} = O(1)$. As a result, Eq. (304) implies that

$$[B_z(r, 0)]_w = k/r^{5/4}, \text{ with } k \\ = [\dot{M}(GM)^{1/2}/(2\beta_\phi)]^{1/2}, \quad (308)$$

where the w subscript indicates the wind region of the disk. Of course at a sufficiently small radius, denoted r_{wi} , the outflow ceases, and the dependence of $B_z(r, 0)$ reverts to approximately the stellar dipole field, μ/r^3 . As a consistency condition we must have

$$\mathcal{E} = (k/r_{wi}^{5/4}) / (\mu/r_{wi}^3) = \left[\frac{\dot{M}(GM)^{1/2} r_{wi}^{7/2}}{\mu^2 (2\beta_\phi)} \right]^{1/2} \\ < 1. \quad (309)$$

The transition between the dipole and outflow field dependences is handled by letting $B_z(r, 0) = (\mu/r^3)g(r) + (k/r^{5/4})[1 - g(r)]$, where, for example, $g(r) = \{1 + \exp[(r - r_{wi})/\Delta r]\}^{-1}$ and $\Delta r/r_{wi} \ll 1$.

Eqs. (302)–(307) can be used to obtain the disk parameters in the region of outflow. As shown below the viscous dissipation is much larger than the Ohmic, and Eq. (305) then gives $T = [81\dot{M}^2(GM)^{1/2}\kappa/(128\pi^2\alpha D\beta_r^2 ac)]^{1/4} r^{-7/8}$. For illustrative values, $M = 1 M_\odot$, $\dot{M} = 10^{17}$ g/s $\approx 1.6 \times 10^{-9} M_\odot/\text{yr}$, $\alpha = 0.1$, $\beta_r = 0.58$, and $D = 1$, we find at the representative distance $r = 10^8$ cm that $T \approx 0.44 \times 10^6$ K, $v_K = 1.15 \times 10^9$ cm/s, $c_s = 7.6 \times 10^6$ cm/s, $u = 0.88 \times 10^6$ cm/s, $\sigma = 180$ g/cm², and $h/r = 6.6 \times 10^{-3}$. The ratio of the ohmic dissipation to that due to viscosity is: $(4/27)\alpha D\beta_r^3 \ll 1$. The ratio of the viscous dissipation to the power output of the outflows (the $\pm z$ Poynting fluxes) (per unit area of the disk) is: $(9/2)(h/r)(\beta_r D)^{-1} \ll 1$. Thus, most of the accretion power for $r > r_{wi}$ goes into the outflows. However, the fraction of the total accretion power in outflows is small if $r_{wi} \gg r_*$, where r_* is the star’s radius ($\sim 10^6$ cm for a neutron star). Note that $\dot{M} = 10^{17}$ g/s and $M = 1 M_\odot$ correspond to a total accretion power or luminosity $L_0 = GMM/r_* \approx 1.33 \times 10^{37}$ (erg/s)(10^6 cm/ r_*).

Conservation of the poloidal flux threading the disk implies that there is an outer radius, denoted r_{wo} , of the outflow from the disk. That is, we have $\int_{r_{wi}}^{r_{wo}} dr(k/r^{5/4}) = \int_{r_{wi}}^{r_{wo}} r dr(\mu/r^3)$. Thus, the outer radius is $r_{wo} \approx r_{wi}(f\mathcal{E})^{-4/3}$, where $f \approx 1$ for $1 - \mathcal{E} \ll 1$ and $f = 3/4$ for $\mathcal{E} \ll 1$. For $r > r_{wo}$, $B_z(r, 0)$ rapidly approaches zero.

Eq. (307) gives the disk thickness. From Eq. (308), we have $\epsilon = rB_z^2/(2\pi\sigma v_K^2) = (u/c_s)(c_s/v_K)/(2\beta_\phi)$. The magnetic compression of the disk is small if $\epsilon < c_s/v_K$ or equivalently if $u/c_s < 1$. Our numerical solutions have $u/c_s < 1$ in the region of outflow.

5.1.6. Necessary condition for MHD outflows

A necessary condition on β_r for MHD outflows from the disk can be obtained by considering the net force \mathcal{F}_p on a fluid particle in the direction of its

poloidal motion above the disk. Notice that for stationary flows, the poloidal flow velocity v_p is parallel to \mathbf{B}_p owing to the assumed axisymmetry and perfect conductivity. However, in general $v \times \mathbf{B} \neq 0$ so that the fluid particles do not move like “beads on a wire”. Above, but close to the disk ($h \leq z \ll r$), we assume that the poloidal field lines are approximately straight. Thus, the poloidal position of a fluid particle above the disk is $\mathbf{r} = (r_o + S \sin(\theta))\hat{\mathbf{r}} + S \cos(\theta)\hat{\mathbf{z}}$, where S is the distance along the path from the starting value $S_o = h / \cos(\theta)$ at a radius r_o , $\tan(\theta) = (B_r)_h / B_z = \beta_r$, and $z = S \cos(\theta)$. The effective potential is $U(S) = -(1/2)\omega_o^2(r_o + S \sin(\theta))^2 - GM/|\mathbf{r}|$ (LRN), and the force in the direction of the particle’s poloidal motion is $\mathcal{F}_p = -\partial U / \partial S$. For distances z much less than the distance to the Alfvén point, $\omega_o \approx \omega_K(r_o)$. In this way we find

$$\mathcal{F}_p = -(\omega_K^2 - \omega^2)r \left(\frac{B_r}{|\mathbf{B}_p|} \right) + \omega_K^2 z (3\beta_r^2 - 1) \left(\frac{B_z}{|\mathbf{B}_p|} \right), \quad (310)$$

for $h \leq z \ll r$, where we assume $B_z > 0$.

The slow magnetosonic point of the outflow occurs where $\mathcal{F}_p = 0$ (LRC) at the distance

$$z_s = r \left(1 - \frac{\omega^2}{\omega_K^2} \right) \frac{\beta_r}{3\beta_r^2 - 1}. \quad (311)$$

The factor $1 - (\omega/\omega_K)^2$ can be obtained from the radial force balance equation (303). The radial pressure force is small compared with the magnetic force for the conditions we consider, $\alpha\beta_r^2/(3\beta_\phi) > h/r \ll 1$. Thus,

$$\frac{z_s}{h} = \left(\frac{2\alpha D B_z^2 r}{3M\omega_K} \right) \frac{\beta_r^3}{3\beta_r^2 - 1}. \quad (312)$$

For $r_{wi} < r < r_{wo}$, the quantity in brackets is simply $\alpha/(3\beta_\phi)$ owing to Eq. (308). Note that the minimum of $\beta_r^3/(3\beta_r^2 - 1)$ is $1/2$ at $\beta_r = 1$. If the gas near the surface of the disk ($h \lesssim z \leq z_s$) is assumed isothermal with temperature $T_1 \ll T$ and sound speed $c_{s1} \equiv (k_B T_1 / m)^{1/2}$, then the density at the slow magnetosonic point ρ_s can be obtained using the MHD form of Bernoulli’s equation. At the slow magnetosonic point, the poloidal flow speed is $v_p = c_{s1} |\mathbf{B}_p| / |\mathbf{B}| \equiv$

v_{sm} , the slow magnetosonic speed, and $\rho_s = \rho_h \exp\{-1/2 - [U(z_s) - U(h)]/c_{s1}^2\}$, where U is now regarded as a function of z . In turn, the mass flux density from the $+z$ surface of the disk is $\rho_s v_{sm} \cos(\theta) = \rho_s c_{s1} B_z / |\mathbf{B}|$.

The consistency of the magnetically driven outflow solutions requires $z_s \gtrsim h$. If this were not the case, the outflows would be matter rather than field dominated near the disk. There are two possible regimes having $z_s \gtrsim h$: one is with $\alpha D / (3\beta_\phi) < 1$ [or $\alpha D / (3\beta_\phi) \ll 1$] and $\beta_r \gtrsim 1/\sqrt{3}$; another is with $\alpha D / (6\beta_\phi) > 1$ and $\beta_r > 1$. In the present work, we consider the first regime which is consistent in the following respect: The magnetic pinching force on the inner part of the outflow ($r < r_{wo}$) increases as the mass flux in the outflow increases (LBC). In turn, an increase in the pinching force acts to decrease $\beta_r = (B_r)_h / B_z$ thereby increasing z_s/h and decreasing the mass flux in the outflow.

In addition to the condition $z_s \gtrsim h$, the slow magnetosonic point must be at a distance z_s not much larger than h , say $2h$, in order for the outflow to have a non-zero mass flux. At the inner radius of the outflow, r_{wi} , the $B_z(r, 0)$ field in the disk is $\mu / (2r_{wi}^3)$ as discussed in Section 5.1.5. We then have

$$\begin{aligned} r_{wi} &\gtrsim \left[\frac{\alpha D \mu^2}{24 \dot{M} (GM)^{1/2}} \right]^{2/7} \\ &\approx 0.75 \times 10^8 \text{ cm} \\ &\times \left[\left(\frac{\alpha D}{0.1} \right) \left(\frac{\mu}{10^{30} \text{ G cm}^3} \right)^2 \left(\frac{10^{17} \text{ g/s}}{\dot{M}} \right) \right. \\ &\left. \times \left(\frac{M_\odot}{M} \right)^{1/2} \right]^{2/7}, \end{aligned} \quad (313)$$

from Eq. (312). Note that from Eq. (309), we get $\mathcal{E} \gtrsim [\alpha D / (48\beta_\phi)]^{1/2}$ or $\mathcal{E} \gtrsim 0.046$ and $r_{wo} \lesssim 90 r_{wi}$ for $\alpha = 0.1$, $D = 1$ and $\beta_\phi = 1$.

5.1.7. MHD outflows and spin-up ($r_{to} < r_{cr}$)

We have numerically integrated Eqs. (302)–(307) assuming magnetically driven outflows from the disk. We integrate the equations inward starting from a large radial distance $r < r_{wo}$. The inner radius of the region of outflow is determined as discussed above. For $r < r_{wi}$, $dF/dr = 0$, and the solutions in this range of r all exhibit a “turn-over radius”, r_{to} , where $d\omega/dr = 0$. This “turn over” results from the

radially outward magnetic force in Eq. (303) which becomes stronger as r decreases. In the region close to the turnover, the magnetic compression of the disk becomes strong in that $\epsilon = O(1)$. From a least squares fitting of many integrations, we find

$$r_{to} \approx 0.91 \times 10^8 \text{ cm} \left(\frac{\alpha D}{0.1}\right)^{0.3} \left(\frac{\mu}{10^{30} \text{ G cm}^3}\right)^{0.57} \times \left(\frac{10^{17} \text{ g/s}}{\dot{M}}\right)^{0.3} \left(\frac{M_\odot}{M}\right)^{0.15}. \quad (314)$$

The turn-over radius is less than but in all cases close to r_{wi} . Thus, Eq. (314) is compatible with (313). Our radius r_{to} has a role similar to that of the Alfvén radius r_A of Ghosh and Lamb (1978, 1979a,b). The dependences we find of r_{to} on μ , \dot{M} , and M are close to those of r_A . However, our analysis shows an important dependence on αD which is proportional to the magnetic diffusivity of the disk. Furthermore, our r_{to} is smaller than r_A by a factor of about $(\alpha D/12)^{0.3}$, which is ≈ 0.24 for $\alpha D = 0.1$.

The turn-over radius is important in the respect that the inward angular momentum flux carried by the disk ($\dot{M}F$) is $\dot{M}\omega_{to}r_{to}^2$ because $d\omega/dr = 0$ at $r = r_{to}$. [Note that we do not consider here the possibility of significant poloidal current flow along the open field lines extending from the polar caps of the star ($B_\phi > 0$ for $z > 0$ in Fig. 9) which would act to remove angular momentum from the star to infinity.] From numerical integrations, we find to a good approximation that $\omega_{to} = (GM/r_{to}^3)^{1/2}$, so that the influx of angular momentum to the star is $\dot{M}F_{to} = \dot{M}(GMr_{to})^{1/2}$. Thus, the rate of increase of the star’s angular momentum J is:

$$\frac{dJ}{dt} = \dot{M}(GMr_{to})^{1/2}. \quad (315)$$

With I the moment of inertia of the star, $J = I\omega_*$, and $dJ/dt = (dI/dM)\dot{M}\omega_* + I(d\omega_*/dt)$. For the situation of interest, the term proportional to dI/dM is negligible because r_{to} is much larger than the star’s radius. Thus, we have “spin-up” of the star,

$$\frac{d\omega_*}{dt} = \frac{\dot{M}(GMr_{to})^{1/2}}{I},$$

or

$$\frac{1}{P} \frac{dP}{dt} \approx -5.8 \times 10^{-5} \frac{1}{\text{yr}} \left(\frac{P}{1\text{s}}\right) \left(\frac{\dot{M}}{10^{17} \text{ g/s}}\right) \times \left(\frac{10^{45} \text{ g cm}^2}{I}\right) \left(\frac{M}{M_\odot}\right)^{1/2} \left(\frac{r_{to}}{10^8 \text{ cm}}\right)^{1/2}, \quad (316)$$

where $P = 2\pi/\omega_*$ is the pulsar period. Because the total accretion luminosity $L = GMM/r_*$ with r_* the star’s radius, $\dot{P} \propto -P^2 L^{0.85} \mu^{0.285}$ for constant αD , r_* , and M .

Our outflow solutions are consistent only in the case where $\omega_{to} = (GM/r_{to}^3)^{1/2} > \omega_*$. In this case, with r decreasing from r_{to} , the rotation rate of the disk $\omega(r)$ decreases and approaches the rotation rate of the magnetosphere ($\approx \omega_*$) from above where it matches onto the magnetospheric rotation through a radially thin turbulent boundary layer. We find no consistent stationary solutions when $\omega(r)$ decreases below ω_* . The condition $\omega_{to} > \omega_*$ is the same as

$$r_{to} < r_{cr} \equiv \left(\frac{GM}{\omega_*^2}\right)^{1/3} \approx 1.5 \times 10^8 \text{ cm} \left(\frac{M}{M_\odot}\right)^{1/3} \left(\frac{P}{1\text{s}}\right)^{2/3}, \quad (317)$$

where r_{cr} is commonly referred to as the “co-rotation radius”. Note that r_{cr} decreases during spin-up. Thus, r_{cr} approaches r_{to} if r_{to} does not decrease rapidly.

5.1.8. Magnetic braking of star by disk; spin-up or spin-down ($r_{to} > r_{cr}$)

For $r_{to} > r_{cr}$, the B field in the outer part of the disk ($r \gg r_{cr}$) is open as discussed above, but there are no consistent stationary MHD outflows, $(B_\phi)_h = 0$, $\beta_r = hu/\eta_t \ll 1$, and the Ohmic dissipation is small compared with that due to viscosity. Thus, the outer part of the disk obeys essentially the equations of Shakura and Sunyaev (1973) for a Keplerian disk with $F = \text{const.} \equiv F_\infty$ in Eq. (304) undetermined. We show below that F_∞ can be determined self-consistently by considering the region near r_{cr} where the Keplerian accretion flow is brought into co-rotation with the star. Because there are no outflows, the angular momentum influx to the star is $\dot{M}F_\infty$ which is equal to dJ_*/dt .

In the region of the disk where $\omega(r)$ is close to ω_* ,

that is, where $r \sim r_{\text{cr}}$, $|(B_\phi)_h/B_z|$ given by Eq. (300) is *not* much larger than unity. In this region, closed but twisted field lines link the star and the disk. The twist of the field acts to remove (or add) angular momentum from (to) the disk if $B_\phi B_z > 0$ (or < 0). The angular momentum removed from the disk is deposited on the star via the B field. In this region of the disk the key equations are (300) and (304) which we rewrite as

$$\begin{aligned} \frac{d\omega}{dr} &= \frac{u}{r^2 \nu_t} (F - \omega r^2), \quad \frac{dF}{dr} \\ &= \frac{hr}{D \nu_t} (\omega - \omega_*) \left(\frac{r^2 B_z^2}{M} \right) H\left(\frac{\tau}{\tau_{\text{max}}} \right). \end{aligned} \quad (318)$$

Here, $H(x)$ is a Heaviside function such that $H(x) = 1$ for $|x| < 1$ and $H(x) = 0$ for $|x| > 1$;

$$\tau(r) \equiv \frac{(B_\phi)_h(r)}{B_z(r, 0)} = - \frac{hr}{D \nu_t} (\omega - \omega_*)$$

is a measure of the field twist; $\tau_{\text{max}} = \text{const}$ is the maximum value of the twist; and

$$F(r) \equiv r^2 \omega + \frac{r^2 \nu_t}{u} \frac{d\omega}{dr}.$$

We consider τ_{max} to be a universal constant. For $|\tau| > \tau_{\text{max}}$ the field configuration becomes open. In Eqs. (316), B_z is assumed to be the star's dipole field. The other equations of Section 5.1.4 are still needed. Note that both the viscous and Ohmic heating must be retained in the energy equation (305). The viscous dissipation is dominant for $r > r_{\text{cr}}$, while the Ohmic dissipation dominates for $r < r_{\text{cr}}$. Eqs. (303) and (306) can be combined to give u as a function of r , T , and ω . In turn, this expression for u can be combined with the energy conservation equation (305) to give both u and T as functions of r , ω , and $\partial\omega/\partial r$ if viscous heating dominates, or as functions of r and ω if Ohmic heating dominates. Furthermore, $\nu_t = (2/3)\alpha c_s h$ in Eq. (318) can be derived from T and h/r from Eq. (38) using β_r from Eq. (37), $\beta_\phi = -\tau$, and ϵ from B_z and u .

We have solved the equations (303), (305)–(307), and (318) by numerical integration starting from the outside, at a distance where $\tau > \tau_{\text{max}}$ and $F = \text{const} = F_\infty$, and integrating inward through r_{cr} . The fact that the value of F_∞ is not known a priori points to the use of a “shooting method” for its de-

termination. Using this approach, we find that there is in general a unique value of F_∞ , denoted F_∞^0 , such that the solution for $\omega(r)$ smoothly approaches ω_* for r decreasing below r_{cr} . If F_∞ is smaller than F_∞^0 , then $\omega(r)$ follows the Keplerian law as r decreases below r_{cr} . On the other hand, if F_∞ is larger than F_∞^0 , then $\omega(r)$ goes through a maximum and decreases rapidly to values much less than ω_* . The only physical solution is that with $F_\infty = F_\infty^0$. Hereafter, the zero superscript on F_∞ is implicit.

The behavior of Eqs. (318) can be understood qualitatively by noting that if $\omega(r)$ were to decrease linearly through r_{cr} , then the radial width of the region of braking, $dF/dr < 0$ where $\omega < \omega_*$, would equal that the width of the region of acceleration, $dF/dr > 0$ where $\omega > \omega_*$. Consequently, F would change by only a small fractional amount. However, if within the braking region $F(r)$ attains a value equal to ωr^2 , then $d\omega/dr = 0$ at this point and $d\omega/dr$ remains small and $\omega \approx \omega_*$ for smaller r . A rough estimation gives the radial width of the braking region as $\Delta r \sim \tau_{\text{max}} D c_s / \omega_K$, where c_s is based on the temperature just outside of this region, and the jump in F as $\Delta F \sim \tau_{\text{max}} \Delta r (r^2 B_z^2 / M)$.

Fig. 11 shows the dependence of F_∞ on μ and on \dot{M} for sequences of cases where r_{cr} is assumed comparable to r_{to} . This is clearly not a necessary choice; that is, r_{to} could differ significantly from r_{cr} . However, with $r_{\text{cr}} = r_{\text{to}}$, Fig. 11 allows a direct comparison of the angular momentum influx to the star ($\dot{M} F_K$) for the case of outflows ($r_{\text{to}} \leq r_{\text{cr}}$) with the influx ($\dot{M} F_\infty$) in the case of no outflows and magnetic braking ($r_{\text{to}} > r_{\text{cr}}$). Fig. 11 suggests that a bimodal behavior can occur where the star switches between spin-up and spin-down, owing to some extraneous perturbation.

5.2. Magnetic propeller regime

5.2.1. Introduction

Observations of some X-ray pulsars show remarkable “jumps” between states where the pulsar is spinning-down to one where it is spinning-up. Examples include the objects Cen X-3 (Bildsten et al., 1997) and GX 1+4 (Chakrabarty et al., 1997; Cui, 1997). The theoretical problem of disk accretion on to a rotating magnetized star has been discussed in

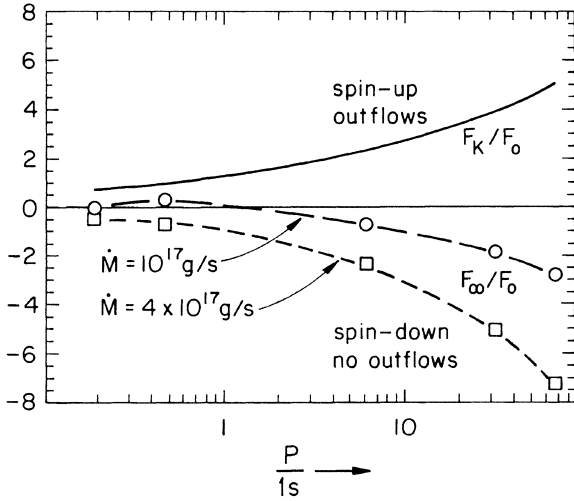


Fig. 11. The figure shows the dependence of F_∞ and $F_K = (GM_{cr})^{1/2}$ on the pulsar period P assuming $r_{cr} = r_{to}$ for $\dot{M} = 10^{17}$ g/s and 4×10^{17} g/s. The other parameters have been taken to be $\alpha = 0.1$, $D = 1$, $\tau_{max} = 5$, and $M = M_\odot$. Thus, each $\dot{M} = \text{const.}$ curve corresponds to different magnetic moments as $\mu \propto P^{1.17}$. F_∞ and F_K are measured in units of $(GM_{cr})^{1/2}$ with $r_o = 10^8$ cm. This plot allows a comparison of the angular momentum influx to the star ($\dot{M}F_K$) in the case of outflows and spin-up ($r_{to} < r_{cr}$) with the case of magnetic braking where the influx is $\dot{M}F_\infty$ ($r_{to} > r_{cr}$).

many works over a long period (Pringle and Rees, 1972; Lynden-Bell and Pringle, 1974; Ghosh and Lamb, 1979a,b; Wang, 1979; Lipunov, 1993; Lovelace et al., 1995 (referred to as LRBK95); Li and Wickramasinghe, 1997). However, except for the work by Li and Wickramasinghe (1997), the studies do not specifically address the “propeller” regime (Illarionov and Sunyaev, 1975) where the rapid rotation of the star’s magnetosphere acts to expel most of the accreting matter and where the star spins-down. Recent computer simulation studies of disk accretion on to a rotating star with an aligned dipole magnetic field (Hayashi et al., 1996; Goodson et al., 1997) provide evidence of time-dependent outflows but do not give definite evidence for a “propeller” regime with spin-down of the star. Recent computer simulation studies of disk accretion on to a rotating star with an aligned dipole magnetic field (Hayashi et al., 1996; Goodson et al., 1997; Miller and Stone, 1997) provide evidence of time-dependent outflows but do not give definite evidence for a “propeller” regime with spin-down of the star.

Lovelace et al. (1999b, hereafter LRBK99) de-

veloped a model for magnetic “propeller”-driven outflows which were first considered by Illarionov and Sunyaev (1975). Such outflows can cause a rapidly rotating magnetized star accreting from a disk to spin-down. Energy and angular momentum lost by the star goes into expelling most of the accreting disk matter. The envisioned geometry is shown in Fig. 9. The theory gives an expression for the effective Alfvén radius R_A (where the inflowing matter is effectively stopped) which depends on the mass accretion rate, the star’s mass and magnetic moment, and the star’s rotation rate. The model points to a mechanism for “jumps” between spin-down and spin-up evolution and for the reverse transition, which are changes between two possible equilibrium configurations of the system. In for example the transition from spin-down to spin-up states the Alfvén radius R_A decreases from a value larger than the corotation radius to one which is smaller. In this transition the “propeller” goes from being “on” to being “off.” The ratio of the spin-down to spin-up torque (or the ratio for the reverse change) in a jump is shown to be of order unity.

5.2.2. Theory

Consider disk accretion on to a rapidly rotating star so that the disk-star configuration is as sketched in Fig. 12. Consider the flow of mass, angular momentum, and energy into and out of the annular region indicated by the box $A'ACC'$ in this figure, where $A'A$ is at radius r_1 and CC' is at r_2 . Notice that at this point the values of r_1 and r_2 are *unknown*. They are determined by the physical considerations discussed here.

Consider first the outer surface CC' through the disk. The influx of mass into the considered region is

$$\dot{M}_{accr} = 2\pi r_2 \int_{-h}^h dz [\rho (-v_r)]_2 > 0, \quad (319)$$

where h is the half-thickness of the disk, and the 2 subscript indicates evaluation at $r = r_2$. We assume that mass accretion rate for $r \geq r_2$ is approximately constant equal to \dot{M}_{accr} . That is, we consider that outflow from the disk is negligible for $r \geq r_2$. The influx of angular momentum into the considered region is

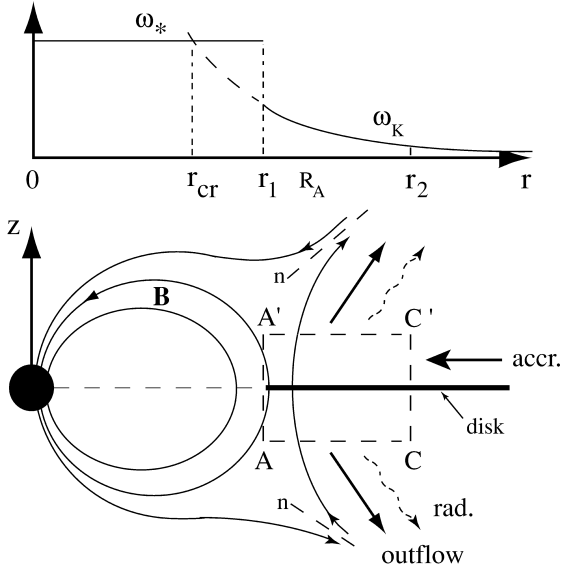


Fig. 12. Geometry of disk accretion on to a rapidly rotating star with an aligned dipole magnetic field considered by LRBK99. Here, r_1 and r_2 are the boundaries of the region; R_A is the effective radius where the outflow begins; ω_* is the star's rotation rate; ω_K is the Keplerian rotation rate of the accretion disk; and $r_{cr} \equiv (GM/\omega_*^2)^{1/3}$ is the corotation radius. The magnetic field in the vicinity of r_1 has an essential time-dependence owing to the continual processes of stellar flux leaking outward into the disk, the resulting field loops being inflated by the differential rotation (LRBK95), and the reconnection between the open disk field and the closed stellar field loops. The dashed lines marked by the letters “n” indicate neutral surfaces along which reconnection occurs.

$$\begin{aligned} \dot{L}_{\text{accr}} &= \dot{M}_{\text{accr}}(rv_\phi)_2 - T_2, \\ T_2 &= 2\pi r_2^2 \int_{-h}^h dz (T_{r\phi}^{\text{vis}})_2, \end{aligned} \quad (320)$$

where $T_{r\phi}^{\text{vis}}$ is the viscous contribution to the stress tensor which includes *both* the turbulent hydrodynamic and turbulent magnetic stresses. The influx of energy into the considered region is

$$\dot{E}_{\text{accr}} = \dot{M}_{\text{accr}} \left(-\frac{GM}{2r_2} + w_2 \right) - \omega_2 T_2, \quad (321)$$

where $\omega \equiv v_\phi/r \approx v_K/r$ with $v_K \equiv \sqrt{GM/r}$ the Keplerian speed and M the mass of the star, and where w_2 is the enthalpy. For conditions of interest here the disk at r_2 is geometrically thin so that $w \sim c_s^2 \ll v_K^2$, where c_s is the sound speed.

Consider next the fluxes of mass, angular momentum, and energy across the surface AA' in Fig. 12. For the physical regime considered, where $v_K(r_1)/r_1 \ll \omega_*$ (= the angular rotation rate of the star), the mass accretion across the AA' surface is assumed to be small compared with \dot{M}_{accr} . The reason for this is that any plasma which crosses the AA' surface will be “spun-up” to an angular velocity ω_* (by the magnetic force) which is substantially larger than the Keplerian value, and thus it will be thrown outwards. Thus the efflux of angular momentum across this surface from the considered region is $\dot{L}_1 = -T_1$. The efflux of energy across this surface is $\dot{E}_1 = -\omega_* T_1$, where ω_* is the angular rotation rate of the star and the inner magnetosphere as shown in Fig. 12. For the conditions considered, the star slows down and loses rotational energy so that $T_1 > 0$.

We have $\dot{E}_1/\dot{L}_1 = \omega_*$. Because the interaction of the star with the accretion flow is by assumption entirely across the surface AA' , this is consistent with the spin-down of a star with constant moment of inertia I ; that is, $\Delta E_*/\Delta L_* = I_* \omega_* \Delta \omega_*/(I_* \Delta \omega_*) = \omega_*$.

Next we consider the mass, angular momentum, and energy fluxes across the surfaces $A'C'$ and AC in Fig. 12. As mentioned, accretion on to the star is small for $r_{cr} \ll r_1$ where r_{cr} is the corotation radius as indicated in Fig. 12. Thus, the mass accretion goes mainly into outflows, $\dot{M}_{\text{out}} \approx \dot{M}_{\text{accr}}$, where “out” stands for outflows. The angular momentum outflow across the surfaces $A'C'$ and AC , \dot{L}_{out} , must be the difference between the angular momentum lost by the star and the incoming angular momentum of the accretion flow. The angular momentum carried by radiation from the disk is negligible because $(v_K/c)^2 \ll 1$, where c is the speed of light. That is, $\dot{L}_{\text{out}} = \dot{L}_{\text{accr}} - \dot{L}_1$. The energy outflow across the $A'C'$ and AC surfaces is $\dot{E}_{\text{out}} + \dot{E}_{\text{rad}} = \dot{E}_{\text{accr}} - \dot{E}_1$, where \dot{E}_{rad} is the radiation energy loss rate from the disk surfaces between $r = r_1$ and r_2 , and \dot{E}_{out} is the rate of energy loss carried by the outflows.

Angular momentum conservation gives

$$\dot{L}_{\text{out}} = \dot{M}_{\text{accr}}(rv_\phi)_2 - T_2 + T_1. \quad (322)$$

We have

$$\dot{E}_{\text{out}} + \dot{E}_{\text{rad}} = -\frac{GM\dot{M}_{\text{accr}}}{2r_2} - \omega_2 T_2 + \omega_* T_1. \quad (323)$$

We can solve Eq. (322) for T_2 and thereby eliminate this quantity from the energy equation (323). This gives

$$\dot{E}_{\text{out}} + \dot{E}_{\text{rad}} = -\frac{3GMM_{\text{accr}}}{2r_2} + \omega_2 \dot{L}_{\text{out}} + (\omega_* - \omega_2)T_1. \quad (324)$$

The preceding equations are independent of the nature of the outflows from the disk. At this point we consider the case of magnetically driven outflows as treated by Lovelace et al. (1991), hereafter LBC). In the LBC model the outflows come predominantly from an annular inner region of the disk of radius $\sim R_A$ where the disk rotation rate is $\omega_0 = \sqrt{GM/R_A^3}$. Thus we assume that the outflows come from a region of the disk which is approximately in Keplerian rotation. For the present situation, shown in Fig. 1, it is clear that we must have $r_1 < R_A < r_2$. Further, we will assume R_A is close in value to r_1 with $(R_A - r_1)/R_A \lesssim 1$. For conditions where the outflow from the disk is relatively low temperature (sound speed much less than Keplerian speed), Eqs. (16) and (18) of LBC imply the general relation $\dot{E}_{\text{out}} = \omega_0 \dot{L}_{\text{out}} - 3GMM_{\text{out}}/(2R_A)$. This equation can be used to eliminate \dot{L}_{out} in favor of \dot{E}_{out} in Eq. (324). Recalling that $\dot{M}_{\text{out}} = \dot{M}_{\text{accr}}$ we have

$$(1 - \delta^{3/2})\dot{E}_{\text{out}} + \dot{E}_{\text{rad}} = (\omega_* - \omega_2)T_1 - \frac{3GMM_{\text{accr}}}{2r_2}(1 - \delta^{1/2}), \quad (325)$$

where $\delta \equiv R_A/r_2 < 1$.

The energy dissipation in the region of the disk $r = r_1$ to r_2 heats the disk and this heat energy is transformed into outgoing radiation \dot{E}_{rad} . Thus we have

$$\dot{E}_{\text{rad}} = \frac{3}{2} \int_{r_1}^{r_2} dr \frac{GMM_{\text{disk}}(r)}{r^2}, \quad (326)$$

(Shakura, 1972; Shakura and Sunyaev, 1973), where $\dot{M}_{\text{disk}}(r_2) = \dot{M}_{\text{accr}}$ and $\dot{M}_{\text{disk}}(r_1) \approx 0$. The essential change in $\dot{M}_{\text{disk}}(r)$ occurs in the vicinity of R_A so that $\dot{E}_{\text{rad}} \approx (3GMM_{\text{accr}}/2)(R_A^{-1} - r_2^{-1})$. Thus Eq. (325) becomes

$$(1 - \delta^{3/2})\dot{E}_{\text{out}} = (\omega_* - \omega_2)T_1 - \frac{3GMM_{\text{accr}}}{2R_A}(1 - \delta^{3/2}). \quad (327)$$

Thus the power from the spin-down of the star $\omega_* T_1$ must be larger than a certain value in order to drive the outflow.

For magnetically driven outflows, the value of \dot{E}_{out} can be written as

$$\dot{E}_{\text{out}} = \frac{3}{2} \mathcal{F}_0^{2/3} \omega_0^{4/3} R_A^{8/3} B_0^{4/3} \dot{M}_{\text{accr}}^{1/3}, \quad (328)$$

[Eq. (34) of LBC], where \mathcal{F}_0 is a dimensionless numerical constant ≥ 0.234 , and B_0 is the poloidal magnetic field at the base of the outflow at $r = R_A$. We take the simple estimate $B_0 = \mu/R_A^3$, which omits corrections for example for compression of the star's field by the inflowing plasma.

Next we consider the torque on the star T_1 . Because most of the matter inflowing in the accretion disk at $r = r_2$ is driven off in outflows at distances $r > r_1$, the stress is necessarily due to the magnetic field. The magnetic field in the vicinity of r_1 has an essential time-dependence owing to the continual processes of stellar flux leaking outward into the disk, the resulting field loops being inflated by the differential rotation (LRBK95), and the reconnection between the open disk field and the closed stellar field loops. The time scale of these processes is $t_1 \lesssim 2\pi r_1/v_K(r_1)$. We make the estimate of the torque $T_1 = -2\pi r_1^2 \langle 2\Delta z \rangle \langle B_r B_\phi \rangle_1 / (4\pi)$, where Δz is the vertical half-thickness of the region where the magnetic stress is significant, and where the angular brackets denote a time average of the field quantities at $r \sim r_1$. The magnetic field components, B_r, B_ϕ , with $B_\phi \propto -B_r$ necessarily, must be of magnitude less than or of the order of the dipole field $B_1 = \mu/r_1^3$ at $r = r_1$. The fact that B_ϕ has the opposite sign to that of B_r is due to the fact that the B_ϕ field arises differential rotation between the region $r < r_1$, which rotates at rate ω_* , and the region $r > r_1$, which rotates at rate $\omega_K(r_1) < \omega_*$. Also, it is reasonable to assume $\Delta z \lesssim r_1$. Therefore,

$$T_1 \approx \bar{\alpha} r_1^3 B_1^2 \equiv \bar{\alpha} \frac{\mu^2}{R_A^3}, \quad (329)$$

where $\bar{\alpha} \leq 1$ (the time average of $\alpha(t)$) is a dimen-

sionless constant analogous to the α – parameter of Shakura (1972) and Shakura and Sunyaev (1973). (Note that because $r_1 \lesssim R_A$, $\bar{\alpha}$ and $\bar{\alpha}_1 = (r_1/R_A)^3 \bar{\alpha}$ are of the same order of magnitude.)

Substituting Eqs. (328) and (329) into Eq. (327) gives

$$\begin{aligned} & \frac{3}{2} (1 - \delta^{3/2}) \mathcal{F}_o^{2/3} \left(\frac{r_A}{R_A} \right)^{7/3} \\ &= \frac{\bar{\alpha} r_A^{7/2}}{R_A^2 r_{\text{cr}}^{3/2}} \left[1 - \left(\frac{r_{\text{cr}}}{R_A} \right)^{3/2} \delta^{3/2} \right] \\ & - \frac{3}{2} (1 - \delta^{3/2}). \end{aligned} \quad (330)$$

Here, we have introduced two characteristic radii — the corotation radius,

$$r_{\text{cr}} \equiv \left(\frac{GM}{\omega_*^2} \right)^{1/3} \approx 1.5 \times 10^8 \text{ cm } M_1^{1/3} P_1^{2/3},$$

with $P_1 \equiv (2\pi/\omega_*)/1\text{s}$ the pulsar period and $M_1 \equiv M/M_\odot$. [For a young stellar object, $r_{\text{cr}} \approx 1.36 \times 10^{12} M_1^{1/3} P_{10d}^{2/3}$, where P_{10d} is the period in units of 10 days.] The second is the *nominal* Alfvén radius

$$\begin{aligned} r_A &\equiv \left[\frac{\mu^2}{\dot{M}_{\text{accr}} \sqrt{GM}} \right]^{2/7} \approx 3.6 \times 10^8 \text{ cm} \\ &\times \frac{\mu_{30}^{4/7}}{\dot{M}_{17}^{2/7} M_1^{1/7}}, \end{aligned} \quad (330a)$$

where the accretion rate $\dot{M}_{17} \equiv \dot{M}_{\text{accr}}/(10^{17} \text{ g/s})$ with $10^{17} \text{ g/s} \approx 1.6 \times 10^{-9} M_\odot/\text{yr}$ and $\mu_{30} \equiv \mu/(10^{30} \text{ G cm}^2)$ with the magnetic field at the star's equatorial surface $\mu/r^3 = 10^{12} \text{ G}(10^6 \text{ cm}/r)^3$. [For a young stellar object $r_A \approx 1.81 \times 10^{12} \text{ cm } \mu_{36.5}^{4/7}/(\dot{M}_{17}^{2/7} M_1^{1/7})$, where the normalization corresponds to a stellar radius of 10^{11} cm , a surface magnetic field of $3 \times 10^3 \text{ G}$, and an accretion rate of $1.6 \times 10^{-8} M_\odot/\text{yr}$.] The corotation radius is the distance from the star where the centrifugal force on a particle corotating with the star ($\omega_*^2 r$) balances the gravitational attraction (GM/r^2). The Alfvén radius r_A is the distance from a *non-rotating* star where the free-fall of a quasi-spherical accretion flow is stopped, which occurs (approximately) where the kinetic energy-density of the flow equals the energy-density of the star's dipole field. Note that the assumptions leading to Eq. (330a) require $R_A > r_{\text{cr}}$.

Notice that R_A (or $r_1 \sim R_A$) is the *effective* Alfvén radius for a *rotating* star. It depends on *both* r_A and r_{cr} in contrast with the common notion that the Alfvén radius is given by r_A even for a rotating star. From Eq. (329), the *spin-down* rate of the star is $I(d\omega_*/dt) = -\bar{\alpha} \mu^2/R_A^3$, where I is the moment of inertia of the star (assumed constant). Thus the spin-down rate depends on both r_A and r_{cr} .

Fig. 13 shows the dependence of R_A on r_A and r_{cr} for a sample case. For conditions of a newly formed disk around a young pulsar, the initial system point would be on the upper left-hand part of the curve. Due to the pulsar slowing down (assuming μ and \dot{M} constant), the system point would move downward and to the right as indicated by the arrow. In this region of the diagram, $R_A \approx \sqrt{\bar{\alpha}} r_A^{7/4}/r_{\text{cr}}^{3/4} \propto \sqrt{\omega}$ (for $\delta \ll 1$), so that the torque on the star is $T_1 \approx (GMM)^{3/2}/(\mu\sqrt{\bar{\alpha}}\omega^{3/2})$. Thus the braking index is

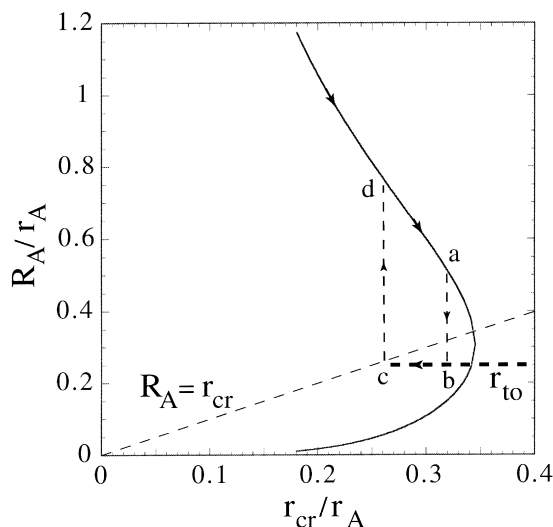


Fig. 13. *Effective* Alfvén radius R_A (normalized by the *nominal* Alfvén radius r_A) as a function of the normalized corotation radius r_{cr}/r_A for $\bar{\alpha} = 0.2$ obtained from Eq. (330). We have neglected the $\delta^{3/2} = (R_A/r_2)^{3/2}$ terms compared with unity and taken the value $\mathcal{F}_o = 0.234$ from LBC. Only the part of the solid curve above the dashed line $R_A = r_{\text{cr}}$ is consistent with our assumptions. The dashed horizontal line r_{to} indicates the “turnover radius” of the disk rotation curve or effective Alfvén radius in the regime discussed by LRBK95 where \dot{M}_{accr} falls onto the star and the star spins-up. For this line the turbulent magnetic diffusivity of the disk is taken to be $\alpha D = 0.1$. The points $a b c d$ and the associated vertical lines represent possible transitions between spin-down and spin-up of the pulsar as discussed in the text.

$n = -3/2$, where n is defined by the relation $\dot{\omega}_* = -\text{const } \omega_*^n$. Numerically,

$$\frac{1}{P} \frac{dP}{dt} = \frac{1.55 \times 10^{-5}}{\text{yr}} \frac{P_1^{5/2} (M_1 \dot{M}_{17})^{3/2}}{\sqrt{\bar{\alpha}} \mu_{30} I_{45}}, \quad (331)$$

where $I_{45} \equiv I/(10^{45} \text{ g cm}^2)$. For $R_A \gg r_{\text{cr}}$, the mass accretion rate to the star is small compared with \dot{M}_{accr} , but some accretion may occur due to “leakage” of relatively low angular momentum plasma across field lines near r_1 (Arons and Lea, 1976).

As R_A decreases, the spin-down torque on the star increases. Over a long interval, R_A will decrease to a value larger than r_{cr} but not much larger. In this limit, mass accretion on to the star \dot{M}_1 may become significant. Our treatment can be extended to this limit by noting that $\dot{M}_1 = \dot{M}_2 - \dot{M}_{\text{out}}$, $\dot{L}_1 = \dot{M}_1 \omega_1 r_1^2 - T_1$, and $\dot{E}_1 = \dot{M}_1 (-GM/2r_1) - \omega_* T_1$, where T_1 is given by Eq. (329). In this limit the accretion luminosity is GMM_1/r_* , where r_* is the star’s radius. Fig. 13 is not changed appreciably for $\dot{M}_1 < \dot{M}_{\text{accr}}$.

Further spin-down of the star will cause the system point in Fig. 13 to approach the right-most part of the curve. Further spin-down of the star is impossible. At this point of the evolution, the only possibility is a transition to the spin-up regime. In this regime the effective Alfvén radius is the “turn-over radius” r_{to} of the disk rotation curve calculated by LRBK99, the star spins-up at the rate $I d\omega_*/dt = \dot{M}_{\text{accr}} (GM r_{\text{to}})^{1/2}$, and most of the disk accretion \dot{M}_{accr} falls onto the star. The dashed horizontal line in Fig. 13 indicates r_{to} which is necessarily less than r_{cr} .

The location of the turnover line r_{to} in Fig. 13 suggests the possible evolution shown by the sequence of points $a \rightarrow b \rightarrow c \rightarrow d \rightarrow a$. The system can jump down from point a where the star spins-down to point b where it spins-up. The spin-down torque at a is $-\bar{\alpha} \mu^2 / R_{Aa}^3$ (where R_{Aa} is the effective Alfvén radius at point a), whereas the spin-up torque at b is $\dot{M}_{\text{accr}} (GM r_{\text{to}})^{1/2}$. The magnitude of the ratio of these torques is

$$\frac{\text{spin-down}}{\text{spin-up}} = \bar{\alpha} \left(\frac{r_A}{R_{Aa}} \right)^{7/2} \left(\frac{R_{Aa}}{r_{\text{to}}} \right)^{1/2}. \quad (332)$$

With the system on the r_{to} line, it evolves to the left. Because $r_{\text{to}} \leq r_{\text{cr}}$, there must be an upward jump from point c to point d . For this case the torque ratio is given by Eq. (322) with $R_{Aa} \rightarrow R_{Ad}$. From point d

the system evolves to the right. For the example shown in Fig. 2, the torque ratio is ≈ 3.45 for $a \rightarrow b$ whereas it is ≈ 0.87 for $c \rightarrow d$. The vertical line $c \rightarrow d$ is at the left-most position allowed for the considered conditions, but this transition could also occur if the line is shift to the right. The line $a \rightarrow b$ can be displaced slightly to the right or it can be displaced to the left to be coincident with the $c \rightarrow d$ line. In the latter case the torque ratio for the spin-down to spin-up jump is approximately equal to the torque ratio for the spin-up to spin-down jump and is ≈ 0.87 . The smaller the horizontal separation of the $a \rightarrow b$ and the $c \rightarrow d$ lines, the shorter is the time interval between jumps.

Summarizing, we can say that the horizontal locations of the transitions, $a \rightarrow b$, and $c \rightarrow d$, are indeterminate within a definite range. The locations of the jumps in the (R_A, r_{cr}) plane may in fact be a stochastic or chaotic in nature and give rise to chaotic hysteresis in the of the spin-down/spin-up behavior of the pulsar. The jumps could be triggered by small variations in the accretion flow (\dot{M} for example) and magnetic field configuration (the time-dependence of α in the torque T_1). Analysis of the accreting neutron star system Her X-1 (Voges et al., 1987; Morfill et al., 1989) suggests that the intensity variations are described by a low dimensional deterministic chaotic model. The transitions between spin-down and spin-up and the reverse transitions may be described by an analogous model.

The allowed values in Fig. 2 have $r_{\text{cr}}/r_A \leq \text{const} \equiv k$, where $k \approx \bar{\alpha}^{2/3}$. This corresponds to pulsar periods

$$P \leq 5.2\text{s} \left(\frac{\bar{\alpha}}{M_1^{5/7}} \right) \left(\frac{\mu_{30}^2}{\dot{M}_{17}} \right)^{3/7}. \quad (333)$$

For some long period pulsars such as GX 1+4 this inequality points to magnetic moment values μ_{30} appreciably larger than unity. Periods much longer than allowed by (333) can result for pulsars which accrete from a stellar wind (Bisnovatyi-Kogan, 1991). [For a young stellar object, Eq. (333) gives $P \leq 8d(\bar{\alpha}/M_1^{5/7})(\mu_{36.5}^2/\dot{M}_{18})^{3/7}$.]

5.3. Cyclotron emission from magnetic poles of X-ray pulsars

The accretion flow of plasma to a strongly mag-

netized neutron star is channeled by the magnetic field and falls mainly into the magnetic poles (see, e.g., Toropin et al., 1999). The spectra of X-ray pulsars are formed from a combination of black body photons from the star's surface and Comptonized photons from the hot coronal layer. In presence of a strong magnetic field $\sim 10^{10}$ – 10^{13} G, the cyclotron or synchrotron emission of electrons also falls into the X-ray band. There are many observations of a spectral feature, interpreted as a cyclotron line in the X-ray spectrum of the pulsar Her X-1 (Trümper et al., 1978; Tueller et al., 1984; Ubertini et al., 1980; Voges et al., 1982; Gruber et al., 1980; McCray et al., 1982; Mihara et al., 1990; Sheepmaker et al., 1981) at 39–58 KeV (see Table 2). The magnetic field strength is usually calculated from the non-relativistic formula

$$H = \frac{mc\omega}{e}, \quad (334)$$

where ω is the gyration frequency and m is the electron rest mass. From observations of the line frequency in Table 2, the magnetic field strengths are of the order of $(3\text{--}5) \times 10^{12}$ G.

But these large values of the field strength are in conflict with: (1) theoretical models for the rate of change of the pulsar spin (Bisnovaty-Kogan and Komberg, 1973), (2) the condition for the transparency for the outgoing radiation (Bisnovaty-Kogan, 1973, 1974), (3) consideration of the interrelation between radio and X-ray pulsars (Bisnovaty-Kogan and Komberg, 1974), and (4) interpretation of beam variability during the 35-day cycle (Sheffer et al., 1992; Deeter et al., 1998; Scott et al., 2000; see also Lipunov, 1987). A likely reason for this conflict is that the non-relativistic formula (334) is not applicable in this case. Bisnovaty-Kogan and Fridman (1969) find that the temperature of the electrons

emitting a cyclotron line could be $\sim 10^{11}$ K, and therefore they are ultrarelativistic. The mean energy of the cyclotron line is then broadened and shifted relativistically by a factor of $\gamma \approx kT/mc^2$. Baushev and Bisnovaty-Kogan (1999) have calculated the spectral profile of the cyclotron line for various electron distributions. Furthermore, a model of the hot spot on the pulsar magnetic pole was developed, and it was shown that the overall observed X-ray spectrum (from 0.2 to 120 KeV) could result in presence of a surface magnetic field $\sim 5 \times 10^{10}$ G, which is well below those obtained from (334). Monte Carlo calculations of resonant radiative transfer has been discussed by Wang et al. (1988).

5.3.1. Spectrum of cyclotron radiation of anisotropic relativistic electrons

Bisnovaty-Kogan (1973) and Gnedin and Sunyaev (1973) showed that in the magnetic field near the pulsar the component of an electron's momentum perpendicular to the magnetic field decays rapidly owing to cyclotron/synchrotron emission, while the parallel momentum component remains constant. Hence the electron momentum distribution is anisotropic with

$$p_{\perp}^2 \ll p_{\parallel}^2, \quad (335)$$

where $p_{\perp} \ll mc$, $p_{\parallel} \gg mc$. Assume for simplicity that the transverse electron distribution is a two-dimensional Maxwellian,

$$dn = \frac{N}{T_1} \exp\left(-\frac{mu^2}{2T_1}\right) d(mu^2/2), \quad (336)$$

where $T_1 \ll mc^2$. Let us calculate the cyclotron emission of N such particles moving with speed V along the magnetic field.

Table 2
Observations of the cyclotron line in Her X-1

Date	References	ω_{\max} (KeV)	Line width (KeV)
May 1978	Trümper et al. (1978)	58	11^{+26}_{-11}
September 1977	Voges et al. (1982)	51	21^{+9}_{-7}
February 1978	Gruber et al. (1980)	48	28 ± 7
April 1980	Gruber et al. (1980)	54	11^{+14}_{-11}
May 1980	Ubertini et al. (1980)	49.5	18^{+6}_{-3}
September 1980	Tueller et al. (1984)	39	27^{+21}_{-20}

For a single particle having a transverse velocity u ,

$$j(\theta) = \frac{e^4 H^2 u^2 \left(1 - \frac{V^2}{c^2}\right)^2 \left[(1 + \cos \theta) \left(1 + \frac{V^2}{c^2}\right) - 4 \frac{V}{c} \cos \theta \right]}{8 \pi c^5 m^2 \left(1 - \frac{V}{c} \cos \theta\right)^5}, \quad (337)$$

(Ginzburg, 1975) where θ is the angle between the magnetic field and the direction to the observer. Integration over the distribution (336), gives

$$J(\theta) = \int j(\theta) dn = N \frac{e^4 H^2 T_1 \left(1 - \frac{V^2}{c^2}\right)^2 \left[(1 + \cos \theta) \left(1 + \frac{V^2}{c^2}\right) - 4 \frac{V}{c} \cos \theta \right]}{4 \pi c^5 m^3 \left(1 - \frac{V}{c} \cos \theta\right)^5}. \quad (338)$$

For the spectrum we find

$$\omega(\theta) = \omega_H \frac{\sqrt{1 - \frac{V^2}{c^2}}}{1 - \frac{V}{c} \cos \theta}, \quad \omega_H = \frac{eH}{mc}. \quad (339)$$

When $V \approx c$ the cyclotron/synchrotron radiation is highly directed with a pencil beam radiation pattern along V ($\theta \approx 0$). Under these conditions ($\theta = 0$, $V \approx c$) we obtain from (338) and (339)

$$J(0) = \frac{2Ne^4 H^2 T_1}{\pi c^5 m^3 \left(1 - \frac{V}{c}\right)}, \quad (340)$$

$$\omega(0) = \omega_H \sqrt{\frac{1 + \frac{V}{c}}{1 - \frac{V}{c}}} \approx 2\omega_H \frac{E_{\parallel}}{m_e c^2}. \quad (341)$$

This gives

$$1 - \frac{V}{c} = \frac{2\omega_H^2}{\omega^2}. \quad (342)$$

Consider now the parallel momentum distribution of the electrons,

$$dn = f(p_{\parallel}) dp_{\parallel}. \quad (343)$$

Substituting of dn for N and using

$$p_{\parallel} = \frac{mc}{2} \frac{\omega}{\omega_H}; \quad 1 - \frac{V}{c} = \frac{2\omega_H^2}{\omega^2}, \quad (344)$$

we obtain for the spectral density

$$J_{\omega} = \frac{e^2 T}{2\pi c^2 \omega_H} \omega^2 f\left(-\frac{mc}{2} \frac{\omega}{\omega_H}\right) d\omega. \quad (345)$$

Let us consider two important cases. When f is a relativistic Maxwell,

$$f = \frac{n_0 c}{T_2} \exp\left(-\frac{p_{\parallel} c}{T_2}\right), \quad T_2 \gg mc^2 \gg T_1, \quad (346)$$

where n_0 is a number of emitting electrons. Then the spectrum is:

$$J_{\omega} = \frac{n_0 e^2}{2\pi c \omega_H} \frac{T}{T_2} \omega^2 \exp\left(-\frac{mc^2 \omega}{2\omega_H T_2}\right) d\omega. \quad (347)$$

This spectrum has a single maximum at

$$\frac{\omega}{\omega_H} = \frac{4T_2}{mc^2}. \quad (348)$$

In the second case consider the distribution function f ,

$$f = \frac{n_0}{\sqrt{\pi}\sigma} \exp\left(-\frac{(p_{\parallel} - a)^2}{\sigma^2}\right). \quad (349)$$

The spectrum of radiation is

$$J_{\omega} = \frac{n_0 e^2}{2\pi c^2 \omega_H} \omega^2 \exp\left(-\frac{\left(\frac{mc}{2} \frac{\omega}{\omega_H} - a\right)^2}{\sigma^2}\right) d\omega. \quad (350)$$

When $\sigma \ll a$ this spectrum has a single maximum at

$$\omega \approx \frac{2a}{mc} \omega_H. \quad (351)$$

Notice that in all cases the maximum of the spectrum is shifted to

$$\frac{\omega}{\omega_H} \sim \frac{\bar{E}_e}{mc^2}. \quad (352)$$

This is a general property of the relativistic cyclotron line which is independent of the form of f .

Fig. 14 shows the observed X-ray spectrum (solid line) (Mihara et al., 1990) and the model calculation

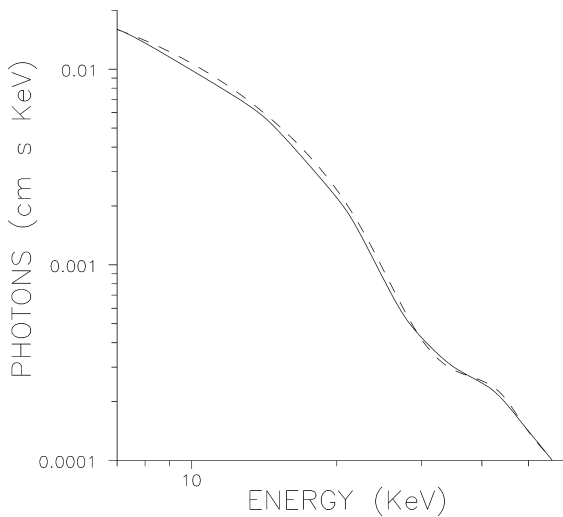


Fig. 14. Comparison of observed and calculated X-ray spectra including the cyclotron line. The solid curve is the observed spectrum from Mihara et al. (1990). The dashed curve is a model consisting of a Comptonized spectrum and the line feature (350) with $a = 7 \times 10^{-4}$ eV s/cm, and $\sigma = 2 \times 10^{-4}$ eV s/cm, from Baushev and Bisnovatyi-Kogan (1999).

using (350) which gives a better fit to the observed spectrum. The spectrum from McCray et al. (1982) was also approximated by (350) as shown in Fig. 15.

Taking the values suggested by Bisnovatyi-Kogan and Fridman (1969), the parallel electron temperature as 2×10^{11} K (that is, $T_2 = 2 \times 10^{11}$ K) and $a = 7 \times 10^{-4}$ eVs/cm, we obtain for the magnetic field strength $B = 4 \times 10^{10}$ G, 8×10^{10} G, and 4×10^{10} G, respectively. Here we estimate the spectral form of the cyclotron line averaged over the pulsar period, supposing a uniform distribution of $f(p_{||})$ over the polar cap. In this model the beam of the cyclotron feature is determined by the number distribution of the emitting relativistic electrons, moving predominantly along the magnetic field, above the polar cap.

5.3.2. Model of the X-ray spectrum of Her X-1

In order to obtain a complete model of the observed spectrum of Her X-1, the following model of the hot spot is considered (see Fig. 16). A collisionless shock wave is assumed to be present in the accretion flow near the surface on the magnetic pole of the neutron star. In this shock front ultrarelativistic electrons are generated having small

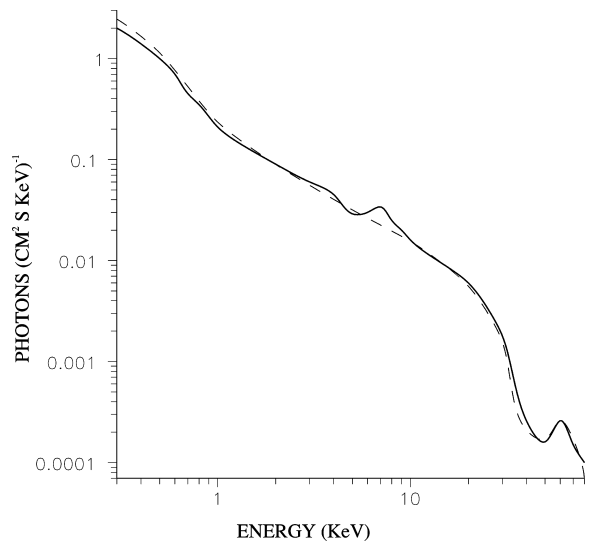


Fig. 15. Comparison of observed and calculated X-ray spectra of Her X-1. The solid curve is the observed spectrum from McCray et al. (1982) and the dashed curve is a model consisting of a Comptonized spectrum and the cyclotron feature (350) with $T_s = 0.9$ KeV, $T_e = 8$ KeV, $\tau_e = 14$, $a = 7 \times 10^{-4}$ eV s/cm, $\sigma = 10^{-4}$ eVs/cm, $B = 4 \times 10^{10}$ G, from Baushev and Bisnovatyi-Kogan (1999).

pitch-angles so that condition (335) is fulfilled automatically. Behind the shock there is a hot turbulent zone with a temperature T_e , and optical depth τ_e . Under this zone there is a heated spot on the surface of the neutron star with a lower temperature. Fig. 16 shows a schematic drawing of the emission region of Her X-1 and the spectrum.

There are three main regions of the spectrum: a quasi-Planckian spectrum between 0.3 and 0.6 KeV which is generated near the magnetosphere of the X-ray pulsar; a power-law spectrum (0.6–20) KeV with a rapid decrease at 20 KeV, and the cyclotron line feature.

The power-law spectrum area appears as follows. The star surface emits a black-body spectrum with temperature T_s . As this radiation travels through the turbulent zone it is Comptonized. This Comptonized spectrum has been calculated according to Sunyaev and Titarchuk (1980); see also Zel'dovich and Shakura (1969). Taking the neutron star radius to be 10 km, the distance of the X-ray pulsar 6 Kpc, the hot spot area $S = 2 \times 10^{12}$ cm², we have found the best fitting spectrum for $T_s = 1$ KeV, $T_e = 8$ KeV, and

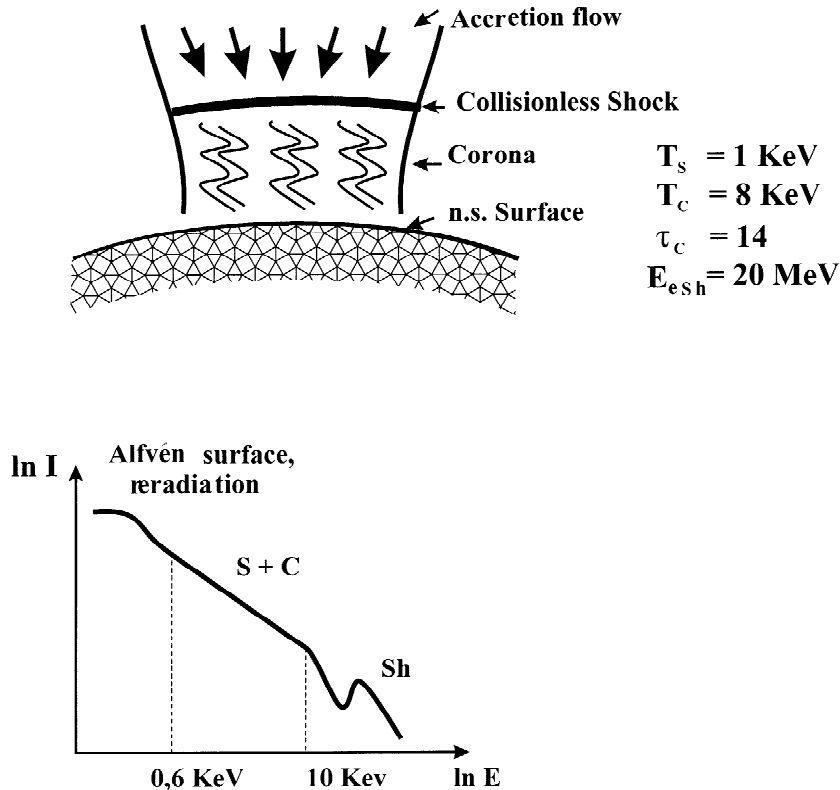


Fig. 16. Schematic structure of the accretion column near the magnetic pole of the neutron star (top), and its radiation spectrum (bottom) from Bisnovaty-Kogan (1999b).

$\tau_e = 14$. This spectrum is shown in Fig. 15 by the dashed line. It agrees nicely with the observed solid curve.

Observations of the variability of the cyclotron line are reported in Mihara et al. (1997). The Ginga satellite detected changes of the cyclotron line energies of 4 pulsars. The change was as large as 40% in the case of 4U 0115+63. The larger luminosity of this source corresponds to smaller average energy of the cyclotron feature. These changes can readily be explained in our model. The velocity of the accretion flow decreases as the pulsar's luminosity increases. This is because locally the luminosity is close to the Eddington limit. As a result the shock wave intensity drops and the energy of the ultrarelativistic electrons decreases. The cyclotron energy decreases in accordance with (352).

Observations taken by Beppo-Sax and RXTE satellites (Santangelo et al., 1999; Heindl et al.,

1999) revealed 4 cyclotron-like spectral features (harmonics) in the spectrum of the X-ray pulsar 4U 0115+63. Interpretation of these features is still not completed.

6. Magnetohydrodynamic origin of jets from accretion disks

6.1. Introduction

Powerful, highly-collimated, oppositely directed jets are observed in active galaxies and quasars (see for example Bridle and Eilek, 1984), and in old compact stars in binaries — the “microquasars” (Mirabel and Rodriguez, 1994; Eikenberry et al., 1998). Further, highly collimated emission line jets are seen in young stellar objects (Mundt, 1985; Bührke et al., 1988). Different ideas and models

have been put forward to explain astrophysical jets (see reviews by Begelman et al., 1984; Bisnovaty-Kogan, 1993b; Lovelace et al., 1999c). Recent observational and theoretical work favors models where twisting of an ordered magnetic field threading an accretion disk acts to magnetically accelerate the jets as first proposed by Lovelace (1976) and Blandford (1976). The nature of the ordered magnetic field threading an accretion disk envisioned by Bisnovaty-Kogan and Ruzmaikin (1976) is shown in Fig. 17. Fig. 18 shows the outflows from a disk with such an ordered field from Lovelace (1976). Two main regimes have been considered in theoretical models, the *hydromagnetic regime* where the energy and angular momentum is carried by both the electromagnetic field and the kinetic flux of matter, and the *Poynting flux regime* where the energy and angular momentum outflow from the disk is carried predominantly by the electromagnetic field.

The theory of the origin of hydromagnetic outflows has been developed by many authors (Blandford and Payne, 1982; Pudritz and Norman, 1986; Sakurai, 1987; Koupelis and Van Horn, 1989; Lovelace et al., 1991, 1993; Pelletier and Pudritz, 1992; Königl and Ruden, 1993; Cao and Spruit, 1994; Contopoulos and Lovelace, 1994; Con-

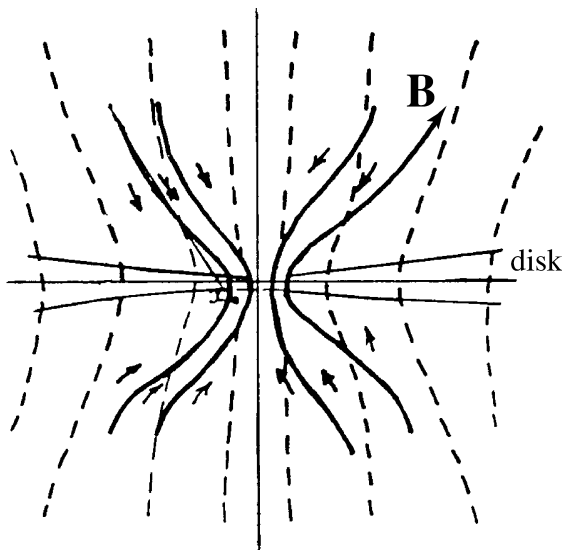


Fig. 17. Sketch of the magnetic field threading an accretion disk shown increase of the field owing to flux freezing in the accreting disk matter from Bisnovaty-Kogan and Ruzmaikin (1976).

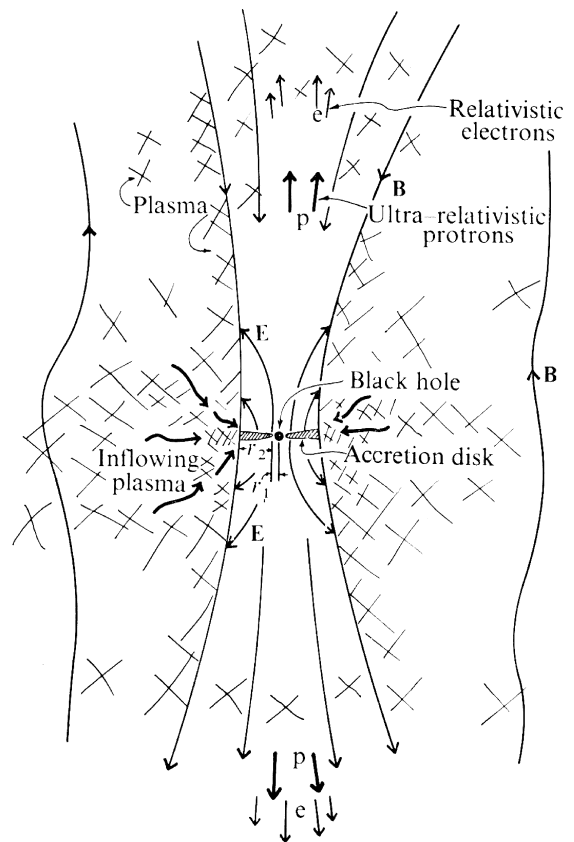


Fig. 18. Sketch of the electromagnetic outflows from the two sides of the disk owing to the Faraday unipolar dynamo action of a rotating magnetized disk from Lovelace (1976).

topoulos, 1995; Ostriker, 1997). Physical understanding of the hydromagnetic outflows from disks has developed from MHD simulations (Uchida and Shibata, 1985; Shibata and Uchida, 1986; Bell, 1994; Ustyugova et al., 1995, 1999; Koldoba et al., 1995; Romanova et al., 1997, 1998; Meier et al., 1997; Ouyed and Pudritz, 1997; Krasnopolsky et al., 1999; Koide et al., 2000; and Meier et al., 2001).

Recent work on hydromagnetic outflows assumes the geometry sketched in Fig. 19. A strong case for hydromagnetic jets as an explanation of jets in protostellar systems emerges because the temperature of the inner regions of these systems is insufficient to permit driving by thermal or radiation pressure (Königl and Ruden, 1993). Part of the investigations have been analytical or semi-analytical and outgrowths of the self-similar solution of Blandford and

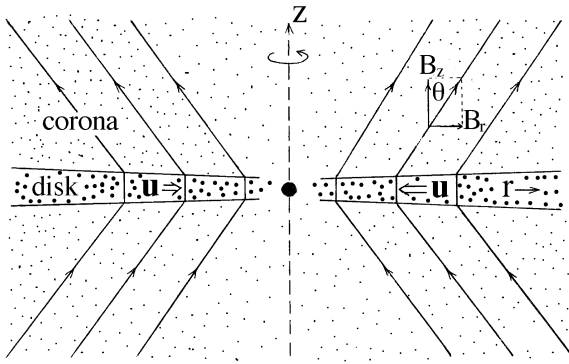


Fig. 19. Sketch of an accretion disk threaded by a magnetic field for conditions which may lead to hydromagnetic jet formation.

Payne (1982) (Pudritz and Norman, 1986; Königl, 1989; Pelletier and Pudritz, 1992; Contopoulos and Lovelace, 1994). The outflows in this model are often referred to as “centrifugally driven” owing to the driving force close to the disk: Close to the disk, MHD fluid particles move along the magnetic field lines (sometimes described as “beads on a wire”). If the poloidal magnetic field lines threading the disk diverge away from the z -axis as shown in Fig. 17 (making an angle with the z -axis of more than 30°), then the sum of the gravitational and centrifugal forces is outward, away from the disk. The self-similar models are unsatisfactory in the respect that they must be cutoff at small cylindrical radii, $r \leq r_{\min}$. This is the most important region of the jet flow. Observations of optical stellar jets (Mundt, 1985) reveal jet velocities ~ 200 – 400 km/s, which are comparable to the Keplerian disk velocity close to the star’s surface. This suggests that the jets originate from the inner region of the disk close to the star (Pringle, 1989; Shu et al., 1988).

The limitations of analytical models has motivated efforts to study jet formation using MHD simulations. Simulation studies of hydromagnetic jet formation have addressed two main regions: The jet formation region where the matter enters with sub slow-magnetosonic speed and exits with super fast-magnetosonic speed. The second region includes the disk and the problem of the Velikhov (1959) — Chandrasekhar (1981) instability (Balbus and Hawley, 1998) and the resulting 3D MHD turbulence. A number of studies have addressed the coupled problem of the disk and near jet regions (Uchida and

Shibata, 1985; Shibata and Uchida, 1986; Stone and Norman, 1994; Bell and Lucek, 1995;). MHD simulations of the near jet region have been carried out by several groups (Bell, 1994; Ustyugova et al., 1995, 1999; Koldoba et al., 1995; Romanova et al., 1997, 1998; Meier et al., 1997; Ouyed and Pudritz, 1997).

The powerful jets observed from active galaxies and quasars are probably *not* hydromagnetic outflows but rather Poynting flux dominated jets. The motion of these jets measured by very long baseline interferometry correspond to bulk Lorentz factors of $\Gamma = \mathcal{O}(10)$ which is much larger than the Keplerian disk velocity predicted for hydromagnetic outflows. Furthermore, the low Faraday rotation measures observed for these jets at distances $< \text{kpc}$ from the central object implies a very low plasma densities. Similar arguments indicate that the jets of microquasars are *not* hydromagnetic outflows but rather Poynting jets. Poynting jets have been proposed to be the driving mechanism for gamma ray burst sources (Katz, 1997) Theoretical studies have developed models for Poynting jets from accretion disks (Lovelace et al., 1987, 2001; Colgate and Li, 1998; Lynden-Bell, 1996; Romanova and Lovelace, 1997; Levinson, 1998; Romanova, 1999; and Li et al., 2001). Stationary Poynting flux dominated outflows were found by Romanova et al. (1998) and Ustyugova et al. (2000) in axisymmetric MHD simulations of the opening of magnetic loops threading a Keplerian disk.

6.2. Basics of MHD outflows from disks

The main forces which drive a hydromagnetic outflow from a disk threaded by a magnetic field are the centrifugal force and the magnetic pressure gradient force. If disk has a hot corona, the pressure gradient may also be important. We neglect the radiative force but in this regard see Phinney (1987). Accreting matter of the disk carries magnetic field inward thus generating a B_r component of the magnetic field as sketched in Fig. 19. On the other hand, rotation of the disk acts to generate a toroidal component of the field B_ϕ (< 0 if $B_z > 0$).

For a sufficiently inclined magnetic field (θ in Fig. 19 sufficiently large), outflows can result from the centrifugal force (Blandford and Payne, 1982) and/or the magnetic pressure gradient force ($-\nabla_z B_\phi^2 /$

(8π) (Lovelace et al., 1989, 1991; Koupelis and Van Horn, 1989). This depends on the ratio of energy densities at the base of the outflow at the inner radius of the disk denoted r_i . Thus, the main parameters are $\varepsilon_{\text{th}} = (c_s/v_K)_i^2$ and $\varepsilon_B = (v_A/v_K)_i^2$, where v_K is Keplerian velocity, c_s the sound speed, v_A the Alfvén speed, and the i subscript indicates evaluation on the surface of the disk at its inner radius, $r = r_i$. For $\varepsilon_B \sim 1$ the outflow is magneto-centrifugally driven, whereas for $\varepsilon_{\text{th}} \sim 1$, the flow is thermally driven.

Processes in the disk are of course coupled to the outflows (Lovelace et al., 1994, 1997; Falcke et al., 1995). However, it is difficult to simultaneously simulate the disk and the outflow regions because the time scales of the accretion and outflow are in general very different. The radial accretion speed of the disk is typically $|v_r| \ll c_s \ll v_K$, where c_s is the sound speed in the disk, and v_K is the Keplerian velocity. On the other hand the velocity of magnetic outflows from disks is of the order of v_K . Clearly, it is “easier” (less computation time is required) to simulate the outflows.

Furthermore, processes in the disk may involve the small scale MHD instability of Chandrasekhar–Velikhov instability emphasized by Balbus, and Hawley, and therefore require high spatial resolution. Stone and Norman (1994) attempted to simultaneously simulate the internal MHD dynamics of a disk and MHD dynamics of outflows. This proved impractical because essentially all of the spatial resolution was needed for treating the unstable dynamics of the disk. Also, there was the problem that the initial configuration was far from equilibrium. Simulation of the internal MHD disk dynamics has led several groups to the problem of simulating 3D MHD turbulence in a sheared flow of a patch of a disk (for example, Hawley et al., 1995; Brandenburg et al., 1995). This is a much larger project than that of understanding MHD outflows. At the same time it is widely thought, and observations of cataclysmic variables support the view, that the disk turbulence — including MHD turbulence — can be modeled approximately using the Shakura (1972); Shakura and Sunyaev (1973) “alpha” viscosity model (Eardley and Lightman, 1975; Coroniti, 1981; see also Section 2.5). In contrast with the internal disk dynamics, there is theoretical and simulation evidence that the outflows can be treated using axi-

symmetric (2D) MHD (Blandford and Payne, 1982; Lovelace et al., 1991; Ustyugova et al., 1995). Here, we consider outflows from a disk represented as a boundary condition. This approach has subsequently been adopted by other groups (Meier et al., 1997; Ouyed and Pudritz, 1997). This treatment of the disk is justified for outflows from a disk where the accretion speed is small compared with the Keplerian speed (Ustyugova et al., 1995).

6.3. Theory of stationary MHD flows

The theory of stationary, axisymmetric, ideal MHD flows was developed by Chandrasekhar (1956); Woltjer (1959); Mestel (1968); Kulikovskiy and Lyubimov (1962); and others. Under these conditions the MHD equations can be reduced to a single equation for the “flux function” $\Psi(r, z)$ in cylindrical (r, ϕ, z) coordinates (Heinemann and Olbert, 1978; Lovelace et al., 1986). The flux function Ψ labels flux surfaces so that $\Psi(r, z) = \text{const}$ represents the poloidal projection of a field line. The equation for Ψ is commonly referred to as the Grad–Shafranov equation (Lovelace et al., 1986). The discussion of this section follows that of Ustyugova et al. (1999).

6.3.1. Integrals of motion

For axisymmetric conditions the flow field can be written as $v = v_p + v_\phi \mathbf{e}_\phi$ where v_p is the poloidal (r, z) component, $v_\phi = \omega r > 0$ is the toroidal component, and \mathbf{e}_ϕ is the unit toroidal vector. Similarly, the magnetic field can be written as $\mathbf{B} = \mathbf{B}_p + B_\phi \mathbf{e}_\phi$. The ideal MHD equations then imply that certain quantities are constants on any given flux surface $\Psi(r, z) = \text{const}$ or equivalently they are constants along any given stream line or a given magnetic field line. These integrals are functions of Ψ (see for example Lovelace et al., 1986),

$$\mathbf{v}_p = \frac{K(\Psi)}{4\pi\rho} \mathbf{B}_p \quad (353)$$

$$\omega r^2 - \frac{rB_\phi}{K} = \Lambda(\Psi) \quad (354)$$

$$\omega - \frac{KB_\phi}{4\pi\rho r} = \Omega(\Psi) \quad (355)$$

$$S = S(\Psi) \tag{356}$$

$$w + \Phi - \frac{\Omega^2 r^2}{2} + \frac{\mathbf{v}_p^2}{2} + \frac{1}{2}(\omega - \Omega)^2 r^2 = E(\Psi) \tag{357}$$

Here, S is the entropy, w is the enthalpy, and Φ is the gravitational potential. The quantity K corresponds to the conservation of mass along a stream-line, Λ to the conservation of angular momentum, Ω to the conservation of helicity, S to the conservation of entropy, and E (Bernoulli's constant) to the conservation of energy.

The remaining MHD equation (which cannot be written in the integral form) is the Euler force equation across the poloidal magnetic field line (Bogovalov, 1997),

$$\begin{aligned} &(\mathbf{v}_p^2 - v_{Ap}^2) \frac{\partial \theta}{\partial s} - \frac{\cos \theta}{r} (v_\phi^2 - v_{A\phi}^2) \\ &+ \frac{1}{\rho} \frac{\partial}{\partial n} \left(p + \frac{\mathbf{B}^2}{8\pi} \right) + \frac{\partial \Phi}{\partial n} = 0, \end{aligned} \tag{358}$$

which is equivalent to the Grad–Shafranov equation. Here, $\partial/\partial n$ is the derivative in the direction perpendicular to magnetic field lines and directed outward from the axis, θ is the angle of inclination of the poloidal magnetic field line away from the z -axis, s is the distance from the disk along a magnetic field line, $v_{Ap} \equiv |\mathbf{B}_p|/\sqrt{4\pi\rho}$ and $v_{A\phi} \equiv |B_\phi|/\sqrt{4\pi\rho}$ are the poloidal and azimuthal Alfvén velocities. The quantity $\partial\theta/\partial s$ is the curvature of magnetic field line. The first two terms in Eq. (6) are determined by the non-diagonal (tension) part of the stress tensor, $\rho v_i v_k + (p + \mathbf{B}^2/8\pi)\delta_{ik} - B_i B_k/4\pi$. The third term is determined by the total (matter plus magnetic) pressure $p + \mathbf{B}^2/8\pi$ and the gravity force $\partial\Phi/\partial n$.

To clarify the physical sense of the integrals of motion, it is useful to derive the fluxes of mass, angular momentum (about the z -axis), and energy. The corresponding conservation laws for stationary conditions are

$$\nabla \cdot (\rho \mathbf{v}_p) = 0, \tag{359}$$

$$\nabla \cdot \left(r \rho \mathbf{v}_p v_\phi - \frac{\mathbf{B}_p r B_\phi}{4\pi} \right) = 0, \tag{360}$$

$$\nabla \cdot \left[\rho \mathbf{v}_p \left(\frac{\mathbf{v}^2}{2} + \frac{\mathbf{B}^2}{4\pi\rho} + w + \Phi \right) - \frac{\mathbf{B}_p (\mathbf{v} \cdot \mathbf{B})}{4\pi} \right] = 0. \tag{361}$$

Because $v_p \parallel \mathbf{B}_p$, the vector flux densities are directed along the field lines.

Consider the fluxes through an annular region with surface area element $d\mathbf{S}$. The matter flux through the axisymmetric surface \mathbf{S} extending out from the z -axis is

$$\mathcal{F}_M = \int_S d\mathbf{S} \cdot \rho \mathbf{v}_p = \frac{1}{4\pi} \int_S d\mathbf{S} \cdot \mathbf{B}_p K(\Psi), \tag{362}$$

where we took into account the integral (353). $d\mathbf{S} \cdot \mathbf{B}_p$ is the magnetic flux through the annular region bounded by flux surfaces Ψ and $\Psi + d\Psi$. Thus we can change from space integration to integration over Ψ . Because $B_r = -(1/r) \partial\Psi/\partial z$ and $B_z = (1/r) \partial\Psi/\partial r$, we have

$$\mathcal{F}_M(\Psi) = \frac{1}{2} \int_0^\Psi d\Psi' K(\Psi'), \tag{363}$$

where $\Psi = 0$ corresponds to the z -axis. Similarly,

$$\begin{aligned} \mathcal{F}_L(\Psi) &= \int d\mathbf{S} \cdot \left(r \rho \mathbf{v}_p v_\phi - \frac{\mathbf{B}_p r B_\phi}{4\pi} \right) \\ &= \frac{1}{2} \int_0^\Psi d\Psi' \Lambda(\Psi') K(\Psi'), \end{aligned} \tag{364}$$

$$\begin{aligned} \mathcal{F}_E(\Psi) &= \int d\mathbf{S} \cdot \rho \mathbf{v}_p \\ &\times \left[\left(\frac{\mathbf{v}^2}{2} + \frac{\mathbf{B}^2}{4\pi\rho} + w + \Phi \right) - \frac{\mathbf{B}_p \mathbf{v} \cdot \mathbf{B}}{4\pi} \right] \\ &= \frac{1}{2} \int_0^\Psi d\Psi' (E + \Lambda\Omega) K. \end{aligned} \tag{365}$$

Thus, $K d\Psi/2$ is the matter flux between the flux surfaces separated by $d\Psi$, $\Lambda K d\Psi/2$ is the angular momentum flux, and $(E + \Lambda\Omega) K d\Psi/2$ is the energy flux. Note that $\Lambda(\Psi)$ is the specific angular momentum carried along the magnetic field line $\Psi = \text{const}$, $E(\Psi) + \Lambda\Omega(\Psi)$ is the specific energy, and $\Omega(\Psi)$ is

the angular velocity of the disk at the point where the magnetic field line or flux surface $\Psi = \text{const}$ intersects the disk (for $|v_p| \rightarrow 0$ at the disk).

6.3.2. Alfvén surface

Conditions at the Alfvén surface are known to be important for the global properties of MHD flows (Weber and Davis, 1967). Eqs. (2) and (3) constitute a linear system of equations for ω and B_ϕ . The determinant of this system is zero if $K^2 = 4\pi\rho$. Under this condition a solution exists if $\Lambda = r^2\Omega$ (Weber and Davis, 1967) which corresponds to $v_p = \mathbf{B}_p/\sqrt{4\pi\rho} = v_{Ap}$. This is the condition which defines the Alfvén surface. Fig. 20 shows the Alfvén surface for a sample case. The radius at which this field line intersects the disk is $r_d(\Psi)$. The radius at which it crosses the Alfvén surface is $r_A(\Psi)$. The density at this point on the Alfvén surface is $\rho_A(\Psi)$. Thus,

$$\begin{aligned} \rho_A(\Psi) &= K^2(\Psi)/4\pi, \\ r_A^2(\Psi) &= \Lambda(\Psi)/\Omega(\Psi). \end{aligned} \quad (366)$$

Eqs. (354) and (355) give

$$\omega = \Omega \frac{1 - \rho_A r_A^2 / \rho r^2}{1 - \rho_A / \rho}, \quad (367)$$

$$B_\phi = r\Omega\sqrt{4\pi\rho_A} \frac{1 - r_A^2/r^2}{1 - \rho_A/\rho}. \quad (368)$$

Taking into account Eqs. (366)–(368), one can express the fluxes of mass, angular momentum and energy, using only the values of physical quantities on the Alfvén surface:

$$\mathcal{F}_M(\Psi) = \int_0^\Psi d\Psi' \sqrt{\pi\rho_A}, \quad (369)$$

$$\mathcal{F}_L(\Psi) = \int_0^\Psi d\Psi' \sqrt{\pi\rho_A} \Omega r_A^2, \quad (370)$$

$$\mathcal{F}_E(\Psi) = \int_0^\Psi d\Psi' \sqrt{\pi\rho_A} (E + \Omega^2 r_A^2). \quad (371)$$

6.3.3. Forces

For understanding the plasma acceleration, we project the different forces onto the poloidal magnetic field lines. As mentioned, in a stationary state, matter flows along the poloidal magnetic field lines. The acceleration in the poloidal (r, z) plane is

$$(\mathbf{v}_p \cdot \nabla) \mathbf{v}_p + v_\phi (\mathbf{e}_\phi \cdot \nabla) (v_\phi \mathbf{e}_\phi). \quad (372)$$

The last term represents the centrifugal acceleration $-(v_\phi^2/r)\mathbf{e}_r = -r\omega^2\mathbf{e}_r$. To get the force per unit mass along a magnetic field line, we multiply the Euler equation by a unit vector $\hat{\mathbf{b}}$ parallel to \mathbf{B}_p . This gives

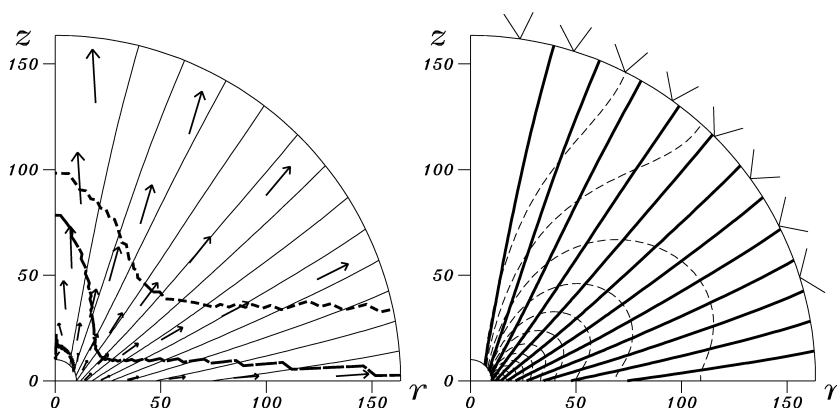


Fig. 20. Simulation results for stationary MHD outflow obtained using a spherical coordinate system (Ustyugova et al., 1999). The solid lines represent the poloidal magnetic field, and the arrows the velocity vectors. The dashed lines in the left-hand plot represent the slow magnetosonic surface (the lowest dashed line), the Alfvén surface (the middle line), and the fast magnetosonic surface (the top line). In the right-hand panel, the dashed lines are surfaces of constant toroidal current density, while the lines on the outer boundary are the projections of the fast magnetosonic Mach cones.

$$f = \omega^2 r \sin \theta - \frac{1}{\rho} \frac{\partial p}{\partial s} - \frac{\partial \Phi}{\partial s} + \frac{1}{4\pi\rho} \hat{\mathbf{b}} \cdot [(\nabla \times \mathbf{B}) \times \mathbf{B}], \quad (373)$$

where θ is the inclination angle of the field line to the z -axis. The final term of (373) is the projection of the magnetic force in the direction of $\hat{\mathbf{b}}$, which can be transformed to

$$f_M = \frac{1}{4\pi\rho} \hat{\mathbf{b}} \cdot [(\nabla \times \mathbf{B}) \times \mathbf{B}] = -\frac{1}{8\pi\rho r^2} \frac{\partial (rB_\phi)^2}{\partial s},$$

which is useful for understanding our results.

When magnetic field lines are inclined outward, away from the symmetry axis, the gravitational force $f_G = \partial\Phi/\partial s$ opposes the outflow of matter from the disk. If the matter is relatively cold then the pressure gradient force $f_p = -(1/\rho)(\partial p/\partial s)$ is unimportant. Then matter is accelerated outward by the centrifugal force $f_C = \omega^2 r \sin \theta$ and/or the magnetic force f_M . This determines the driving mechanisms of the outflow, centrifugal and/or magnetic. The centrifugal force always acts to accelerates matter outward if the distance between magnetic field line and the axis increases. However, under the same condition, the magnetic force can act to accelerate or decelerate the flow depending on the direction of $-\nabla(rB_\phi)^2$ (see discussion in Ustyugova et al., 1999).

Thus, magnetic and centrifugal forces may both accelerate matter, but this depends on the configuration of magnetic field and current-density lines.

6.3.4. Collimation of outflows

Consider now the collimation of the flow. From Eq. (358), taking into account that $\cos \theta = \partial r/\partial n$, we have

$$(\mathbf{v}_p^2 - v_{Ap}^2) \frac{\partial \theta}{\partial s} = -\frac{1}{8\pi\rho r^2} \frac{\partial}{\partial n} (rB_\phi)^2 + \frac{\cos \theta v_\phi^2}{r} - \frac{1}{\rho} \frac{\partial}{\partial n} \left(p + \frac{\mathbf{B}_p^2}{8\pi} \right) - \frac{\partial \Phi}{\partial n}. \quad (374)$$

At large distances from the Alfvén surface $r \gg r_A$, the density $\rho \ll \rho_A$, but values ρr^2 and v_p^2 remain finite (Heyvaerts and Norman, 1989). Then $v_{Ap}^2 = (\rho/\rho_A)^2 v_p^2 \ll v_p^2$, so that the second term on the left-hand side of (374) is negligible. On the right-hand

side, only the first term is important for $r \gg r_A$. Then, Eq. (374) simplifies to

$$v_p^2 \frac{\partial \theta}{\partial s} = -\frac{1}{8\pi\rho r^2} \frac{\partial}{\partial n} (rB_\phi)^2. \quad (375)$$

Thus, the curvature of magnetic field lines in the region $r \gg r_A$ is determined by the gradient $(rB_\phi)^2$. This force can act either to “collimate” the flow or “anticollimate” it depending on the orientation of the $rB_\phi(r, z) = \text{const}$ and $\Psi(r, z) = \text{const}$ surfaces (Ustyugova et al., 1999). The simulation study of Ustyugova et al. (1999) in fact finds only very small collimation of the hydromagnetic outflows over distances of the order of 100 times the inner disk radius. Recent work by Ustyugova et al. (2000) extends this conclusion by showing only small collimation out to distances of > 1000 times the inner disk radius. The collimation observed in protostellar jets at small distances, for example, in HH 30 observed with the space telescope, may result from the pressure of the external medium (Lovelace et al., 1991).

The conclusion by Heyvaerts and Norman (1989) that the magnetic collimation of MHD jets is a mathematical rather than physical result. The conclusion is based on the premise that the entire half-space above the disk is described by a stationary solution $\Psi(r, z)$ of the Grad–Shafranov equation. In reality, MHD jets result from initial conditions at the disk (as in the simulation studies) which result in the outward propagation of the jet into a highly conducting ionized external (interstellar or intergalactic) medium. At a given time, the region inside the surface $r = \mathcal{R}(z, t)$ is filled by the jet flow and the region outside it is filled by external plasma. The net axial current carried by the jet $2\pi \int_0^{\mathcal{R}} r dr J_z$ (for say $z > 0$) is necessarily zero for any (z, t) . Therefore, the toroidal magnetic field is zero on the surface \mathcal{R} , and there is *no* magnetic confinement of the flow. Of course, it is possible that a fraction of the flux Ψ is collimated along the z -axis while the remaining flux is “anti-collimated” (that is, pushed away) from the z -axis. Exactly such a case is discussed in Section 2.5 below for the case of Poynting jets. This case also has the physical condition that the jet carries no net magnetic flux, $2\pi \int_0^{\mathcal{R}} r dr B_z = 0$. As in Landau’s (1946) treatment of the damping of plasma waves,

the physically correct treatment of the collimation of MHD jets requires consideration of an initial value problem.

6.4. Numerical simulations of MHD outflows

In order to test and more fully understand analytical models of stationary outflows, MHD simulations of flows from a disk treated as a boundary condition have been carried out by a number of groups.

6.4.1. Non-stationary outflows

The initial magnetic field configuration was chosen so that the magnetic field was significantly inclined to the disk ($\theta > 30^\circ$) over most of the disk surface (Ustyugova et al., 1995; Koldoba et al., 1995). The simulations involve solving the complete system of ideal non-relativistic MHD equations using a Godunov-type code assuming axisymmetry but taking into account all three components of velocity and magnetic field. Matter of the corona was initially in thermal equilibrium with the gravitating center. At $t = 0$, the disk is set into rotation with Keplerian velocity and at the same time matter is pushed from the disk with a small poloidal velocity equal to a fraction of the slow magnetosonic velocity ($v_p = \alpha v_{sm}$, with $\alpha = 0.1-0.9$). A relatively high temperature and small magnetic field was considered. We found that at the maximum of the outflow, matter is accelerated to speeds in excess of the escape speed and in excess of the fast magnetosonic speed within the simulation region ($\sim 100r_i$). The acceleration is due to both thermal and magnetic pressure gradients. The outflow collimates within the simulation region due to strong amplification, “wrapping up” of the toroidal magnetic field and the associated pinching force.

However, the outflows are *not stationary*. The matter flux grows to a peak and then decreases to relatively small values. The strong collimation of the outflow reduces the divergence of the field away from the z -axis ($\theta < 30^\circ$) and this “turns off” the outflow of matter and leads to flow velocities less than the escape speed. Thus, this simulation is an example of a temporary outburst of matter to a jet. Unfortunately, this type of flow has a significant dependence on the initial conditions.

6.4.2. Stationary outflows

More recently, stationary magnetohydrodynamic outflows from a rotating accretion disk have been obtained by time-dependent axisymmetric simulations by Romanova et al. (1997) and systematically analyzed by Ustyugova et al. (1999). The initial magnetic field in the latter work was taken to be a split-monopole poloidal field configuration (Sakurai, 1987) frozen into the disk. The disk was treated as a perfectly conducting, time-independent density boundary [$\rho(r)$] in Keplerian rotation which is different from the earlier specification of a small velocity outflow (Section 5.3.1, Ustyugova et al., 1995). The outflow velocity from the disk is determined self-consistently from the MHD equations. The temperature of the matter outflowing from the disk is small in the region where the magnetic field is inclined away from the symmetry axis ($c_s^2 \ll v_K^2$), but relatively high ($c_s^2 \approx v_K^2$) at very small radii in the disk where the magnetic field is not inclined away from the axis. We have found a large class of stationary MHD winds.

Fig. 20 shows the nature of the stationary MHD outflows found by Ustyugova et al. (1999). The outflows are approximately spherical, with only small collimation within the simulation region. The *collimation distance* over which the flow becomes collimated (with divergence less than, say, 10°) is much larger than the size of our simulation region. Because the flow is super fast-magnetosonic (see below), the flow is not expected to magnetically collimate at larger distances. Notice for example that the solar wind is also super fast-magnetosonic and essentially uncollimated. Collimation may however result from the pressure of external plasma (Lovelace et al., 1991).

Fig. 21 shows the variation of the flow speed and other characteristic speeds along a sample streamline. The outflow accelerates from thermal velocity ($\sim c_s$) to a much larger asymptotic poloidal flow velocity of the order of one-half $\sqrt{GM/r_i}$ where M is the mass of the central object and r_i is the inner radius of the disk. This asymptotic velocity is much larger than the local escape speed and is larger than fast magnetosonic speed by a factor of ~ 1.75 . The *acceleration distance* for the outflow, over which the flow accelerates from ~ 0 to, say, 90% of the asymptotic speed, occurs at a flow distance of about

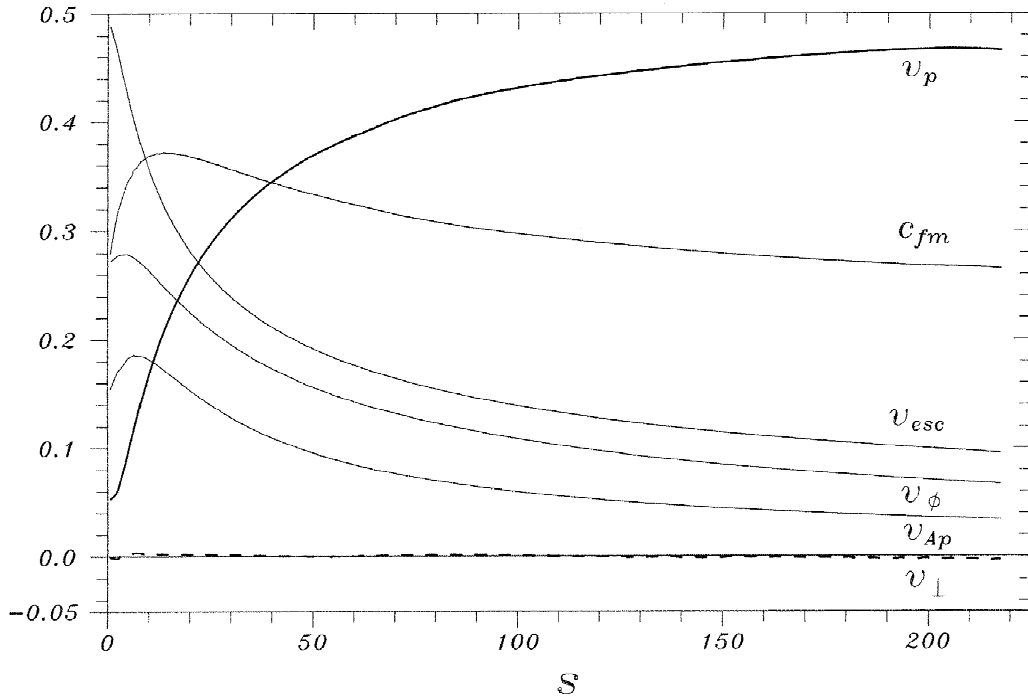


Fig. 21. Dependences of different velocities on distance s measured in units of r_i from the disk along the second magnetic field line away from the axis in Fig. 20 (Ustyugova et al., 1999). This field line “starts” from the disk at $r \approx 6r_i$, where it has an angle $\theta \approx 28^\circ$ relative to the z -axis. The velocities are measured in units of $\sqrt{GM/r_i}$. Here, v_p is the poloidal velocity along the field line and v_\perp is the poloidal velocity perpendicular to the field line. Also, v_{Ap} is the poloidal Alfvén velocity, c_{fm} is the fast magnetosonic velocity, and v_{esc} is the local escape velocity.

$80r_i$. Close to the disk the outflow is driven by the centrifugal force while at all larger distances the flow is driven by the magnetic force which is proportional to $-\nabla(rB_\phi)^2$, where B_ϕ is the toroidal field.

The stationary MHD flow solutions allow us (353) to compare the results with MHD theory of stationary flows, (354) to investigate the influence of different outer boundary conditions on the flows, and (355) to investigate the influence of the shape of the simulation region on the flows. The ideal MHD integrals of motion (constants on flux surfaces discussed by Lovelace et al., 1986) were calculated along magnetic field lines and were shown to be constants with accuracy 5–15%. Other characteristics of the numerical solutions were compared with the theory, including conditions at the Alfvén surface.

Different outer boundary conditions on the toroidal component of the magnetic field can significantly influence the calculated flows. The commonly used

“free” boundary condition on the toroidal field leads to artificial magnetic forces on the outer boundaries, which can give spurious collimation of the flows. New outer boundary conditions which do not give artificial forces have been proposed and investigated by Ustyugova et al. (1999).

The simulated flows may also depend on the shape of the simulation region. Namely, if the simulation region is elongated in the z -direction, then Mach cones on the outer cylindrical boundaries may be partially directed inside the simulation region. Because of this, the boundary can have an artificial influence on the calculated flow. This effect is reduced if the computational region is approximately square or if it is spherical as in Fig. 20. Simulations of MHD outflows with an elongated computational region can lead to *artificial* collimation of the flow.

Recent simulation studies have treated MHD outflows from disks with more general initial \mathbf{B} field configurations, for example, that where the poloidal

field has different polarities as a function of radius (Hayashi et al., 1996; Goodson et al., 1997; Romanova et al., 1998). The differential rotation of the foot-points of \mathbf{B} field loops at different radii on the disk surface causes twisting of the coronal magnetic field, an increase in the coronal magnetic energy, and an opening of the loops in the region where the magnetic pressure is larger than the matter pressure ($\beta \lesssim 1$) (Romanova et al., 1998). In the region where $\beta \lesssim 1$, the loops may be only partially opened. Current layers form in the narrow regions which separate oppositely directed magnetic field. Reconnection occurs in these layers as a result of the small numerical magnetic diffusivity. In contrast with the case of the solar corona, there can be a steady outflow of energy and matter from the disk surface. We find that the power output mainly in the form of a Poynting flux. Opening of magnetic field loops and subsequent closing can give reconnection events which may be responsible for X-ray flares in disks around both stellar mass objects and massive black holes (Hayashi et al., 1996; Goodson et al., 1997; Romanova et al., 1998).

6.5. Poynting jets

In a very different regime from the hydromagnetic flows discussed in Sections 3–5, a Poynting outflow or jet transports energy and angular momentum mainly by the electromagnetic fields with only a small contribution due to the matter (Lovelace et al., 1987, 2001; Colgate and Li, 1998; Romanova et al., 1998; Ustyugova et al., 2000; Li et al., 2001). A steady Poynting jet can be characterized in the lab frame by its asymptotic (large distance) magnetic field $B_\phi = -B_0[r_o/r_j(z)]$ at the jet's edge, $r = r_j(z)$, where r_o is the jet's radius at $z = 0$ and B_0 is the poloidal field strength at this location. The electric field in the jet is $\mathbf{E} = -v \times \mathbf{B}/c$ and consequently the energy flux or luminosity of the jet is $L_j = vB_0^2 r_o^2 / 8 \sim 4 \times 10^{45} \text{ erg/s} (v/c)(r_o/10^{14} \text{ cm})^2 (B_0/10^4 \text{ G})^2$. Propagating disturbances in such field dominated jets provide a simple, but self-consistent physical model for the gamma ray flares observed in Blazars (Romanova and Lovelace, 1997; Levinson, 1998; Romanova, 1999). Owing to pair production close to the black hole, the main constituent of a Poynting flux jet may be electron–positron pairs.

6.5.1. Theory of Poynting jets

Consider the coronal magnetic field of a differentially rotating Keplerian accretion disk for a given poloidal field threading the disk. That is, the disk is perfectly conducting with a very small accretion speed. Further, consider “coronal or force-free” magnetic fields in the non-relativistic limit. We use cylindrical (r, ϕ, z) coordinates as in Section 4 and consider axisymmetric field configurations. Thus the magnetic field has the form $\mathbf{B} = \mathbf{B}_p + B_\phi \hat{\phi}$, with $\mathbf{B}_p = B_r \hat{r} + B_z \hat{z}$. Because $\nabla \cdot \mathbf{B} = 0$, $\mathbf{B} = \nabla \times \mathbf{A}$ with \mathbf{A} the vector potential. Consequently, $B_r = -(1/r)(\partial \Psi / \partial z)$, $B_z = (1/r)(\partial \Psi / \partial r)$, where $\Psi(r, z) \equiv rA_\phi(r, z)$. The $\Psi(r, z) = \text{const}$ lines label the poloidal field lines; that is, $(\mathbf{B}_p \cdot \nabla)\Psi = 0 = \mathbf{B} \cdot \nabla \Psi = 0$. Note that $2\pi\Psi(r, z)$ is the magnetic flux through a horizontal, coaxial circular disk of radius r .

The magnetic field threading the disk at $z = 0$ is assumed to evolve slowly so that it can be considered approximately time-independent, $\Psi(r, z = 0) = \Psi_0(r)$. However, the magnetic field above the disk will in general be time-dependent, $\Psi = \Psi(r, z, t)$, due to the differential rotation of the disk. Fig. 22 shows a possible vacuum poloidal magnetic field threading the disk. This field may be regarded as the “initial” field for the considered case where the space exterior to the disk is filled with a low density plasma.

The non-relativistic equation of plasma motion in the corona of an accretion disk is

$$\rho \, d\mathbf{v}/dt = -\nabla p + \rho \mathbf{g} + \mathbf{J} \times \mathbf{B}/c, \quad (376)$$

where v is the flow velocity, p is the pressure, and \mathbf{g} is the gravitational acceleration. The equation for the \mathbf{B} field is $\nabla \times \mathbf{B} = 4\pi\mathbf{J}/c$, because the displacement current is negligible in the non-relativistic limit. In the “coronal or force-free plasma limit,” the magnetic energy density $\mathbf{B}^2/(8\pi)$ is much larger than the kinetic or thermal energy densities; that is, sub-Alfvénic flow speeds v , $v^2 \ll v_A^2 = \mathbf{B}^2/4\pi\rho$, where v_A is the Alfvén velocity. Eq. (376) then simplifies to $0 \approx \mathbf{J} \times \mathbf{B}$; therefore, $\mathbf{J} = \lambda\mathbf{B}$ (Gold and Hoyle, 1960). Because $\nabla \cdot \mathbf{J} = 0$, $(\mathbf{B} \cdot \nabla)\lambda = 0$ and consequently $\lambda = \lambda(\Psi)$, as well-known. Thus Ampère's law becomes $\nabla \times \mathbf{B} = 4\pi\lambda(\Psi)\mathbf{B}/c$.

The r and z components of this equation imply $rB_\phi = H(\Psi)$, and $dH(\Psi)/d\Psi = 4\pi\lambda(\Psi)/c$, where $H(\Psi)$ is another function of Ψ . Thus, $H(\Psi) = \text{const}$

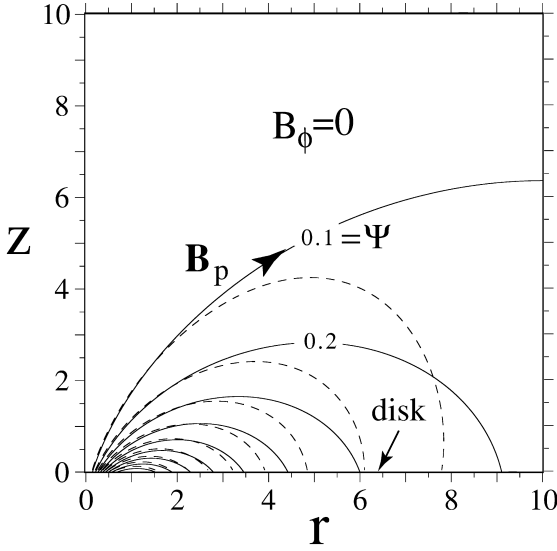


Fig. 22. “Initial” dipole-like vacuum magnetic field from Lovelace et al. (2001). In this and subsequent plots, r and z are measured in units of the radius r_0 of the O -point in the disk plane. The solid lines are the magnetic field lines for the case where the flux function on the disk surface is $\Psi(r, z=0) = a^3 r^2 K / (a^2 + r^2)^{3/2}$ with $a = r_0 / \sqrt{2}$. In this and subsequent plots Ψ is measured in units of $\Psi_0 = r_0^2 K / 3^{3/2}$. Note that $B_z(0) = 6\sqrt{3}\Psi_0 / r_0^2 \approx 10.4\Psi_0 / r_0^2$. The dashed lines are the field lines for the case where the outer boundaries ($R_{\max} = 10, Z_{\max} = 10$) are perfectly conducting; for this case $\Psi(r, z=0) \rightarrow \Psi(r, 0)[1 - (r/r_0 - 1)^2/81]$ so that the O -point is still at r_0 and Ψ_0 is unchanged. Because of axisymmetry and reflection symmetry about the $z=0$ plane, the field need be shown in only one quadrant.

are lines of constant poloidal current density; $\mathbf{J}_p = (c/4\pi)(dH/d\Psi)\mathbf{B}_p$ so that $(\mathbf{J}_p \cdot \nabla)H = 0$. The toroidal component of Ampère’s law gives

$$\Delta^* \Psi = -H(\Psi) \frac{dH(\Psi)}{d\Psi}, \quad (377)$$

which is the Grad–Shafranov equation for Ψ (see for example Bateman, 1980; Lovelace et al., 1986). Here, $\Delta^* \equiv \partial^2/\partial r^2 - (1/r)(\partial/\partial r) + \partial^2/\partial z^2$ is the adjoint Laplacian operator. Note that $\Delta^* \Psi = r(\nabla^2 - 1/r^2)A_\phi$ and that $H(dH/d\Psi) = 4\pi r J_\phi/c$. From Ampère’s law, $\oint d\mathbf{l} \cdot \mathbf{B} = (4\pi/c) \int d\mathbf{S} \cdot \mathbf{J}$, so that $rB_\phi(r, z) = H(\Psi)$ is $(2/c)$ times the current flowing through a circular area of radius r (with normal $\hat{\mathbf{z}}$) labeled by $\Psi(r, z) = \text{const}$. Equivalently, $-H[\Psi(r, 0)]$ is $(2/c) \times$ the current flowing into the area of the disk $\leq r$. For all cases studied here, $-H(\Psi)$ has a maximum so that the total current flowing into the

disk for $r \leq r_m$ is $I_{\text{tot}} = 2/c(-H)_{\max}$, where r_m is such that $-H[\Psi(r_m, 0)] = (-H)_{\max}$ so that r_m is less than the radius of the O -point, r_0 . The same total current I_{tot} flows out of the region of the disk $r = r_m$ to r_0 .

The function $H(\Psi)$ must be determined before the GS equation can be solved. Lynden-Bell and Boily (1994) determined the form of $H(\Psi)$ by requiring that the solution $\Psi(\mathbf{r})$ be a self-similar function of $|\mathbf{r}|$. Their stationary solution has *no* energy or angular momentum outflow from the disk. However, in general the magnetic field threading a disk will have definite length-scales and the field solution will not be self-similar.

For definiteness we consider the *initial value problem* where the disk at $t=0$ is threaded by a poloidal field such as shown in Fig. 22. Such a field can arise from a disk-dynamo driven by star-disk collisions as discussed by Pariev et al. (2001). We assume for simplicity that the field threading the disk has the symmetry of a dipole although it is predicted in the reference above that the quadrupole field grows somewhat faster.

The form of $H(\Psi)$ is then determined by the differential rotation of the disk: The azimuthal *twist* of a given field line going from an inner footpoint at r_1 to an outer footpoint at r_2 is fixed by the differential rotation of the disk. The field line slippage speed through the disk due to the disk’s finite magnetic diffusivity is estimated to be negligible compared with the Keplerian velocity. For a given field line we have $r d\phi/B_\phi = ds_p/B_p$, where $ds_p \equiv \sqrt{dr^2 + dz^2}$ is the poloidal arc length along the field line, and $B_p \equiv \sqrt{B_r^2 + B_z^2}$. The total twist of a field line loop is

$$\Delta\phi(\Psi) = \int_1^2 ds_p \frac{-B_\phi}{rB_p} = -H(\Psi) \int_1^2 \frac{ds_p}{r^2 B_p}, \quad (378)$$

with the sign included to give $\Delta\phi > 0$. For a Keplerian disk around an object of mass M the angular rotation is $\omega_K = \sqrt{GM/r^3}$ so that the field line twist after a time t is

$$\begin{aligned} \Delta\phi(\Psi) &= \omega_0 t \left[\left(\frac{r_0}{r_1} \right)^{3/2} - \left(\frac{r_0}{r_2} \right)^{3/2} \right] \\ &= (\omega_0 t) \mathcal{F}(\Psi/\Psi_0) \end{aligned} \quad (379)$$

where r_0 is the radius of the O -point, $\omega_0 \equiv \sqrt{GM/r_0^3}$, and \mathcal{F} is a dimensionless function (the quantity in the square brackets). At sufficiently small r_1 one reaches the inner radius of the disk r_i ($\ll r_0$) where we assume ω_k saturates at the value $\omega_{ki} = \sqrt{GM/r_i^3}$. For the dipole-like field of Fig. 22, $\mathcal{F} \approx 3^{9/8}(\Psi_0/\Psi)^{3/4}$ for $\Psi/\Psi_0 \ll 1$, while $\mathcal{F} \approx 3.64(1 - \Psi/\Psi_0)^{1/2}$ for $1 - \Psi/\Psi_0 \ll 1$.

The quantity $T \equiv \omega_0 t$ (in radians) we refer to as the “twist” of the disk. For the dashed field lines of Fig. 22, T is the twist $\Delta\phi(\Psi_1)$ of the field line with $\Psi_1/\Psi_0 \approx 0.932$ which has footpoints at $r_1 \approx 0.73r_0$ and $r_2 \approx 1.4r_0$. For $\Psi/\Psi_0 = 0.1$, where the footpoints are at $r_1 \approx 0.14r_0$ and $r_2 \approx 7.8r_0$, the field line twist is $\Delta\phi \approx 18.3$ rad. for $T = 1$.

For example, for an accretion disk around a massive black hole $M = M_8 10^8 M_\odot$ in the nucleus of galaxy, the twist is $T = (t/3.17d)(r_0/10^{15} \text{ cm})^{3/2}/\sqrt{M_8}$. The inner radius of the disk is $r_i \approx M_8 9 \times 10^{13}$ cm for a Schwarzschild black hole.

The Grad–Shafranov equation (377) is an elliptic equation and can be readily solved by the method of Successive Over-Relaxation (SOR) (see for example Potter, 1973). $H(\Psi)$ is determined iteratively so that Eqs. (377)–(378) are all satisfied to a high accuracy (Finn and Chen, 1990; Li et al., 2001b). Fig. 23 shows a sample high twist solution exhibiting a Poynting jet (Lovelace et al., 2001). These high-twist solutions consist of a region near the axis which is *magnetically collimated* by the toroidal B_ϕ field and a region far from the axis, on the outer radial boundary, which is *anti-collimated* in the sense that it is pushed against the outer boundary. The field lines returning to the disk at $r > r_0$ are anti-collimated by the pressure of the toroidal magnetic field.

Fig. 24 shows a three dimensional view of two sample field lines for the same case as Fig. 23.

6.5.2. Analytic model of Poynting jets

Fig. 24 shows that most of the twist $\Delta\phi$ of a field line occurs along the jet from $z = 0$ to Z_{\max} . Because $-r^2 d\phi/H(\Psi) = dz/B_z$, we have

$$\frac{\Delta\phi(\Psi)}{-H(\Psi)} = \frac{(\omega_0 t)\mathcal{F}(\Psi/\Psi_0)}{-H(\Psi)} \approx \frac{Z_{\max}}{r^2 B_z}, \quad (380)$$

where $r^2 B_z(r, z)$ is evaluated on the straight part of

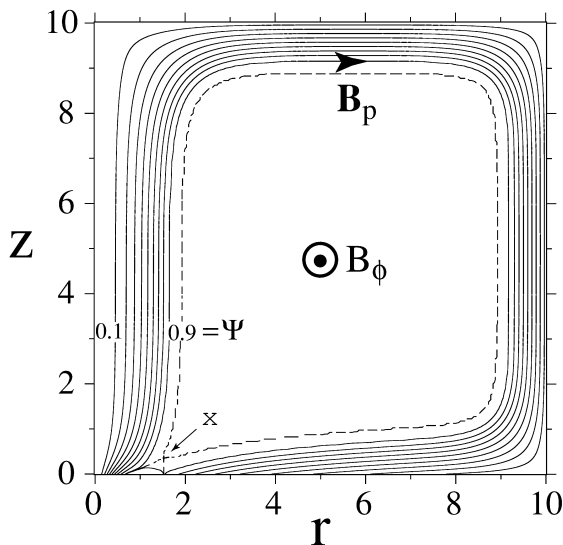


Fig. 23. Poloidal field lines for Poynting jet case for twist $T = 1.84$ rad. and $(-H)_{\max} = 1.13\Psi_0/r_0$ with $\Psi = \text{const}$ contours measured in units of Ψ_0 which is the maximum value of Ψ from Lovelace et al. (2001). The outer boundaries at $r = R_{\max}$ and $z = Z_{\max}$ are perfectly conducting and correspond to an external plasma. This external plasma will expand in response to the magnetic pressure of the jet so that R_{\max} and Z_{\max} will increase with time. The initial poloidal magnetic field is shown by the dashed lines in Fig. 22. The dashed contour is the separatrix with the X-point indicated. Note that the radial width of the upgoing field lines along the axis is about one-half the width of downgoing field lines at the outer wall as required for equilibrium.

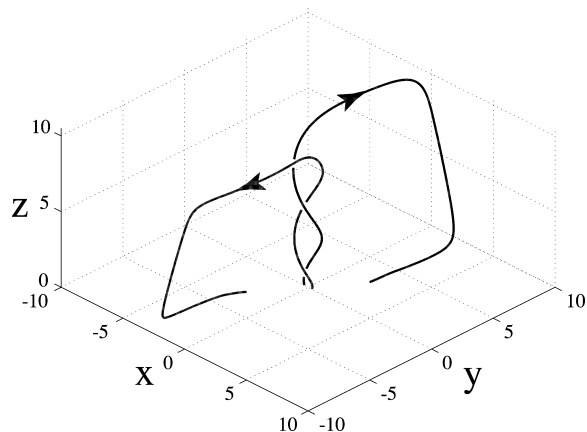


Fig. 24. Three dimensional view of two field lines originating from the disk at $x = \pm 0.32 r_0$ ($\Psi = 0.4\Psi_0$) for the Poynting jet of Fig. 23 from Lovelace et al. (2001). Each field line has a twist of ≈ 8.22 rad. or about 1.31 rotations about the z -axis from its beginning at r_1 and end at r_2 . The z -axis is tilted towards the viewer by 30° .

the jet at $r = r(\Psi)$. In the core of the jet $\Psi \ll \Psi_0$, we have $\mathcal{F} \approx 3^{9/8}(\Psi_0/\Psi)^{3/4}$, and in this region we can take

$$\Psi = C\Psi_0\left(\frac{r}{r_0}\right)^q, \\ H = -\mathcal{H}\left(\frac{\Psi_0}{r_0}\right)\left(\frac{\Psi}{\Psi_0}\right)^s, \quad (381)$$

where C , q , \mathcal{H} , and s are dimensionless constants. The GS equation for the straight part of the jet, $\Psi_{rr} - \Psi_r/r = -HH'$ implies $q = 1/(1-s)$ and $C^{2(1-s)} = s(1-s)^2\mathcal{H}^2/(1-2s)$. In turn, Eq. (381) implies $s = 1/4$ so that $q = 4/3$, $C = [9/32]^{2/3}\mathcal{H}^{4/3}$, and $\mathcal{H} = 3^{1/8}4(r_0\omega_0 t/Z_{\max})$.

In order to have a Poynting jet, we must have \mathcal{H} larger than ≈ 0.5 . For the case of uniform expansion of the top boundary, $Z_{\max} = V_z t$, this condition is the same as $V_z < 9.2(r_0\omega_0)$. For the case of Figs. 23 and 24, $\mathcal{H} \approx 0.844$.

The field components in the straight part of the jet are

$$B_\phi = -\sqrt{2}B_z = -\sqrt{2}\left(\frac{3}{16}\right)^{1/3}\mathcal{H}^{4/3}\left(\frac{\Psi_0}{r_0}\right)\left(\frac{r_0}{r}\right)^{2/3}. \quad (382)$$

These field components of course satisfy the radial force balance equation $d(B_z^2)/dr + (1/r^2)d(r^2B_\phi^2)/dr = 0$ which is equivalent to the GS equation. These dependences agree approximately with those found independently in the numerical simulations of Poynting jets by Ustyugova et al. (2000). On the disk, $\Psi \approx 3^{3/2}\Psi_0(r/r_0)^2$ for $r < r_0/3^{3/4}$. Using this and the equation for $\Psi(r)$ gives the relation between the radius of a field line in the disk, denoted r_d , and its radius in the jet, $r/r_0 = 2^{5/2}3^{1/8}(r_d/r_0)^{3/2}\mathcal{H}^{-1}$. Thus the power laws apply for $r_1 < r < r_2$, where $r_1 = 3^{1/8}2^{5/2}r_0(r_i/r_0)^{3/2}/\mathcal{H}$ and $r_2 = (2^{5/2}/3)r_0/\mathcal{H}$, with r_i the inner radius of the disk. The outer edge of the Poynting jet has a transition layer where the axial field changes from $B_z(r_2)$ to zero while (minus) the toroidal field increases from $-B_\phi(r_2)$ to $(-H)_{\max}/r_2$. Using Eqs. (19), which are only approximate at r_2 , gives $(-H)_{\max} \approx (3/2)^{1/2}\mathcal{H}\Psi_0/r_0$. This expression agrees approximately with our numerical results.

6.5.3. Occurrence of Poynting jets and the Kink instability

The rate at which toroidal flux Φ_t is created in the region above the disk is $d\Phi_t/dt \approx -12\omega_0\Phi_0$ (Lovelace et al., 2001). If the area $R_m Z_m$ of this region is fixed owing to a very dense external plasma, the average value of $-B_\phi > 0$ in it increases. On the other hand if the area $R_m Z_m$ increases rapidly enough, $-B_\phi$ will decrease. The Poynting jets occur under conditions where $-B_\phi$ increases to a sufficient extent to cause pinching of the poloidal magnetic field. Because the most rapid expansion of the \mathbf{B} field of occurs in the z -direction, a necessary condition for occurrence of a Poynting jet is that the rate of expansion of the boundary $V_z = dZ_m/dt$ be bounded by some constant. In fact the condition obtained in Section 5 for occurrence of Poynting jets has this form, $V_z < 9.2(\omega_0 r_0)$.

Note that there may be “self-regulation” in the respect that the field configuration which occurs is at the “boundary” between low and high-twist solutions. In view of Fig. 7, the low-twist field gives a gradual expansion of the boundaries which allows build up of toroidal flux whereas the high-twist field gives a more rapid expansion which tends to give a slower increase of Φ_t .

The region of collimated field (see Fig. 23) — the Poynting jet — has $v^2 \ll v_A^2$ and is kink unstable according to the standard non-relativistic analysis (e.g., Bateman, 1980, ch. 6). The instability will lead to a helical distortion of the jet with the non-linear amplitude of shift of the helix $\Delta r \sim v_A t$ and with the helix having the same twist about the z -axis as the axisymmetric \mathbf{B} field. Note however that for the astrophysical conditions of interest $v_A \equiv |\mathbf{B}|/\sqrt{4\pi\rho}$ is likely to be larger than the speed of light. A relativistic perturbation analysis is then required including the displacement current. The physical Alfvén speed is $V_A = c/(1 + c^2/v_A^2)^{1/2} < c$. Thus the speed of lateral displacement of the helix is less than c . The evolution of the Poynting jet evidently depends on both V_A and the velocity of propagation of the “head” of the jet V_z (Section 6) which may be relativistic. Relativistic propagation of the jet’s head may act to limit the amplitude of helical kink distortion of the jet. On the other hand a sub-relativistic propagation of the head may allow the helix amplitude to grow but this amplitude can be

limited by flux conservation as discussed by Kadomtsev (1963).

6.5.4. MHD simulations of Poynting jets

Ustyugova et al. (2000) did full, axisymmetric MHD simulations of a Keplerian disk initially threaded by a dipole-like magnetic field as shown in Fig. 22. For these simulations the outer boundaries at $r = R_{\max}$ and $z = Z_{\max}$ were treated as free boundaries following the methods of Ustyugova et al. (1999). These simulations established that a quasi-stationary collimated Poynting jet arises from the inner part of the disk while a steady uncollimated hydromagnetic outflow arises in the outer part of the disk. Fig. 25 shows the evolution towards a stationary Poynting jet.

Quasi-stationary Poynting jets from the two sides of the disk within r_0 , give an energy outflow per unit radius of the disk $d\dot{E}_B/dr = rv_K(-B_\phi B_z)_h$, where the h subscript indicates evaluation at the top surface of the disk. This outflow is $\sim r_0 d\dot{E}_B/dr \sim v_K(r_0)(\Psi_{\max}/r_0)^2 \sim 10^{45}(\text{erg/s})r_{015}^{3/2}\sqrt{M_8}[B_z(0)/6\text{kG}]^2$ where r_{015} is in units of 10^{15} cm, and M_8 in units of $10^8 M_\odot$. This formula agrees approximately with the values derived from the simulations. The jets also give an outflow of angular momentum from the disk which causes disk accretion (without viscosity) at the rate $\dot{M}_B(r) \equiv -2\pi\Sigma v_r = -2(r^2/v_K)(B_\phi B_z)_h \sim 2\Psi_{\max}^2/[r_0^2 v_K(r_0)]$, where Σ is the disk's surface mass density. (Lovelace et al., 1997). The Poynting jet has a net axial momentum flux $\dot{P}_z = (1/4)\int r dr(B_\phi^2 - B_z^2) \sim 0.5(\Psi_{\max}/r_0)^2$, which acts to drive the jet outward through an external medium. Further, the Poynting jet generates toroidal magnetic flux at the rate $\dot{\Phi}_t \sim -12[v_K(r_0)/r_0]\Psi_{\max}$.

For long time-scales, the Poynting jet is of course time-dependent due to the angular momentum it extracts from the inner disk ($r < r_0$). This loss of angular momentum leads to a ‘‘global magnetic instability’’ and collapse of the inner disk (Lovelace et al., 1997). An approximate model of this collapse can be made if the inner disk mass M_d is concentrated near the O -point radius $r_0(t)$, if the field line slippage through the disk is negligible (Lovelace et al., 1997), $\Psi_{\max} = \text{const}$, and if $(-rB_\phi)_{\max} \sim \Psi_{\max}/r_0(t)$ (as found here). Then, $M_d dr_0/dt = -2\Psi_{\max}^2(GMr_0)^{-1/2}$. If t_i denotes the time at which

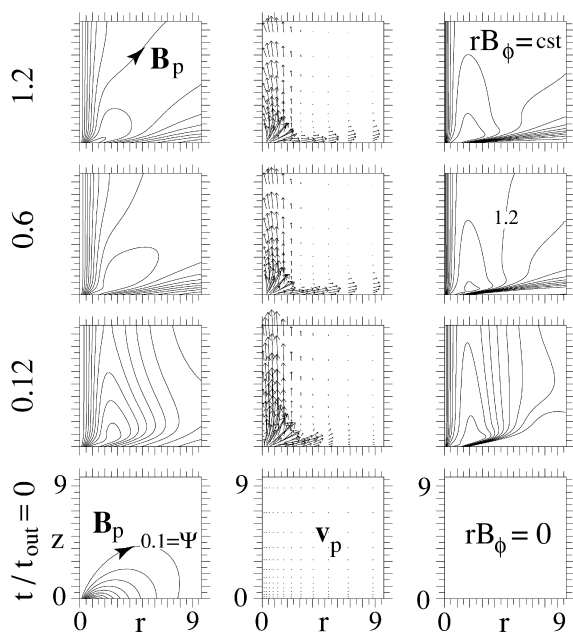


Fig. 25. Time evolution of dipole-like field threading the disk from the initial configuration $t = 0$ (bottom panels) to the final quasi-stationary state $t = 1.2t_{\text{out}}$, where t_{out} is the rotation period of the disk at the outer radius R_{\max} of the simulation region from Ustyugova et al. (2000). The left-hand panels show the poloidal field lines which are the same as $\Psi(r, z) = \text{const}$ lines; Ψ is normalized by Ψ_{\max} and the spacing between lines is 0.1. The middle panels show the poloidal velocity vectors v_p . The right-hand panels show the constant lines of $-rB_\phi(r, z) > 0$ in units of Ψ_{\max}/r_0 and the spacing between lines is 0.1. For this calculation a 100×100 inhomogeneous grid was used with Δr_j and Δz_k growing with distance r and z geometrically as $\Delta r_j = \Delta r_1 q^j$ and $\Delta z_k = \Delta z_1 q^k$, with $q = 1.03$ and $\Delta r_1 = \Delta z_1 = 0.05r_0$.

$r_0(t_i) = r_i$ (the inner radius of the disk), then $r_0(t) = r_i[1 - (t - t_i)/t_{\text{coll}}]^{2/3}$, for $t \leq t_i$, where $t_{\text{coll}} = \sqrt{GM_d}r_i^{3/2}/(3\Psi_{\max}^2)$ is the time-scale for the collapse of the inner disk. (Note that the time-scale for r_0 to decrease by a factor of 2 is $\sim t_i(r_0/r_i)^{3/2} \gg t_i$ for $r_0 \gg r_i$.) The power output to the Poynting jets is $\dot{E}(t) = (2/3)(\Delta E_{\text{tot}}/t_{\text{coll}})[1 - (t - t_i)/t_{\text{coll}}]^{-5/3}$, where $\Delta E_{\text{tot}} = GMM_d/2r_i$ is the total energy of the outburst. Roughly, $t_{\text{coll}} \sim 2 \text{ day } M_8^2(M_d/M_\odot)(6 \times 10^{32} \text{G cm}^2/\Psi_{\max})^2$ for a Schwarzschild black hole, where validity of the analysis requires $t_{\text{coll}} \gg t_i$.

6.6. Summary regarding jets from accretion disks

An ordered magnetic field threading an accretion

disk can give powerful outflows or jets of matter, energy, and angular momentum. Most of the studies have been in the hydromagnetic regime where there is appreciable mass outflow and find asymptotic flow speeds of the order of the maximum Keplerian velocity of the disk, v_{K_i} . These flows are clearly relevant to the jets from protostellar systems which have flow speeds of the order of v_{K_i} . In contrast, observed VLBI jets in quasars and active galaxies point to bulk Lorentz factors $\Gamma \sim 10$ — much larger than the disk Lorentz factor. In the jets of gamma ray burst sources, $\Gamma \sim 100$. The large Lorentz factors as well as the small Faraday rotation measures suggest that these jets are in the Poynting flux regime. Recent work has obtained self-consistent solutions for axisymmetric, non-relativistic plasma equilibria described by the force-free Grad–Shafranov equation (Li et al., 2001; Lovelace et al., 2001). Solutions have been found which are *magnetically collimated* and are termed Poynting jets. These jet solutions are close to those obtained earlier by MHD simulations by Ustyugova et al. (2000). These jets give a *continuous* outflow of energy, angular momentum, and toroidal magnetic flux from the disk into the external space. This behavior contradicts the commonly accepted “theorem” of Solar plasma physics that the motion of the footpoints of a magnetic loop structure leads to a stationary magnetic field configuration with zero power, angular momentum, and flux outflows.

Important issues remain to be investigated — the relativistic expansion of the head of a Poynting jets into an external medium and the three-dimensional kink instability of the jet. The mentioned global magnetic instability of an accretion disk may explain the flares of active galactic nuclei blazar sources (Romanova and Lovelace, 1997; Levinson, 1998; Romanova, 1999) and the outbursts of gamma ray burst sources (Katz, 1997). Further, the magnetic extraction of energy from a rotating black hole may be important (Blandford and Znajek, 1977; Livio et al., 1999).

7. Discussion

Observational evidence for massive black holes at the center of our Galaxy and in the nuclei of other

galaxies (Cherepashchuk, 1996; Ho, 1999; Haswell, 1999; Richstone et al., 1998; Gebhardt et al., 2000; Merritt and Ferrarese, 2001) make it necessary to revise theoretical models of the disk accretion. A large part of the high energy radiation originates close to the black hole, where the standard accretion disk model is not appropriate. Improvements of the accretion models have been made by taking into account the advective terms and including the important consequences of ordered and disordered magnetic fields. The conclusions obtained from ADAF solutions — for optically thin accretion flows at low mass accretion rates — are open to question because of omission of all magnetic field effects. Heating due to the annihilation of the magnetic field in the accretion flow is predicted to be important. Further, the energy exchange between electrons and ions may be increased substantially by the turbulent electric fields in the plasma. Account of the magnetic field leads to the conclusion that the radiative efficiency of the accretion is *not* smaller than about 0.25 the efficiency for standard disk accretion (Bisnovaty-Kogan and Lovelace, 1997, 2000) It is expected that more accurate treatment of the relaxation connected with the plasma turbulence will increase the efficiency further, making it close to unity (see also Fabian and Rees, 1995).

Some observational data which were interpreted as an evidence for the existence of the ADAF regime have disappeared after additional accumulation of data. The most interesting example of this sort is connected with the claim of the proof of the existence of event horizon of the black holes due to manifestation of the ADAF regime of accretion (Narayan et al., 1997). Analysis of a more complete set of observational data (Chen et al., 1998) had shown the disappearance of the statistical effect claimed as an evidence for ADAF. This example shows how dangerous is to base a proof of the theoretical model on the preliminary observational data. It is even more dangerous, when the model is physically not fully consistent. Then even a reliable set of the observational data cannot serve as a proof of the model. The classical example from astrophysics of this kind gives the theory of the origin of the elements presented in the famous book of Gamow (1952), where the model of the hot universe was developed. In addition to rich advantages of this

model, the author also wanted to explain the origin of heavy elements in the primordial explosion, neglecting the problems connected with an absence of the stable elements with the number of barions equal to 5 and 8. Gamow considered the good coincidence of his calculations, where the mentioned problem was neglected, and the observational curve, as a proof of his theory of the origin of the elements. Further developments have shown that his outstanding theory explains many things, but not the origin of the heavy elements which are produced due to stellar evolution.

It appears difficult explain under-luminous AGNs with ADAF solutions where the radiative efficiency is much smaller than for standard accretion disk models. Possible explanations include the fact that the mass accretion rates to the black holes may have been overestimated. More importantly, other mechanisms of energy loss may be involved in the accretion flows, for example, in the form of accelerated particles, as in the radio-pulsars, where the energy carried by the relativistic wind far exceeds the electromagnetic radiation (e.g., the Crab pulsar). Winds and/or jets are likely to happen in the presence of a large scale magnetic field which can have a key role in their the formation. To extend this, we may suggest that under-luminous AGN loose significant part of their energy to the formation of winds and/or jets. A search for a correlation between the occurrence of outflows or jets and low luminosity could be very informative. [Note that the ADAF model of Blandford and Begelman (1999) takes into account outflows, but it requires the same assumption as earlier ADAF models that there is no magnetic field and no heating of electrons by field annihilation. As we have argued, these assumptions are implausible.]

The behavior of accretion disks in the presence of ordered and disordered magnetic fields was discussed. The interaction of an accretion disk with a rotating magnetized star was reviewed including the formation of magnetohydrodynamic (MHD) outflows, magnetic braking of the star's rotation, and the propeller effect. The discussed problems of the MHD origin of jets in both in the hydromagnetic and Poynting flux regimes are currently under active study. Both regimes are being studied by different groups using axisymmetric and more recently 3D

MHD simulations. Many simulation papers have been published on MHD outflows and jets, but the results often represent the time evolution for only a short interval (typically the period of rotation at the inner edge of the disk). These results are therefore strongly dependent on the initial conditions which are unknown. Furthermore, the boundary conditions used in the simulation codes can give false results, for example, collimation of an MHD flow when there actually is no collimation (see e.g. Ustyugova et al., 1999). The difficulty of obtaining generally valid results from MHD simulations is even more challenging in the case of relativistic MHD (Komisarov, 1999) including the Kerr metric near a rapidly rotating black hole (Koide et al., 2000). Energy losses connected with magnetohydrodynamic (MHD) outflows and jets from the accretion disk may be very important and represent an alternative explanation of under-luminous AGN black holes.

Acknowledgements

The authors are indebted to their collaborators for essential contributions to many of the topics discussed in this review. The work of GBK was supported in part by the Russian Fundamental Research Foundation grant No. 99-02-18180, and INTAS-ESO grant No. 120. The work of RVEL was supported in part by NASA grants NAG5-9047 and NAG5-9735 and NSF grant AST-9986936.

References

- Abramowicz, M.A., Czerny, B., Lasota, J.P., Szuszkiewicz, E., 1988. *ApJ* 332, 646.
- Abramowicz, M.A., Zurek, W.H., 1981. *ApJ* 246, 314.
- Abramowicz, M.A., Kato, S., 1989. *ApJ* 336, 304.
- Agol, E., Krolik, J., 1998. *ApJ* 507, 304.
- Agol, E., Krolik, J., Turner, N.J., Stone, J.M., 2000, preprint.
- Aly, J.J., 1984. *ApJ* 283, 349.
- Aly, J.J., 1991. *ApJ Lett.* 375, L61.
- Arons, J., Lea, S.M., 1976. *ApJ* 207; 914; 210, 792
- Artemova, I.V., Bisnovaty-Kogan, G.S., Björnsson, G., Novikov, I.D., 1996. *ApJ* 456, 119.
- Artemova, I.V., Bisnovaty-Kogan, G.S., Igumenshchev, I., Novikov, I.D., 2000, astro-ph/0003058; *ApJ* (2001) 549, No. 2.
- Balbus, S.A., Hawley, J.F., 1992. *ApJ* 400, 610.

- Balbus, S.A., Hawley, J.F., 1998. *RvMP* 70, 1.
- Bateman, G., 1980. *MHD Instabilities*. MIT Press, Cambridge, Chapter 6.
- Baushev, A.N., Bisnovaty-Kogan, G.S., 1999. *ARep* 43, 241.
- Benz, A.O., 1997. In: Simnett, G.M., Alissandrakis, C.E., Vlahos, L. (Eds.), *Solar and Heliospheric Plasma Physics*. Springer, Heidelberg, p. 201.
- Begelman, M.C., Blandford, R.D., Rees, M.J., 1984. *RvMP* 56, 255.
- Bell, A.R., 1994. *Phys. Plasmas* 1, 1643.
- Bell, A.R., Lucek, S.G., 1995. *MNRAS* 277, 1327.
- Beloborodov, A.M., 1998. *MNRAS* 297, 739.
- Biermann, L., Lust, R., 1960. Nonthermal phenomena in stellar atmospheres. In: *Stellar Atmospheres*. Univ. Chicago Press, Chapter 6.
- Bildsten, L., Chakrabarty, D., Chiu, J., Finger, M.H., Koh, D.T., Nelson, R.W., Prince, T.A., Rubin, B.C., Scott, D.M., Stollberg, M., Vaughan, B.A., Wilson, C.A., Wilson, R.B., 1997. *ApJS* 113, 367.
- Bisnovaty-Kogan, G.S., 1973. *AZh* 50, 902.
- Bisnovaty-Kogan, G.S., 1974. *AZh* 51, 443.
- Bisnovaty-Kogan, G.S., 1991. *A&A* 245, 528.
- Bisnovaty-Kogan, G.S., 1993a. *A&A* 274, 796.
- Bisnovaty-Kogan, G.S., 1989. *Physical Problems of the Theory of Stellar Evolution*. Nauka, Moscow, in Russian.
- Bisnovaty-Kogan, G.S., 1993b. In: Errico, L., Vittone, A.A. (Eds.), *Stellar Jets and Bipolar Outflows*. Kluwer, Dordrecht, p. 369.
- Bisnovaty-Kogan, G.S., 1994. *MNRAS* 269, 557.
- Bisnovaty-Kogan, G.S., 1999a. *Proc. Conf. Observational Evidences for the Black Holes in the Universe*, Calcutta, 1998. Kluwer, p. 1.
- Bisnovaty-Kogan, G.S. 1999b. *astro-ph/9911275*.
- Bisnovaty-Kogan, G.S., 2001. *Stellar Physics*, Vol. 1. Springer, Heidelberg.
- Bisnovaty-Kogan, G.S., Blinnikov, S.I., 1976. *SvAL* 2, 191.
- Bisnovaty-Kogan, G.S., Blinnikov, S.I., 1977. *A&A* 59, 111.
- Bisnovaty-Kogan, G.S., Blinnikov, S.I., 1978a. *SvAL* 4, 290.
- Bisnovaty-Kogan, G.S., Blinnikov, S.I., 1978b. *Ap* 14, 316.
- Bisnovaty-Kogan, G.S., Blinnikov, S.I., 1979. *Ap* 15, 99.
- Bisnovaty-Kogan, G.S., Blinnikov, S.I., 1981. *SvA* 25, 175.
- Bisnovaty-Kogan, G.S., Friedman, A.M., 1969. *AZh* 46, 721.
- Bisnovaty-Kogan, G.S., Goncharov, A.V., Komberg, B.V., Cherepashchuk, A.M., Yagola, A.G., 1977. *SvA* 21, 133.
- Bisnovaty-Kogan, G.S., Komberg, B.V., 1973. *Astron. cir.* 784, 721.
- Bisnovaty-Kogan, G.S., Komberg, B.V., 1974. *AZh* 51, 373.
- Bisnovaty-Kogan, G.S., Lovelace, R.V.E., 1997. *ApJ Lett.* 486, L43.
- Bisnovaty-Kogan, G.S., Lovelace, R.V.E., 2000. *ApJ* 529, 978.
- Bisnovaty-Kogan, G.S., Ruzmaikin, A.A., 1974. *Ap&SS* 28, 45.
- Bisnovaty-Kogan, G.S., Ruzmaikin, A.A., 1976. *Ap&SS* 42, 401.
- Bisnovaty-Kogan, G.S., Sunyaev, R.A., 1972. *SvA* 15, 697.
- Blackman, E.G., 1999. *MNRAS* 302, 723.
- Blandford, R.D., 1976. *MNRAS* 176, 465.
- Blandford, R.D., Begelman, M.C., 1999. *MNRAS* 303, L1.
- Blandford, R.D., Payne, D.G., 1982. *MNRAS* 199, 883.
- Blandford, R.D., Znajek, R.L., 1977. *MNRAS* 179, 433.
- Blinnikov, S.I., 1975. *SvA* 19, 151.
- Bogovalov, S.B., 1997. *A&A* 323, 634.
- Boldt, E., 1977. *Ann. New York Acad. Sci.* 302, 329.
- Bondi, H., 1952. *MNRAS* 112, 195.
- Bondi, H., Hoyle, F., 1944. *MNRAS* 104, 273.
- Brandenburg, A., Nordlund, A., Stein, R.F., Torkelson, U., 1995. *ApJ* 446, 741.
- Bridle, A.H., Eilek, J.A. (Eds.), 1984. *Physics of Energy Transport in Extragalactic Radio Sources*. NRAO, Greenbank.
- Bührke, T., Mundt, R., Ray, T.P., 1988. *A&A* 200, 99.
- Campbell, C.G., 1992. *Geophys. Astrophys. Fluid Dynamics* 63, 179.
- Cannizzo, J., Ghosh, P., Wheeler, J.C., 1982. *ApJ Lett.* 260, L83.
- Cannizzo, J.K., Greenhill, L.J., Herrnstein, J.R., Moran, J.M., Mushotsky, R.E., 1998. *AAS Meeting*, 192, #41.03.
- Cao, X., Spruit, H.C., 1994. *A&A* 287, 80.
- Chakrabarti, S.K., 1996. *ApJ* 464, 1996.
- Chakrabarti, S.K., Molteni, D., 1993. *ApJ* 417, 671.
- Chakrabarti, D. et al., 1997. *ApJ* 481, L101.
- Chandrasekhar, S., 1956. *ApJ* 124, 232.
- Chandrasekhar, S., 1957. *An Introduction to the Study of Stellar Structure*. Dover Publ.
- Chandrasekhar, S., 1981. *Hydrodynamic and Hydromagnetic Stability*. Dover, New York.
- Chandrasekhar, S., 1989. In: *Selected Papers*, Vol. 1. Univ. Chicago Press, p. 185.
- Chang, K.M., Ostriker, J.P., 1985. *ApJ* 288, 428.
- Chapman, S., Cowling, T.G., 1939. *The Mathematical Theory of Nonuniform Gases*. Cambridge Univ. Press.
- Chen, W., Cui, W., Frank, J., King, A., Livio, M., Zhang, S.N., 1998. *AIP Conf. Proc.* 431, 347.
- Cherepashchuk, A.M., 1996. *Uspekhi Fiz. Nauk* 166, 809.
- Cherepashchuk, A.M., 2000. *SSRv* 93, 473.
- Colgate, S.A., Li, H., 1998. In: *Proc. of VII International Conference and Lindau Workshop on Plasma Astrophysics and Space Physics*, Lindau, Germany.
- Collins, T.J.B., Helfer, H.L., Van Horn, H.M., 1998. *ApJ* 502, 730.
- Colpi, M., Nanmurelli, M., Calvani, M., 1991. *MNRAS* 253, 55.
- Contopoulos, J., Lovelace, R.V.E., 1994. *ApJ* 429, 139.
- Contopoulos, J., 1995. *ApJ* 450, 616.
- Coppi, B., Coppi, P., 2000. *MIT (RLE) Report PTP 00/09 (PhRvL 87 (2001) 05 1101)*.
- Coroniti, F.V., 1981. *ApJ* 244, 587.
- Cui, W., 1997. *ApJ* 482, L163.
- Davidson, K., Ostriker, J.P., 1973. *ApJ* 179, 585.
- Deeter, J.E., Scott, D.M., Boynton, P.E., Miyamoto, S., Kitamoto, S., Takahama, S., Nagase, F., 1998. *ApJ* 502, 802.
- Di Matteo, T., Fabian, A.C., Rees, M.J., Carilli, C.L., Ivison, R.J., 1998. *astro-ph/9807245 (MNRAS 305 (1999) 492)*.
- Dullemond, C.P., Turolla, R., 1998. *ApJ* 503, 361.
- Eardley, D.M., Lightman, A.P., 1975. *ApJ* 200, 187.
- Eikenberry, S., Matthews, K., Morgan, E.H., Remillard, R.A., Nelson, R.W., 1998. *ApJ Lett.* 494, L61.
- Fabian, A.C., Rees, M.J., 1995. *MNRAS* 277, L55.
- Fabbiano, G., Schreier, E.J., 1977. *ApJ* 214, 235.
- Falcke, H., Malkan, M.A., Biermann, P.L., 1995. *A&A* 298, 375.
- Field, G.B., Rogers, R.D., 1993. *ApJ* 403, 94.
- Finn, J.M., Chen, J., 1990. *ApJ* 349, 345.

- Fujita, M., Okuda, T., 1998. *PASJ* 50, 639.
- Fukue, J., 1987. *PASJ* 39, 309.
- Galeev, A.A., Rosner, R., Vaiana, G.S., 1979. *ApJ* 229, 318.
- Galeev, A.A., Sagdeev, R.Z., 1983. Chapter 6. In: Rosenbluth, M.N., Sagdeev, R.Z. (Eds.). *Handbook of Plasma Physics*, Vol. 1. North-Holland Publ, Amsterdam, Chapter. 6.1.
- Gamow, G., 1952. *The Creation of the Universe*. Viking Press, NY.
- Gebhardt, K., Bender, R., Bower, G., Dressler, A., Faber, S.M., Filippenko, A.V., Green, R., Grillmair, C., Ho, L.C., Kormendy, J., Lauer, T.R., Magorrian, J., Pinkney, J., Richstone, D., Tremaine, S., 2000. *ApJ* 439, L13.
- Ghosh, P., Lamb, F.K., 1978. *ApJ* 223, L83.
- Ghosh, P., Lamb, F.K., 1979a. *ApJ* 232, 259.
- Ghosh, P., Lamb, F.K., 1979b. *ApJ* 234, 296.
- Giacconi, R., Gursky, H., Paolini, F.R., Rossi, B.B., 1962. *PhRvL* 9, 439.
- Giacconi, R., Gursky, H., Kellogg, E., Schreier, E., Tananbaum, U., 1971. *ApJ* 167, L67.
- Giacconi, R., 1974. In: *Astrophysics and Gravitation*. l'Universite de Bruxelles, Bruxelles, p. 27.
- Ginzburg, V.L., 1975. *Theoretical Physics and Astrophysics*. Nauka, Moscow.
- Glatzel, W., 1989. *J. Fluid. Mech.* 202, 515.
- Glatzel, W., 1992. *MNRAS* 257, 572.
- Gnedin, Yu.N., Sunyaev, R.A., 1973. *A&A* 25, 233.
- Godon, P., 1996a. *MNRAS* 279, 1071.
- Godon, P., 1996b. *ApJ* 463, 674.
- Gold, T., Hoyle, F., 1960. *MNRAS* 120, 7.
- Goldreich, P., Julian, W.H., 1969. *ApJ* 157, 869.
- Goodson, A.P., Winglee, R.M., Böhm, K.H., 1997. *ApJ* 489, 390.
- Gruber, D.E. et al., 1980. *ApJ Lett.* 240, L27.
- Gursky, H., Schreier, E., 1975. In: Gursky, H., Ruffini, R. (Eds.), *Neutron Stars, Black Holes and Binary X-Ray Sources*. D. Reidel Publishing Company, Dordrecht, p. 175.
- Haswell, C., 1999. In: Chakrabarty, S. (Ed.), *Observational Evidence for Black Holes in the Universe*. Kluwer, Dordrecht.
- Hawley, J.F., Gammie, C.F., Balbus, S.A., 1995. *ApJ* 440, 742.
- Hayashi, M.R., Shibata, K., Matsumoto, R., 1996. *ApJ* 468, L37.
- Heindl, W.A. et al., 1999. *ApJ Lett.* 521, L49.
- Heinemann, M., Olbert, S., 1978. *J. Geophys. Res.* 83, 2457.
- Heyvaerts, J., Norman, C.A., 1989. *ApJ* 347, 1055.
- Herrnstein, J.R., Greenhill, L.J., Moran, J.M., Diamond, P.J., Inoue, M., Nakai, N., Miyoshi, M., 1998. *ApJ Lett.* 497, L69.
- Ho, L., 1999. In: *Proc. Conf. Observational Evidences for Black Holes in the Universe*, Calcutta, 1998. Kluwer, p. 157.
- Holt, S.S., Bolt, E.A., Kaluzienski, L.J., Serlemitsos, P.J., 1975. *Nature* 256, 108.
- Hōshi, R., 1977. *Prog. Theor. Phys.* 58, 1191.
- Hōshi, R., Shibasaki, N., 1977. *Prog. Theor. Phys.* 58, 1759.
- Ichimaru, S., 1977. *ApJ* 214, 830.
- Igumenshchev, I.V., 2000. *MNRAS* 314, 54.
- Igumenshchev, I.V., Abramowicz, M.A., 1999. *MNRAS* 303, 309.
- Igumenshchev, I.V., Abramowicz, M.A., 2000. *ApJS* 130, 463.
- Igumenshchev, I.V., Abramowicz, M.A., Narayan, R., 2000. *ApJ Lett.* 537, L27.
- Illarionov, A.F., Sunyaev, R.A., 1975. *A&A* 39, 185.
- Ipser, J.R., Managan, R.A., 1981. *ApJ* 250, 362.
- James, R.A., 1964. *ApJ* 140, 552.
- Kadomtsev, B.B., 1963. *Rev. Plasma Phys.* 2, 188.
- Kaisig, M., Tajima, T., Lovelace, R.V.E., 1992. *ApJ* 386, 83.
- Kato, S., Fukue, J., Mineshige, S., 1998. *Black-Hole Accretion Disks*. Kyoto Univ. Press, Kyoto.
- Katz, J.I., 1997. *ApJ* 490, 633.
- Klieber, R., Glatzel, W., 1999. *MNRAS* 303, 107.
- Kley, W., 1991. *A&A* 247, 95.
- Koide, S., Meier, D.L., Shibata, K., Kudo, T., 2000. *ApJ* 536, 668.
- Koldoba, A.V., Ustyugova, G.V., Romanova, M.M., Chechetkin, V.M., Lovelace, R.V.E., 1995. *Ap&SS* 232, 241.
- Komissarov, S.S., 1999. *MNRAS* 303, 343.
- Königl, A., 1989. *ApJ* 342, 208.
- Königl, A., Ruden, S.P., 1993. In: Levy, E.H., Lunine, J. (Eds.), *Protostars and Planets III*. Univ. of Arizona Press, Tucson, p. 641.
- Koupelis, T., Van Horn, H.M., 1989. *ApJ* 342, 146.
- Krasnopolsky, R., Li, Z.-Y., Blandford, R.D., 1999. *ApJ* 526, 631.
- Kulikovskiy, A.G., Lyubimov, G.A., 1962. *Magnetic Hydrodynamics*, PhysMatGiz, Moscow (in Russian).
- Lamb, F.K., Pethick, C.J., Pines, D., 1973. *ApJ* 184, 271.
- Landau, L.D., 1937. *Zh. Exp. Theor. Phys.* 7, 203.
- Landau, L.D., 1946. *J. Phys. U.S.S.R.* 10, 25.
- Landau, L.D., Lifshitz, E.M., 1959. *Fluid Mechanics*. Pergamon Press, New York, Chapter 2.
- Lasota, J.-P., Abramowicz, M.A., Chen, X., Krolik, J., Narayan, R., Yi, I., 1996. *ApJ* 462, 142.
- Lesch, H., 1991. *A&A* 245, 48.
- Levinson, A., 1998. *ApJ* 507, 145.
- Li, H., Lovelace, R.V.E., Finn, J.M., Colgate, S.A., 2000. *ApJ* 533, 1023.
- Li, H., Colgate, S.A., Wendroff, B., Liska, R., 2001. *ApJ* 551, 874.
- Li, H., Lovelace, R.V.E., Finn, J.M., Colgate, S.A., 2001b. *Magnetic helix formation driven by Keplerian disk rotation*, *ApJ*, in press.
- Li, J., Wickramasinghe, D.T., 1997. In: *Accretion Phenomena and Related Outflows*, IAU Colloquium 163, ASP Conf. Ser., 121, 241.
- Liang, E.P.T., Thompson, K.A., 1980. *ApJ* 240, 271.
- Lipunov, V.M., 1987. *AZh* 64, 321.
- Lipunov, V.M., 1993. *Astrophysics of Neutron Stars*. Springer-Verlag, Berlin, Chapters 6, 7.
- Livio, M., Ogilvie, G.I., Pringle, J.E., 1999. *ApJ* 512, 100.
- Lovelace, R.V.E., 1976. *Nature* 262, 649.
- Lovelace, R.V.E., Mehanian, C., Mobarry, C.M., Sulkanen, M.E., 1986. *ApJS* 62, 1.
- Lovelace, R.V.E., Wang, J.C.L., Sulkanen, M.E., 1987. *ApJ* 315, 504.
- Lovelace, R.V.E., Mobarry, C.M., Contopoulos, J., 1989. In: Belvedere, G. (Ed.), *Accretion Disks and Magnetic Fields in Astrophysics*. Kluwer, Dordrecht, p. 71.
- Lovelace, R.V.E., Berk, H.L., Contopoulos, J., 1991. *ApJ* 379, 696.
- Lovelace, R.V.E., Romanova, M.M., Contopoulos, J., 1993. *ApJ* 403, 158.
- Lovelace, R.V.E., Romanova, M.M., Newman, W.I., 1994. *ApJ* 437, 136.
- Lovelace, R.V.E., Romanova, M.M., Bisnovaty-Kogan, G., 1995. *MNRAS* 275, 244.

- Lovelace, R.V.E., Newman, W.I., Romanova, M.M., 1997. *ApJ* 424, 628.
- Lovelace, R.V.E., Romanova, M.M., Bisnovatyi-Kogan, G., 1999a. *ApJ* 514, 368.
- Lovelace, R.V.E., Ustyugova, G.S. and Koldoba, A.V., 1999b, in: Terzian, Y., Weedman, D., Khachikian, E. (Eds.), *Active Galactic Nuclei and Related Phenomena*, IAU Symposium 194 (Astron. Soc. of Pacific: San Francisco), p. 208.
- Lovelace, R.V.E., Li, H., Colgate, S.A., Nelson, A.F., 1999c. *ApJ* 513, 805.
- Lovelace, R.V.E., Li, H., Koldoba, A.V., Ustyugova, G.S., Romanova, M.M., 2001a. *Poynting jets from accretion disks*, *ApJ*, submitted.
- Lynden-Bell, D., 1969. *Nature* 223, 690.
- Lynden-Bell, D., 1996. *MNRAS* 279, 389.
- Lynden-Bell, D., Boily, C., 1994. *MNRAS* 267, 146.
- Lynden-Bell, D., Pringle, J.E., 1974. *MNRAS* 168, 603.
- Matsumoto, R., Kato, Sh., Fukue, J., Okazaki, A.T., 1984. *Publ. Astron. Soc. Japan* 36, 71.
- McConnell, M.L., Ryan, J.M., Collmar, N. et al., 2000. *ApJ* 543, 928.
- McCray, R.A., Shull, J.M., Boynton, P.E. et al., 1982. *ApJ* 262, 301.
- Meier, D.L., Edgington, S., Godon, P., Payne, D.G., Lind, K.R., 1997. *Nature* 388, 350.
- Meier, D.L., Koide, S., Uchida, Y., 2001. *Science* 291, 84.
- Menon, K., Quataert, E., Narayan, R., 1999. *Proc. MG8 (Jerusalem, 1997)*. World Scientific, p. 204.
- Merritt, D., Ferrarese, L., 2001. *ApJ* 547, 140.
- Mestel, L., 1968. *MNRAS* 138, 359.
- Meszáros, P., 1975. *A&A* 44, 59.
- Middleditch, J., Nelson, J., 1976. *ApJ* 208, 567.
- Middleditch, J., Puetter, R.C., Pennypacker, C.R., 1985. *ApJ* 292, 267.
- Mihara, T., Makishima, K., Ohashi, T. et al., 1990. *Nature* 346, 250.
- Mihara, T., Makishima, K., Nagase, F., 1997. *Proceedings of International Workshop, All-sky X-ray Observations in the Next Decade*, March 3–5, 135.
- Miller, K., Stone, J., 1997. *ApJ* 489, 890.
- Mirabel, I.F., Rodriguez, L.F., 1994. *Nature* 371, 46.
- Morfill, G.E., Scheingraber, H., Voges, W., 1989. In: Ogelman, H., van den Heuvel, E.P.J. (Eds.), *Timing Neutron Stars*, Kluwer, Denter, p. 71.
- Muchotrzeb, B., Paczyński, B., 1982. *AcA* 32, 1.
- Mundt, R., 1985. In: Black, D.C., Mathews, M.S. (Eds.), *Protostars and Planets II*. Univ. of Arizona Press, Tucson, p. 414.
- Nagase, F., 1981. *SSRv* 30, 395.
- Nagase, F. et al., 1984. *ApJ* 280, 259.
- Nagase, F., 1989. *PASJ* 41, 1.
- Narayan, R., Barret, D., McClintock, J.E., 1996. *A&AS* 120, 187.
- Narayan, R., Garcia, M.R., McClintock, J.E., 1997. *ApJ Lett.* 478, L79.
- Narayan, R., Yi, I., 1995. *ApJ* 452, 710.
- Nayfeh, A., 1973. *Perturbation Methods*. John Wiley and Sons, New York.
- Nayfeh, A., 1981. *Introduction into Perturbation Techniques*. John Wiley and Sons, New York.
- Newman, W.I., Newman, A.L., Lovelace, R.V.E., 1992. *ApJ* 392, 622.
- Novikov, I.D., Thorne, K.S., 1973. In: DeWitt, C., DeWitt (, B. (Eds.), *Black Holes*. Gordon and Breach, New York, p. 345.
- Ostriker, E.C., 1997. *ApJ* 486, 291.
- Ouyed, R., Pudritz, R.E., 1997. *ApJ* 482, 712.
- Paczynski, B., 1991. *ApJ* 370, 597.
- Paczyński, B., Bisnovatyi-Kogan, G.S., 1981. *AcA* 31, 283.
- Paczyński, B., Wiita, P.J., 1980. *A&A* 88, 23.
- Papaloizou, J.C.B., Stanley, G.Q.G., 1986. *MNRAS* 220, 593.
- Parail, V.V., Pogutse, O.P., 1965. In: Leontovich (, M.A. (Ed.). *Reviews of Plasma Physics*, Vol. 11. Consultants Bureau, New York, p. 1.
- Pariev, V., Finn J.M., Colgate, S.A., 2001. *ApJ*, submitted.
- Parker, E.N., 1955. *ApJ* 121, 491.
- Parker, E.N., 1979. *Cosmical Magnetic Fields*. Clarendon Press, Oxford, Chapter 17.
- Parker, E.N., 1990. In: Ulmschneider, P., Priest, E.R., Rosner (, R. (Eds.), *Mechanisms of Chromospheric and Coronal Heating*. Springer-Verlag, Berlin, p. 615.
- Pelletier, G., Pudritz, R.E., 1992. *ApJ* 394, 117.
- Phinney, E.S., 1987. In: Zensus, J.A., Pearson, T.J. (Eds.), *Superluminal Radio Sources*. Cambridge Univ. Press, Cambridge, p. 301.
- Popham, R., Narayan, R., 1991. *ApJ* 370, 604.
- Popham, P., Narayan, R., 1995. *ApJ* 442, 337.
- Popham, P., Kenyon, S., Hartmann, L., Narayan, R., 1996. *ApJ* 473, 422.
- Porter, L.A., Klimchuk, J.A., Sturrock, P.A., 1992. *ApJ* 385, 738.
- Potter, D., 1973. In: *Computational Physics*. John Wiley and Sons, New York, p. 108.
- Poutanen, J., Krolik, J.H., Ryde, F., 1997. *MNRAS* 292, L21.
- Prandtl, L., 1905. *Proc. Third Int. Math. Kongr., Heidelberg*, pp. 484–491.
- Price, R.H., Liang, E.P., 1977. *ApJ* 218, 247.
- Pringle, J.E., 1989. *MNRAS* 236, 107.
- Pringle, J.E., Rees, M.J., 1972. *A&A* 21, 1.
- Pringle, J.E., Rees, M.J., Pacholczyk, A.G., 1973. *A&A* 29, 179.
- Pudritz, R.E., Norman, C.A., 1986. *ApJ* 301, 571.
- Quataert, E., 1998. *ApJ* 500, 978.
- Rappaport, S.A., Joss, P.C., 1977. *Nature* 266, 683.
- Rappaport, S.A., Joss, P.C., 1983. In: Lewin, W.H.G., van den Heuvel (, E.P.J. (Eds.), *Accretion-Driven Stellar X-Ray Sources*. Cambridge University Press, Cambridge, p. 1.
- Rastätter, L., Schindler, K., 1999. *ApJ* 524, 361.
- Richstone, D., Ajhar, E.A., Bender, R., Bower, G., Dressler, A., Faber, S.M., Filippenko, A.V., Gebhardt, K., Green, R., Ho, L.C., Kormendy, J., Lauer, T.R., Magorrian, J., Tremaine, S., 1998. *Nature* 395A, 14.
- Reames, D.V., Barbier, L.M., Von Roseninge, T.T., Mason, G.M., Mazur, J.E., Dwyer, J.R., 1997. *ApJ* 483, 515.
- Regev, O., 1983. *A&A* 126, 146.
- Regev, O., Bertout, C., 1995. *MNRAS* 272, 71.
- Regev, O., Hougerat, A.A., 1988. *MNRAS* 232, 81.
- Riffert, H., Herold, H., 1995. *ApJ* 450, 508.
- Romanova, M.M., 1999. In: Terzian, Y., Weedman, D., Khachikian (, E. (Eds.), *Active Galactic Nuclei and Related Phenomena*,

- IAU Symposium 194. Astron. Soc. of Pacific, San Francisco, p. 256.
- Romanova, M.M., Lovelace, R.V.E., 1992. *A&A* 262, 26.
- Romanova, M.M., Lovelace, R.V.E., 1997. *ApJ* 475, 97.
- Romanova, M.M., Ustyugova, G.V., Koldoba, A.V., Chechetkin, V.M., Lovelace, R.V.E., 1997. *ApJ* 482, 708.
- Romanova, M.M., Ustyugova, G.V., Koldoba, A.V., Chechetkin, V.M., Lovelace, R.V.E., 1998. *ApJ* 500, 703.
- Sakurai, T., 1987. *PASJ* 39, 821.
- Santangelo, A. et al., 1999. *ApJ Lett.* 523, L85.
- Schlichting, H., 1964. *Grenzschrift-Theorie*. Verlag G. Braun, Karlsruhe.
- Schmidt, M., 1963. *ApJ* 136, 164.
- Schreier, E., Levinson, R., Gursky, H., Kellogg, E., Tananbaum, H., Giacconi, R., 1972. *ApJ* 172, L79.
- Schreier, E.J., Fabbiano, G., 1976. In: *X-Ray Binaries*, NASA SP-389, National Technical Information Service, Springfield, Virginia, p. 197.
- Schwartzman, V.F., 1971. *SvA* 15, 377.
- Scott, D.M. et al., 2000. *astro-ph/0002327*
- Shakura, N.I., 1972. *AZh* 49, 921.
- Shakura, N.I., Sunyaev, R.A., 1973. *A&A* 24, 337.
- Shakura, N.I., Sunyaev, R.A., 1988. *Adv. Space Res.* 8 (2), 135.
- Shapiro, S.L., Lightman, A.P., Eardley, D.M., 1976. *ApJ* 204, 187.
- Shapiro, S.L., Teukolsky, S.A., 1983. In: *Black Holes, White Dwarfs, and Neutron Stars*. Wiley and Sons, New York.
- Sheepmaker, T., Jansen, F.A., Deerenberg, A.J.M. et al., 1981. *SSRv* 30, 325.
- Sheffer, E.K., Kopaeva, I.F., Averintsev, M.B., Bisnovaty-Kogan, G.S., Golynskaya, I.M., Gurin, L.S., D'yachkov, A.V., Zenchenko, V.M., Kurt, V.G., Mizyakina, T.A., Mironova, E.N., Sklyankin, V.A., Smirnov, A.S., Titarchuk, L.G., Shamolin, V.M., Shafer, E.Yu., Shmel'kin, A.A., Giovannelli, F., 1992. *SvA-AJ* 36, 41.
- Shibata, K., Uchida, Y., 1986. *PASJ* 38, 631.
- Shorokhov, O.V., 2000. *Diploma Thesis*. MPhTI, Moscow.
- Shu, F., Lizano, S., Ruden, S.P., Najita, J., 1988. *ApJ* 328, L19.
- Spitzer, L., 1940. *MNRAS* 100, 396.
- Stone, J.M., Norman, M.L., 1994. *ApJ* 433, 746.
- Sturrock, P.A., 1991. *ApJ* 380, 655.
- Sunyaev, R.A., Titarchuk, L.G., 1980. *A&A* 86, 121.
- Tananbaum, H., Gursky, H., Kellogg, E.M., Levinson, R., Schreier, E., Giacconi, R., 1972. *ApJ* 174, L143.
- Tassoul, J.-L., 1978. *Theory of Rotating Stars*. Princeton Univ. Press.
- Tjemkes, S.A., Ziuderwijk, E.J., Van Paradijs, J., 1986. *A&A* 154, 77.
- Toropin, Yu.M., Toropina, O.D., Savelyev, V.V., Romanova, M.M., Chechetkin, V.M., Lovelace, R.V.E., 1999. *ApJ* 517, 906.
- Trubnikov, B.A., 1958. *Magnetic Emission of High Temperature Plasma*, Dissertation, Moscow, USAEC Tech. Information Service, AEC-tr-4073 (1960)
- Trubnikov, B.A., 1973. *Voprosy Teorii Plasmy* 7, 274.
- Trümper, J., Pietsch, W., Reppin, C. et al., 1978. *ApJ* 219, 105.
- Tsuneta, S., 1996. *ApJ* 456, 840.
- Tueller, J., Cline, T.L., Teegarden, B.J. et al., 1984. *ApJ* 279, 177–183.
- Turolla, R., Dullemond, C.P., 2000. *ApJ* 531, L49.
- Ubertini, P., Bazzano, A., LaPadula, C.D., et al., 1980. *Proc. 17th Int. Cosmic-Ray Conf.*, Paris, 1, 99.
- Uchida, Y., Shibata, K., 1985. *PASJ* 37, 515.
- Ustyugova, G.V., Koldoba, A.V., Romanov, M.M., Chechetkin, V.M., Lovelace, R.V.E., 1995. *ApJ Lett.* 439, L39.
- Ustyugova, G.V., Koldoba, A.V., Romanova, M.M., Chechetkin, V.M., Lovelace, R.V.E., 1999. *ApJ* 516, 221.
- Ustyugova, G.V., Lovelace, R.V.E., Romanova, M.M., Li, H., Colgate, S.A., 2000. *ApJ Lett.* 541, L21.
- Vasil'eva, A.V., 1959. *Math. Sbornik* 48, 311.
- Velikhov, E.P., 1959. *J. Exper. Theor. Phys.* 36, 1398.
- Voges, W., Pietsch, W., Reppin, C. et al., 1982. *ApJ* 263, 803.
- Voges, W., Atmanspacher, H., Scheingraber, H., 1987. *ApJ* 320, 794.
- Wang, Y.-M., 1979. *A&A* 74, 253.
- Wang, J.C.L., Wasserman, I.M., Salpeter, E.E., 1988. *ApJS* 68, 735.
- Weber, E.J., Davis, L., 1967. *ApJ* 148, 217.
- Woltjer, L., 1959. *ApJ* 130, 405.
- Wrobel, J.M., Herrnshtein, J.R., 2000. *ApJ Lett.* 533, L11.
- Zel'dovich, Ya.B., 1981. *Proc. Roy. Soc. Lond.*, A 374, 299.
- Zel'dovich, Ya.B., Shakura, N.I., 1969. *AZh* 46, 225.
- Zwillinger, D., 1992. *Handbook of Differential Equations*. Academic Press, Boston.